THE UNIVERSITY OF CALGARY

P-S Seismic Inversion: Modeling, Processing, and Field Examples

by

Robert James Ferguson

A THESIS

SUBMITTED TO THE FACULTY OF GRADUATE STUDIES

IN PARTIAL FULFILLMENT OF THE REQUIREMENTS FOR THE

DEGREE OF MASTER OF SCIENCE

DEPARTMENT OF GEOLOGY AND GEOPHYSICS

CALGARY, ALBERTA

NOVEMBER, 1996

ABSTRACT

This thesis presents methods to invert P-S stacking velocities and P-S reflectivity, to estimate shear-wave velocity (Vs). The methods are applied to synthetic data, as well as a survey from the Blackfoot oil field in Alberta, Canada. S-wave velocity estimates are computed using a P-S analogue of the Dix equation, and are found to be consistent with well-log velocities, for offset-depth ratios of about 1.0. Recursive amplitude inversions, using a weighted stack data, are derived. Missing low-frequency and phase error are found to distort inversion results.

Frequency-domain inversion, and constrained linear inversion, when applied to P-S weighted stacks, are use to restore low-frequency, and phase errors are corrected in processing. Frequency-domain inversion is applied to the Blackfoot field data, and the resulting Vs and Vp/Vs anomalies correlate compellingly with a productive oil reservoir in a Cretaceous sandstone.

ACKNOWLEDGMENTS

I would like to thank Dr. Robert R. Stewart for providing enthusiastic support and insightful supervision to the development of this work. I would also like to thank the staff and sponsors of CREWES (Consortium for Research in Elastic Wave Exploration Seismology) for providing expert technical assistance and unrivaled computer facilities. Special thanks to CREWES members, Henry C. Bland, Darren S. Foltinek, Dr. Gary F. Margrave and Susan L. M. Miller.

DEDICATION

For Corrine Denise.

TABLE OF CONTENTS

LIST OF TABLES

LIST OF FIGURES

Chapter 1 INTRODUCTION

1.1 Definitions

S-wave velocity (Vs), P-wave velocity (Vp) and Vp/Vs can be used to describe the lithologic properties of rock. The relationship of these values to various rocks and their saturants can be complex, but when used in conjunction with well-log or other independent measurements, can provide useful information about reservoir rock properties (Tatham and McCormick, 1991). Many authors have described relationships between lithology and seismic velocities. Laboratory measurements indicate that Vp and Vp/Vs decrease with increasing porosity and clay content (Han et al., 1986). Dominico (1984) found that in shaley sandstones Vs was more sensitive to porosity and clay content than Vp. Nur and Simmons (1969a) and Nur (1971) demonstrated that rocks, with a non-random distribution of cracks, exhibit changes in velocity with direction of propagation (elastic-wave anisotropy). Others have found relationships between seismic velocity and depth of burial. Nur and Simmons (1969b), Wang and Nur (1987), Tosaya et al. (1987) have related increasing Vp and Vs with increasing depth of burial and temperature. Wang (1988) has shown that pore shape and fluid saturation play a role in the response of Vp and Vs to burial and temperature.

The effects of different hydrocarbon saturations on Vp, Vs and Vp/Vs have been studied. Wang and Nur (1987) related an increase in the molecular weight of the saturant to increased Vp. At borehole sonic frequencies (kHz), Murphy (1984) found that Vp and Vp/Vs decrease as gas saturation increases in tight sandstones. Gregory (1976) has shown that Vp/Vs can decrease as much as 30% in consolidated rock with increasing gas saturation. Gardner and Harris (1968) found for sands, a Vp/Vs > 2.0 indicated water saturated unconsolidated sands and a Vp/Vs < 2.0 indicated unconsolidated gas saturated

sands. Castanga et al. (1985) show that in wet sandstones Vp/Vs will decrease with increasing Vp.

As lithologic indicators, Vp and Vs have been found to be useful. In a classic paper, Pickett (1963) found that limestones, dolomites and sandstones could be discriminated from each other using Vp/Vs. Anderson and Leiberman (1966) describe distinct differences in Vp/Vs for the rock forming minerals quartz, calcite, dolomite and halite. Dominico (1977) found Vp/Vs to be useful in discriminating sandstone, calcareous sandstone, limestone, dolomite, and shale and show that Vp and Vs are higher for clean sandstones than shaley sandstones. Ito et al. (1979) showed how Poisson's ratio could be used to discriminate between steam and hot water in pore spaces.

It is clear that estimates of Vp and Vs can be used to indicate rock properties in the subsurface. Because seismic techniques have the ability to probe deeper into the earth than most other technologies, we should quite reasonably try to infer seismic velocity from seismic measurements. Until recently, seismic exploration has consisted mainly of the interpretation of P-P data. Inversion of P-P data to yield P-wave velocity has long been part of the interpretation process. Seismic inversion can be thought of as the process of reducing seismic data to obtain information about the physical subsurface (Menke, 1984). In 1955, Hewitt Dix published a classic paper which described how normal-moveout velocity measurements could be inverted to infer low-frequency Vp trends.

Other inversion methods use stacked (zero-offset) seismic data. These methods assume that moveout correction and summation, of common mid-point gathers, will produce a signal representing reflections of normally incident plane-waves in a layered medium (Lines 1988). Thus, the stacked seismic section is assumed to represent the convolution of an embedded wavelet with the reflectivity sequence of the medium (Lines, 1988). Inversion methods, based on stacked seismic data, seek to convert reflectivity to an image of acoustic impedance (Lines, 1988). An example of an inversion method is simple

recursive inversion, where the zero-offset seismic data are directly inverted based on the zero-offset reflectivity equation. It is assumed in recursive inversion that the wavelet has been removed, the data are noise free and any transmission effects have been removed (Cooke and Schneider, 1983). In practice, however, seismic data are rarely a perfect representation of true subsurface reflectivity, the data are often noisy and are generally band-limited, especially at the low-end of the frequency band (Hendrick and Hearn, 1993). As a result, there are zero-offset methods which seek to accommodate such deficiencies in seismic data.

Seismic approximate impedance log (SAIL), as described by Waters (1978), seeks to recover the low-frequencies missing in seismic data by combining acoustic impedance logs with the integrated seismic data in the frequency domain. The final inversion estimate is thus an inverse Fourier transform of this frequency domain impedance combination. Generalized linear inversion (GLI) can be used to constrain the impedance estimate to a known model using linear programming methods (Cooke and Schneider, 1983), thereby combining a priori impedance information with the seismic data. Sparse-spike inversion seeks to construct an impedance structure having a minimum number of layers and estimates reflection coefficients as a discrete set of delta functions (Oldenburg et al., 1983). An inversion method that uses P-wave AVO variations was developed by Smith and Gidlow (1987). In their GEOSTACK method, CDP gathers are processed to yield the relative change in Vp and Vs. Interval velocity models and correctly processed P-wave reflectivity data are required. The resulting weighted stack section is then used to compute fluid factors or Poisson's ratio. Again, the GEOSTACK method is based on P-wave seismic data only.

These inversion methods all seek to estimate acoustic impedance from seismic data for P-waves. Vp can then be extracted from these estimates by making certain assumptions about subsurface density. Such assumptions may mean using an empirical relationship

between density and Vp, such as Gardner's relationship (Gardner et al., 1974), using density information from a well-log, or assuming that density changes occur more slowly in the subsurface than velocity.

Inversion of pure S-wave data (S-S) from an S-wave source/S-wave receiver pair to yield Vs is less common. Difficulties arising from cumbersome S-wave sources, low-frequency events and low signal to noise have meant that S-S seismic data are a rarity. An alternative to pure S-wave recording is the recording of mode converted or P-S data. P-S data are seismic data which use a conventional P-wave source and S-wave receivers at the surface. The reflected energy recorded by such a configuration is assumed to consist of the primary mode converted S-waves. Since the early 1980's, P-S seismic surveying has developed rapidly, and P-S data are increasingly available (Stewart, 1994). Because more P-S data are being acquired, and because Vs is an important indicator of rock lithology, it is desirable to have practical inversion methods for P-S data. One problem is that, in the case of zero-offset plane-wave inversion, P-S data have no energy. Like the P-P common mid-point (CMP) stack however, we can create a zero-offset trace by stacking the offset, NMO-corrected data which do have meaningful amplitudes.

Stewart (1990) proposed a method that incorporated P-wave and mode-converted S-wave seismic gathers in a joint P-P and P-S inversion. This method used the offset reflectivity equations of Aki and Richards (1980) to convert P-P and P-S seismic gathers to stacked traces which, instead of representing seismic reflectivity, represented normalized change in Vp and Vs respectively. Vestrum and Stewart (1993) used synthetic data to show that the joint P-P and P-S inversion was effective in predicting the relative S-wave and P-wave velocities.

The P-S inversion method presented here is an extension of the pre-stack seismic inversion methods of Smith and Gidlow (1987) and Vestrum and Stewart (1993).

1.2 Thesis Objective

The objective of this thesis is to compute estimates of Vs and Vp/Vs from inversion of P-S data. A general processing flow is described, and a P-S weighted stack and inversion sequence are presented. These algorithms are then evaluated in their ability to estimate Vs and Vp/Vs using synthetic and field data. It is hoped that this work will provide a new tool for seismic analysis and geologic interpretation, and will encourage enhanced exploration activity using multicomponent recording.

1.3 Data used

The P-S weighted stack and inversion sequence were evaluated using the following data sets.

1.3.1 Synthetic data

The synthetic P-S data of Sections 2.4.1 and 2.4.2 were generated using blocked models of Vp, Vs and density. These models were raytraced and Zoeppritz reflection coefficients were computed. The resulting P-S reflectivity gather was used to evaluate the performance of the P-S inversion.

The synthetic data of Sections 2.2.2, 3.2.1 and 4.3 were generated using the sonic and density logs of two wells 14-09-23-23 and 08-08-23-23, both sets of well logs were median filtered to remove spurious data. The first well, 14-09-23-23, was a dry well representing a regional position in the Blackfoot prospect. The second well, 08-08-23-23, was an oil producer. There was no S-wave sonic log available from 14-09-23-23 so one was synthesized from the P-wave sonic using a time varying Vp/Vs log derived from event correlation of stacked sections (Miller et al., 1995). To simplify comparison, the target zone velocities and densities of 08-08-23-23 were clipped out and spliced into a copy of 14-09-23-23, in effect replacing the non-productive zone of interest in 14-09-23-23 with a

productive zone from 08-08-23-23. Raytracing of these models provided P-P and P-S gathers, which represented a regional location and one a producing location. These data were then band-pass filtered to represent the pass bands of the three frequency ranges of the Broad-band Blackfoot 3C-2D.

1.3.2 Broad-band Blackfoot 3C-2D

The Blackfoot survey was acquired over the Blackfoot Field in July, 1995. The field is owned and operated by PanCanadian Petroleum Ltd. and is located 15 km east south east of Strathmore, Alberta. The survey was conducted to compare the performance of different 3-C geophone designs with special emphasis on low-frequency performance. The instrument settings, geometry and shot information, and geophone types are summarized in Tables 1.1, 1.2 and 1.3. There was also a line of 10 Hz geophones deployed in arrays and simultaneously acquired, but was not used in this thesis.

Instrument Description	
Instrument Type	ARAM-24
Pre-amp Gain	18 db
Tape Density	3480 bpi
No. Traces	816
Low-cut Filter	Out
Low-cut Slope	Out
Shooting System	Macha
No. of Channels	816
Record Length	6 Sec.
Sample Rate	1 ms
Notch Filter	Out
High Cut Filter	240 Hz
High Cut Slope	70 db/octave

Table 1.1. Field instruments used in the Blackfoot survey.

Geometry	Description
Line Length	4 km
Shot Spacing	20 m (1/2 stn)
Shot Depth	18 m
Charge Size	6 kg
Receiver spacing	20 m
Line Azimuth	NW

Table 1.2. Blackfoot survey acquisition geometry.

Geophones	
Natural Freq. (Hz)	**Deployment**
2 Hz Mark Products L-4A (vertical)	Buried 40 cm
2 Hz Mark Products L-4A (radial)	Buried 40 cm
4.5 Hz Mark Products L-28 3C	Deep plant 30 cm
10 Hz Litton 3-C LRS-1033 3C	Deep plant 30 cm

Table 1.3. Geophones used and deployment for the Blackfoot survey.

1.4 Hardware and software used

The work presented in Chapters 2, 3 and 4 was created on a SUN MICROSYSTEMS network operated by The CREWES Project of the Department of Geology and Geophysics at the University of Calgary. The P-S weighted stack algorithm, a recursive inversion, and a generalized linear inversion were coded in FORTRAN and ported to the PROMAX processing system. Synthetic data were generated using SYNTH, a seismic modeling package developed by Dr. Ed Krebes and Dr. Don Lawton of the University of Calgary, and later ported to run as a MATLAB function by Dr. Gary Margrave also of the University of Calgary. The log data of Chapter 3 were conditioned and displayed using MATLAB and various MATLAB functions written by Dr. Gary Margrave. The Broad-band Blackfoot 3C-2D data were processed to prestack gathers by

Dr. Mark Harrison formerly of Sensor Geophysical Ltd.. The Blackfoot data were further processed prior to inversion using the PROMAX processing system. All images in this thesis were screen captured using XV. Image processing was done on POWER MACINTOSH computers using FETCH, PHOTOSHOP and CANVAS software. Word processing and thesis assembly was done on POWER MACINTOSH computers using MICROSOFT WORD.

Chapter 2 DIRECT INVERSION OF P-S DATA

2.1 Introduction

Two methods to estimate S-wave interval velocity using P-S seismic data are presented. The first is similar to the Dix (1955) interval velocity method. It computes S-wave interval velocity based on normal moveout (NMO) velocity analysis as used in standard seismic processing. The NMO velocity is picked from P-S seismic data using standard semblance picking algorithms, then inverted directly to yield an S-wave interval velocity estimate. The second P-S inversion method is a stacking procedure followed by inversion. P-S data, which have been sorted into common conversion point (CCP) gathers are stacked using a weighted stack derived from a model of the subsurface. The model used is a function of P- and S-wave velocity and density estimates. The resulting stack can be thought of as a normalized change in S-wave velocity ($\Delta\beta/\beta$) section. Inversion of the $\Delta\beta/\beta$ section proceeds in much the same way as for P-P inversion.

2.2 Inversion of P-S stacking velocities

Stewart and Ferguson (1996) outline an inversion procedure for P-S data. They note that estimation of the P-wave interval velocity from the P-wave stacking velocity is a common procedure in processing P-P data. It is assumed that the stacking velocity, calculated from the coherency of hyperbolic events across a gather, is equal to the RMS velocity. From the RMS velocity, a P-wave interval velocity can be computed using the Dix equation (Dix, 1955). The interval velocity can be used in further processes such as migration and inversion. The S-wave interval velocity is also of interest for rock property analysis and three-component seismic processing. Similar to conventional Dix velocity analysis for P-P data, a method can be developed for estimating shear velocity from converted-wave stacking velocities.

The converted-wave stacking velocity can be found using a variety of methods, including standard velocity analysis (hyperbolic scanning). Based on this stacking velocity, again assuming it is equal to the RMS velocity, the S-wave interval velocity is computed. This is done using the standard Dix interval velocity calculation as follows.

2.2.1 Dix interval velocities

In a layered medium (with layers i=1, N) having P-wave and S-wave interval velocities (α_i, β_i) each layer has a set of one-way transit times: t_i^p for one-way P-waves and t_i^s for one-way S-waves (Figure 2.1).

The RMS velocity for P-S data is given by Tessmer and Behle (1988) as

$$V_k^2 = \frac{\sum_{i=1}^{k} \alpha_i \beta_i t_i}{T_k}, \qquad 2.1$$

where $t_i = t_i^p + t_i^s$ 2.2

and $T_k = \sum_{i=1}^{k} t_i$. 2.3

Using a standard procedure for computing the Dix interval velocity (e.g., Sheriff and Geldart, 1983), we have:

$$V_k^2 T_k - V_j^2 T_j = \sum_{i=1}^{k} \alpha_i \beta_i t_i - \sum_{i=1}^{j} \alpha_i \beta_i t_i . \qquad 2.4$$

If k = j + 1, then

$$V_{j+1}^2 T_{j+1} - V_j^2 T_j = \alpha_{j+1} \beta_{j+1} \left(T_{j+1} - T_j \right), \qquad 2.5$$

and

$$\alpha_{j+1} \beta_{j+1} = \frac{V_{j+1}^2 T_{j+1} - V_j^2 T_j}{T_{j+1} - T_j}, \text{ and} \qquad 2.6$$

$$\beta_{j+1} = \frac{V_{j+1}^2 T_{j+1} - V_j^2 T_j}{\alpha_{j+1}(T_{j+1} - T_j)} . \qquad 2.7$$

Thus, by knowing the converted-wave traveltimes (Tj+1, Tj) bounding an interval, the P-S stacking velocity (Vj, Vj+1), and the P-wave interval velocity (αj+1), direct computation of the S-wave interval velocity (βj+1) is possible (Stewart and Ferguson, 1995). Computation of βj+1 in this manner requires correlation of P-P and P-S events to find the associated P-wave velocity (αj+1). However, from the P-S data alone, a general relationship between α and β could be assumed to find the interval shear velocity.

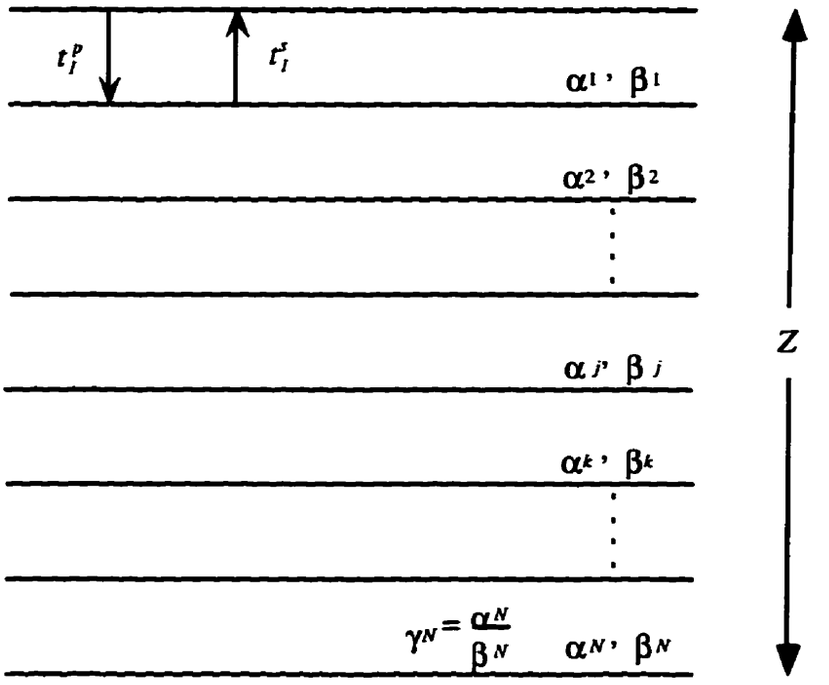

Figure 2.1. Plane-layer elastic medium with N layers.

2.2.2 Synthetic example

An experiment was conducted to test the new Dix interval velocity equation. P-sonic and density logs were obtained from the Blackfoot pool in Southern Alberta (Figure 2.2). Some of the regional markers annotated on Figure 2.2 are: BR - Belly River, MR - Milk River, 2WS - 2nd White Speckled Shale, Viking, Coal 1, Mississippian. An S-wave

velocity log was derived from the P-sonic using a depth-varying γ value (Miller et al., 1995), where γ is the ratio of P-wave velocity to S-wave velocity (Figure 2.3). The P-wave, S-wave and density logs were used to generate a synthetic P-S gather using the SYNTH algorithm (Lawton and Howell, 1992). The resulting gather is shown in Figure 2.4. A stacking velocity, picked according to maximum semblance across a hyperbolic moveout, was obtained from the resultant P-S gather (Figure 2.5).

During velocity analysis a number of stretch mutes were tested and it was found, by allowing only a small amount of NMO stretch, the data were best flattened in the near-offset. Thus, a rather severe mute was used, corresponding to 10% NMO stretch. Note that the correction of the trace gather in Figure 2.5 is good to offset / depth values of about 1.0, beyond which, the gathers are over-corrected. This is a result of the inadequacy of the hyperbolic moveout correction to model P-S reflections, especially for offset / depth values greater than 1.0. A shifted hyperbolic analysis has been shown to be more accurate (Slotboom et al., 1990) and should be implemented in the future.

To avoid having to manually correlate the P-P data to the P-S data it was assumed that $\alpha = \gamma\beta$, were γ is a scalar. This allows a direct, but approximate, calculation of β from P-S data alone. Thus, equation 2.7 becomes,

$$\beta_{j+1} = \left(\frac{V_{j+1}^2 T_{j+1} - V_j^2 T_j}{\gamma (T_{j+1} - T_j)} \right)^{\frac{1}{2}}, \qquad 2.8$$

where $\gamma = \alpha/\beta$.

Note that the effect of γ is reduced in equation 2.8 by the square root factor. This will decrease the dependence of β on the γ value chosen by 1/2. Equation 2.8 was used to convert the stacking velocity picked in Figure 2.5 to interval velocity β. The estimated β for the synthetic data was then compared to the true S-wave velocity (Figure 2.6). A good correlation was found, in a blocky sense, between the well log and the estimate. With γ =

2.3, and using only small offset data, the general log character was recovered. If larger offsets had been used during velocity analysis, the stacking velocity would have been biased to larger values to compensate for the non-hyperbolic moveout. This would have caused the corresponding interval velocities to be too large.

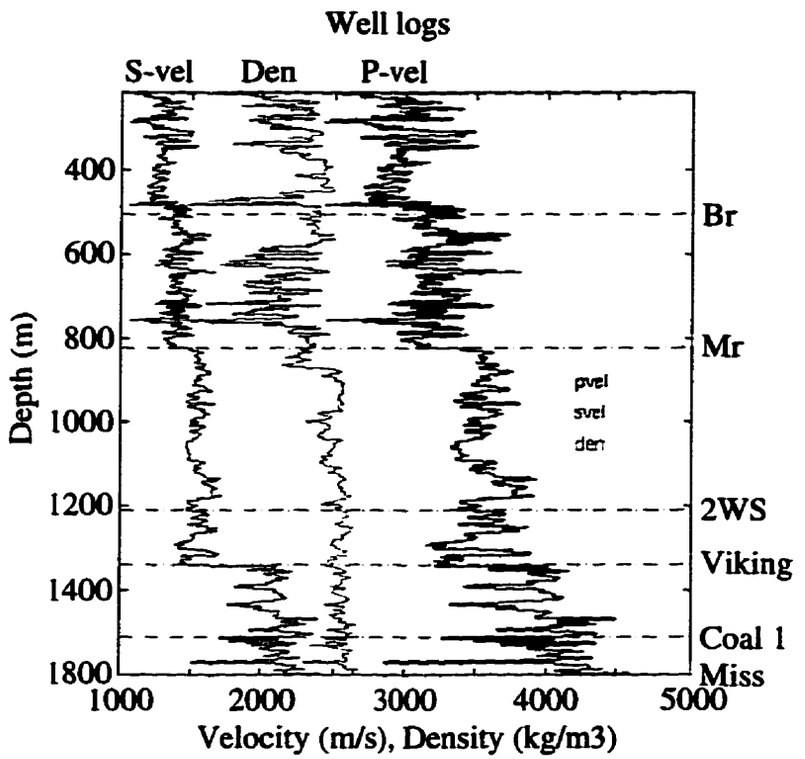

Figure 2.2. Logs used to generate the P-S gather of Figure 2.4. The S-wave velocity was derived from the P-wave velocity using a depth-varying γ (Figure 2.3). The γ estimate was calculated using seismic event timing at the well location (Miller et al., 1995).

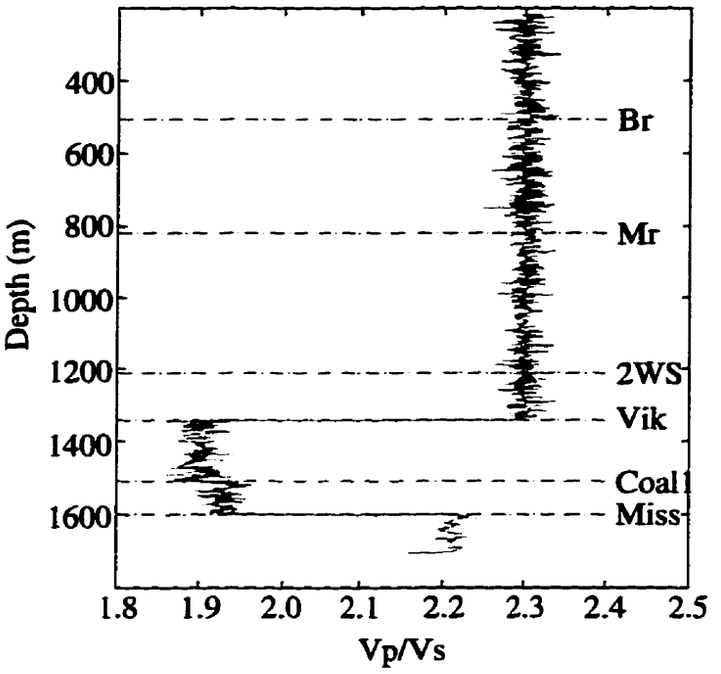

Figure 2.3. Depth-varying γ (Vp/Vs) used to generate the S-wave log in Figure 2.2 (Miller et al., 1995).

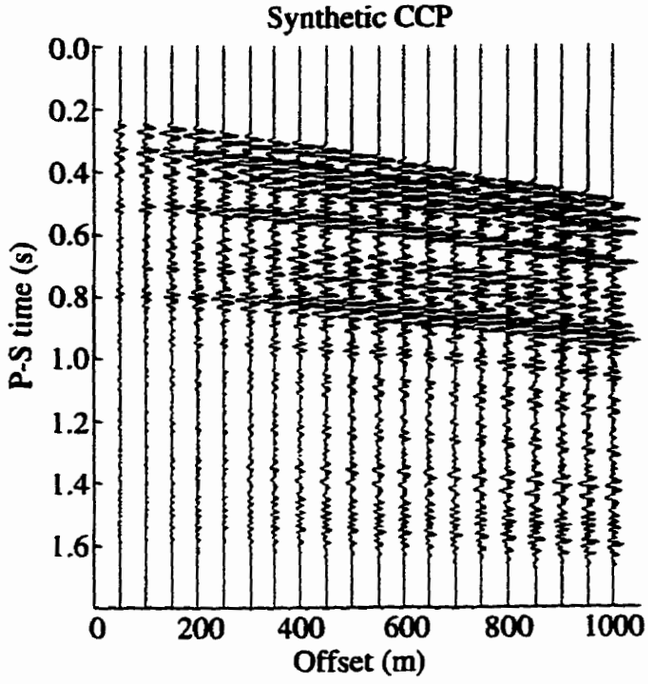

Figure 2.4. Converted-wave gather. Offsets 50 - 1000 m are shown here. The range of offsets used in velocity analysis (Figure 5) extended from 50 m to 2500m.

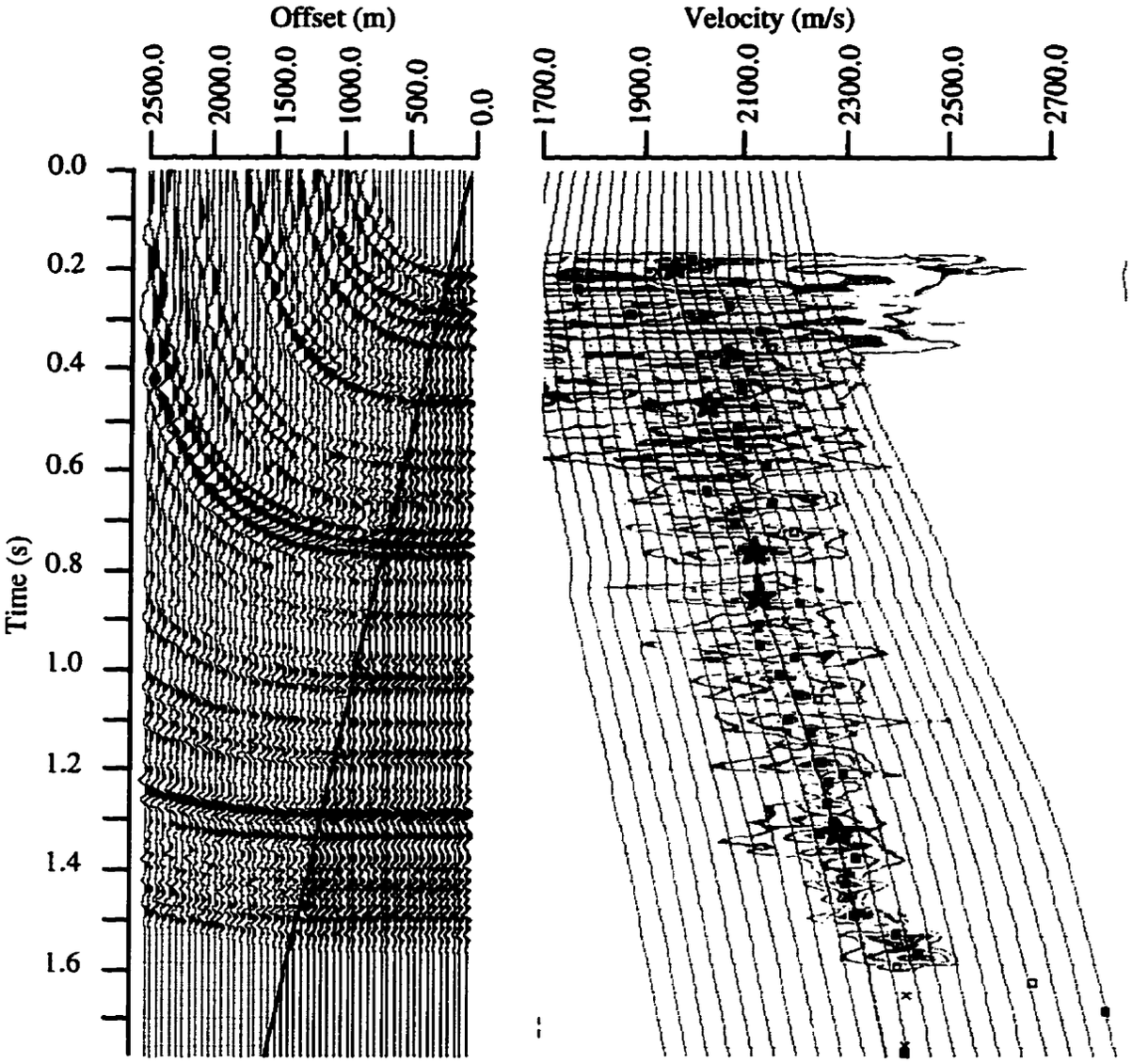

Figure 2.5. Semblance velocity analysis of the P-S gather of Figure 2.4. The gather is shown with the stacking velocity applied (left). The stacking function is marked by stars (right). Note the offset mute required to obtain event flattening (stretch mute = 10%) at near offsets. AGC has been applied prior to coherency analysis to enhance the amplitude of the near offsets to further improve semblance.

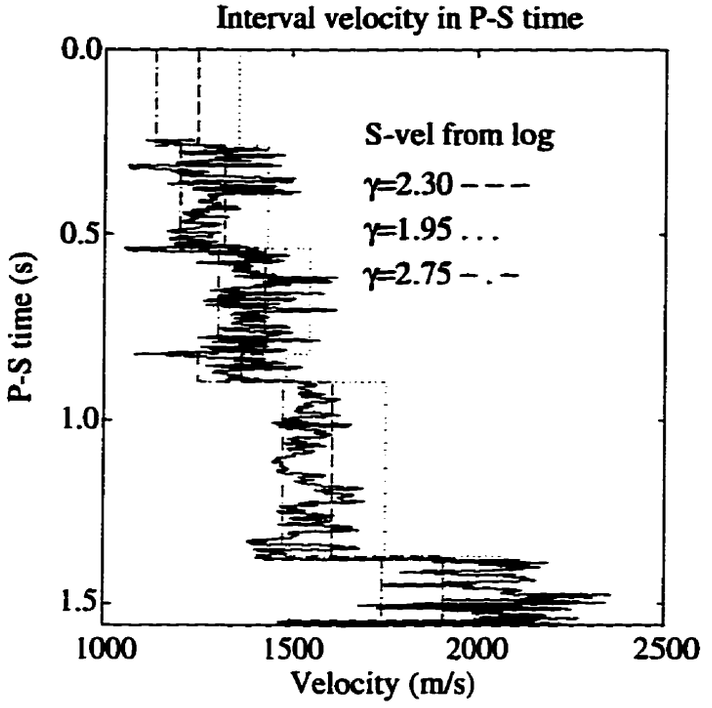

Figure 2.6. Comparison of Dix estimates from the velocity analysis of Figure 2.5 to the S-wave well log. The effect of changing γ (from 1.95 to 2.75) is shown in the plot.

2.2.3 Blackfoot field data

A comprehensive set of seismic experiments was conducted over the Blackfoot oil field in Southern Alberta (Stewart et al., 1996). For details on acquisition parameters and target lithologies please refer to Section 1.3.2. A stacking velocity from the P-S component of the 2D line was acquired (Figure 2.7) and used to compute an S-wave interval velocity. The location at which the stacking velocity was acquired, shotpoint 155, corresponded to the same location as the well in Figure 2.2. Note, the stacking velocity was picked independently by a contractor processing the data using offsets exceeding offset depth values of 1.0. Thus we expect it to give higher values than what a shifted-hyperbola based analysis would find. The stacking velocity was used to calculate an S-wave interval velocity by assuming that γ = 3.25. Figure 2.8 shows the resultant interval velocity

compared to the S-wave log which tied the line. The interval velocity estimate was found to reproduce much of the character of the S-wave log (Figure 2.8).

CCP 100	
Time (ms)	Vel (m/s)
72	1323
170	1374
227	1400
266	1467
348	1630
411	1722
481	1838
578	1916
681	1996
811	2053
896	2088
993	2125
1113	2194
1198	2282
1274	2330
1371	2395
1456	2422
1523	2451
1602	2451

Figure 2.7. Stacking velocity from the Blackfoot 3C-2D.

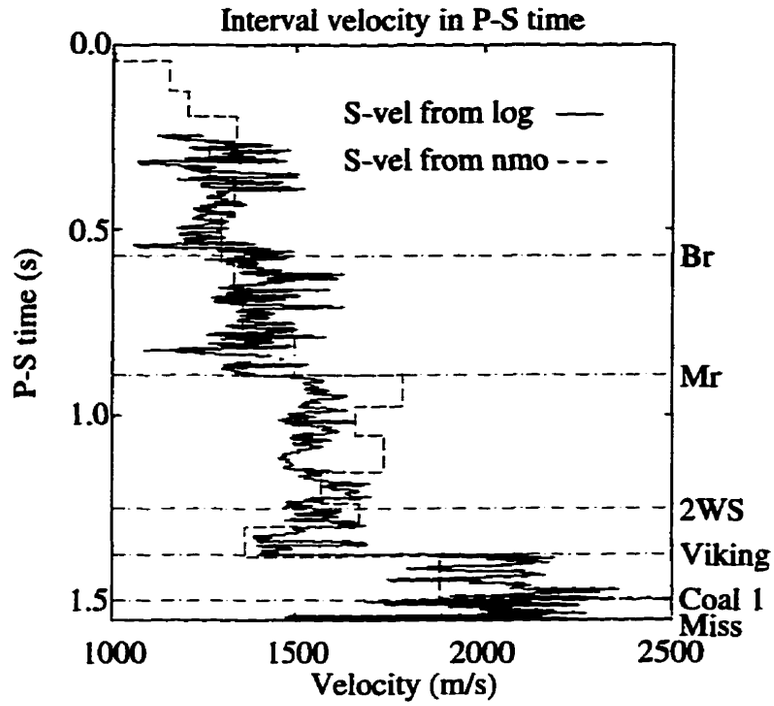

Figure 2.8. Comparison of the Dix estimate to an S-wave log from the area. The γ estimate is high ($\gamma = 3.25$) due to picking the stacking velocities (a) based on large-offset NMO semblance.

2.3 Inversion of P-S gathers

An inversion method was proposed by Stewart (1990) that incorporated P-P and P-S seismic gathers in a joint P-P and P-S inversion. In this method, P-P and P-S seismic gathers were converted to stacked traces which, instead of representing seismic reflectivity, represented normalized change in P-wave velocity (α) and S-wave velocity (β) respectively. This stacking procedure was based on the P-P and P-S reflectivity approximations of Aki and Richards (1980). The resulting sections could then be converted to interval velocity estimates using standard inversion routines (Stewart, 1990).

A first step toward a practical implementation of the above inversion scheme is presented here. This first step involved a simplification which cast the inversion, not as a joint inversion, but, as an inversion of P-S data alone. This approach achieved two results.

First, the potentially awkward step of correlating P-P and P-S gathers in both time and offset was reduced to a simple correlation in time. Second, a method by which standard inversion methods can be used to yield S-wave interval velocity could be developed to complement standard P-P inversion.

P-S inversion requires four sources of data, and two processing steps. The required data are: background (macro or sparse) P- and S-wave velocity models (α and β), a density model (ρ) and seismic traces gathered into asymptotically-approximated common-conversion points (CCPs). The α and β models are interval velocity estimates correlated to P-S time. The ρ model must also be correlated to P-S time. The P-S gather should be scaled to represent true reflectivity, and be as broad-band and noise-free as possible. NMO correction should be applied.

The first processing step takes the above input and computes P-S weighted stack trace for each CCP gather. In the second processing step, each trace of the weighted-stack section is scaled and inverted using a standard inversion technique.

The inversion flow is summarized in Figure 2.9.

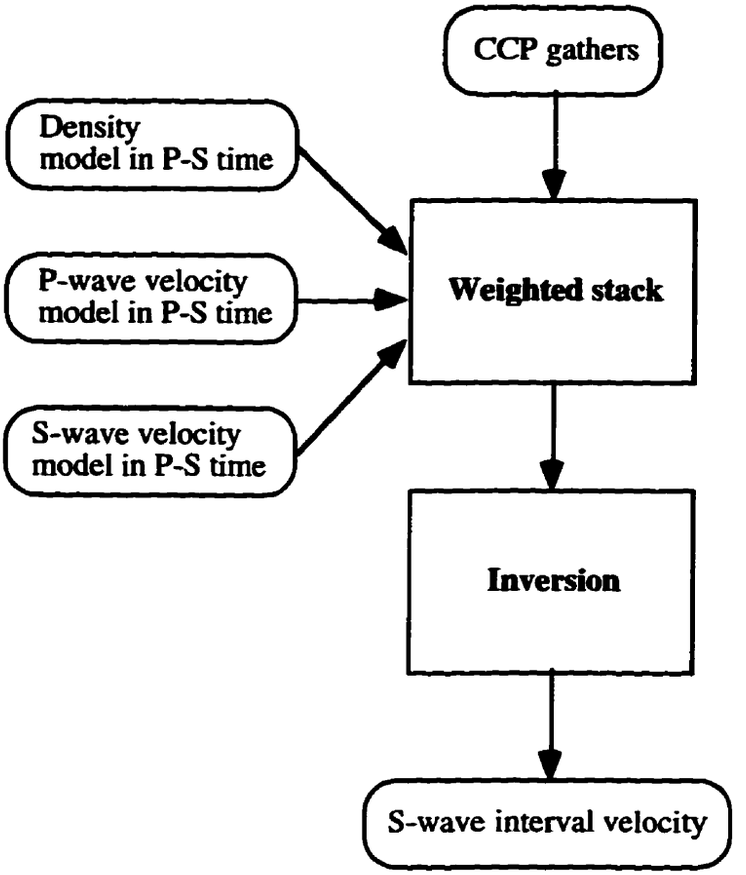

Figure 2.9 . Flow-chart for P-S inversion.

2.3.1 P-S weighted stack

Estimation of S-wave velocity from P-S seismic data requires a relationship between S-wave velocity (β) and P-S reflectivity. A simple relationship is the ratio of velocity change across an interface to the average velocity across the interface (Aki and Richards, 1980) or *P-S weighted stack* ($\Delta\beta/\beta$). This value can be estimated using the following equations. At each conversion point,

$$R^{ps} = 4c\frac{\Delta\rho}{\rho} + d\frac{\Delta\beta}{\beta}, \qquad 2.9$$

where,

$$c = -\frac{\alpha \tan\phi}{8\beta}\left(1 - \frac{2\beta^2}{\alpha^2}\sin^2\theta + \frac{2\beta}{\alpha}\cos\theta\cos\phi\right) \qquad 2.10$$

and,

$$d = \frac{\alpha \tan\phi}{2\beta}\left(\frac{4\beta^2}{\alpha^2}\sin^2\theta - \frac{4\beta}{\alpha}\cos\theta\cos\phi\right) \qquad 2.11$$

R^{PS} is the P-S reflection coefficient as a function of incidence angle. The angles θ and ϕ are calculated as averages across the interface. The values $\Delta\alpha/\alpha$, $\Delta\beta/\beta$, and $\Delta\rho/\rho$ are the relative changes in P-wave velocity S-wave velocity, and density (Aki and Richards, 1980).

Equation (2.9) can be cast as a least-squares problem and solved for $\Delta\beta/\beta$ (Stewart, 1990). The sum of the squares of the error at a single interface is,

$$\varepsilon = \sum_{i=1}^{n}\left(R_i - R_i^{ps}\right)^2 \qquad 2.12$$

where R and R^{PS} are the recorded and modeled P-S reflectivity respectively. Summation is over trace offset in the seismic gather. Expansion of (2.12),

$$\varepsilon = \sum_{i=1}^{n}\left(R_i^{ps}\right)^2 - 8\frac{\Delta\rho}{\rho}\sum_{i=1}^{n}R_i^{ps}c_i - 2\frac{\Delta\beta}{\beta}\sum_{i=1}^{n}R_i^{ps}d_i + 64\left(\frac{\Delta\rho}{\rho}\right)^2\sum_{i=1}^{n}c_i^2 + \left(\frac{\Delta\beta}{\beta}\right)^2\sum_{i=1}^{n}d_i^2 + 8\frac{\Delta\rho}{\rho}\frac{\Delta\beta}{\beta}\sum_{i=1}^{n}c_i d_i \qquad 2.13$$

can then be differentiated with respect to $\Delta\beta/\beta$ to give a value of $\Delta\beta/\beta$ that minimizes the error function ε,

$$0 = \frac{\partial\varepsilon}{\partial\frac{\Delta\beta}{\beta}} = -2\sum_{i=1}^{n}R_i^{ps}d_i + 2\frac{\Delta\beta}{\beta}\sum_{i=1}^{n}d_i^2 + 8\frac{\Delta\rho}{\rho}\sum_{i=1}^{n}c_i d_i \qquad 2.14$$

Rearranging (2.14) to solve for $\Delta\beta/\beta$ yields,

$$\frac{\Delta\beta}{\beta} = \frac{\sum_{i=1}^{n} R_i^{ps} d_i - 4\frac{\Delta\rho}{\rho}\sum_{i=1}^{n} c_i d_i}{\sum_{i=1}^{n} d_i^2} \qquad 2.15$$

The angles θ and ϕ (required by coefficients 'c' and 'd') can be approximated using RMS velocities and Snell's law (Dix, 1955; Zheng and Stewart, 1991; Slawinski et al., 1994). The RMS velocities and $\Delta\alpha/\alpha$ can both be derived from the interval velocity models.

Often, reliable density information for an entire seismic traverse is not available, but α, from P-P seismic inversion or derived from stacking velocities, is available. One may then choose to assume an α to ρ relationship such as Gardner's relationship (Gardner et al., 1974) where,

$$\rho = \kappa\alpha^{\lambda} \qquad 2.16$$

Under this assumption equation (2.15) becomes:

$$\frac{\Delta\beta}{\beta} = \frac{\sum_{i=1}^{n} R_i^{ps} d_i - 4\lambda\frac{\Delta\alpha}{\alpha}\sum_{i=1}^{n} c_i d_i}{\sum_{i=1}^{n} d_i^2} \qquad 2.17$$

using:

$$\frac{\Delta\rho}{\rho} = \lambda\frac{\Delta\alpha}{\alpha} \qquad 2.18$$

Having established relationships between P-S reflection data and $\Delta\beta/\beta$ inversion can be used to convert $\Delta\beta/\beta$ to an estimate of interval velocity β.

2.3.2 Recursive inversion

The P-S weighted stack ($\Delta\beta/\beta$) can be inverted to give an estimate of S-wave velocity (β). The simplest inversion method is to directly compute β from $\Delta\beta/\beta$. This procedure is often referred to as *recursive inversion* because the velocity estimate is computed sequentially, from the top down.

The value $\Delta\beta/\beta$ as being the difference in β divided by the average β across the boundary between two differing rock materials thus,

$$\frac{\Delta\beta}{\beta_j} = 2\frac{(\beta_{j+1} - \beta_j)}{(\beta_{j+1} + \beta_j)} \qquad 2.19$$

solving for $\beta j+1$,

$$\beta_{j+1} = \beta_j \left(\frac{1 + \frac{1}{2}\frac{\Delta\beta}{\beta_j}}{1 - \frac{1}{2}\frac{\Delta\beta}{\beta_j}} \right) \qquad 2.20$$

expanding equation 2.20 as a function of $\beta 1$,

$$\beta_{j+1} = \beta_1 \left(\frac{1 + \frac{1}{2}\frac{\Delta\beta}{\beta_1}}{1 - \frac{1}{2}\frac{\Delta\beta}{\beta_1}} \right) \left(\frac{1 + \frac{1}{2}\frac{\Delta\beta}{\beta_2}}{1 - \frac{1}{2}\frac{\Delta\beta}{\beta_2}} \right) \cdots \left(\frac{1 + \frac{1}{2}\frac{\Delta\beta}{\beta_j}}{1 - \frac{1}{2}\frac{\Delta\beta}{\beta_j}} \right) \qquad 2.21$$

and simplifying the notation,

$$\beta_{j+1} = \beta_1 \prod_{k=1}^{j} \left(\frac{1 + \frac{1}{2}\frac{\Delta\beta}{\beta_k}}{1 - \frac{1}{2}\frac{\Delta\beta}{\beta_k}} \right) . \qquad 2.22$$

Thus, given an estimate of β at $t = t_1$, $\Delta\beta/\beta$ can be directly inverted to provide a value of β for every $t = t_j, j > 1$. Inversion by this method assumes that the reflection series is broad-band and noise free.

2.4 P-S inversion testing

The accuracy of velocity estimates from inversion will be compromised by the realities of seismic acquisition. Seismic data contains noise, is band-limited, may contain phase errors, and is often acquired in areas where there is ambiguity in the background velocity.

Two experiments based on synthetic seismic data were used to evaluate the performance of the P-S inversion. A single interface model was first used to evaluate the effects of errors in user defined background velocity values. Then, a five-layer model was constructed to evaluate the effects of frequency-band limitations and phase error.

2.4.1 Single interface model

The P-S weighted stack of Section 2.3.1 requires a number of user inputs. They are a background S-wave velocity (β), P-wave velocity (α) and a density (ρ).

These inputs can be obtained from a variety of different sources and may contain many sources of error. It is therefore important to understand the effects that errors in these values have on any resulting estimates of β. A model representing the contact of two flat layers of rock material was constructed to test the performance of the P-S weighted stack. The model is shown in Figure 2.10.

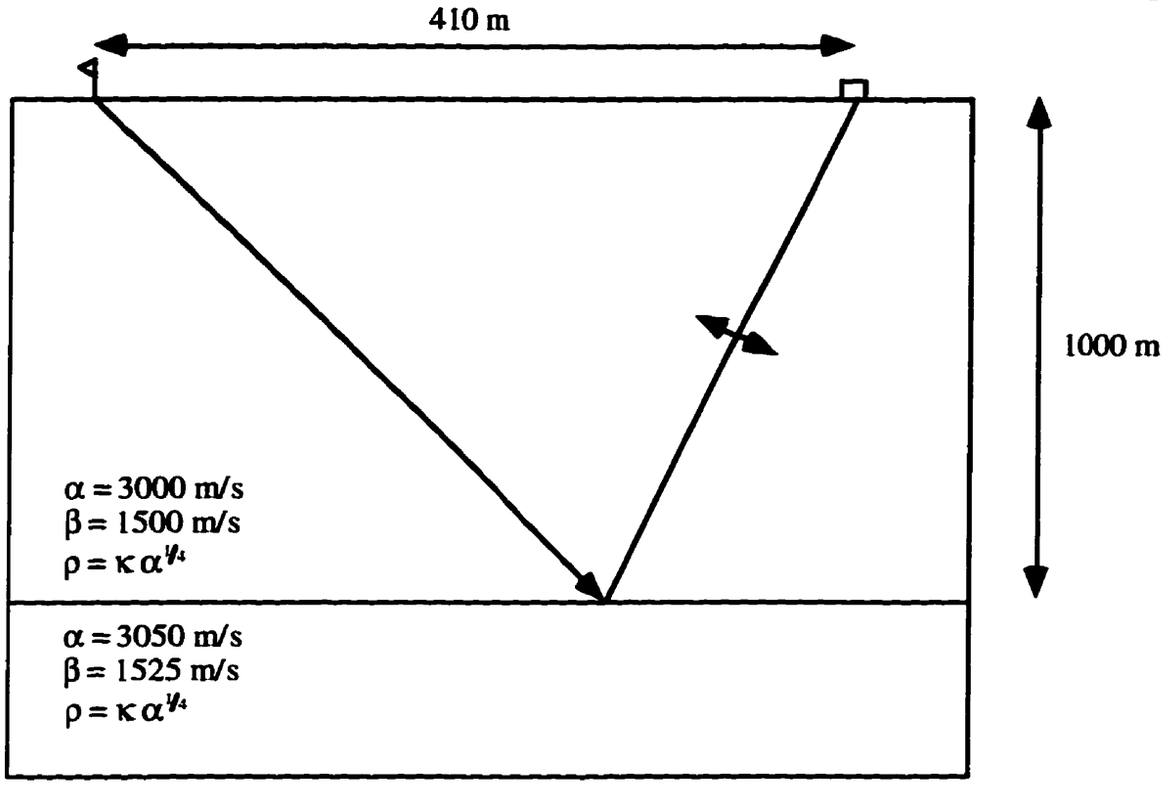

Figure 2.10. Single interface model.

The values of velocity and density in Figure 2.10 were chosen such that they represented small changes in rock properties as required by equation 2.9 (Aki and Richards, 1980). For a perfectly parameterised inversion (i.e. using the correct background model), a change in β, across an interface, of + 25 m/s resulted in a very small error < 0.0001 % as shown in Figure 2.11. A Gardner relationship was assumed in both the computation of the reflection value and the resulting inversions.

In this Section, errors are given in percentages, and are computed such that the error ε in the estimated β is,

$$\varepsilon = 100\,\frac{\beta_T - \beta_E}{\beta_T} \qquad 2.23$$

where,

β_T = true S–velocity

β_E = estimated S–velocity

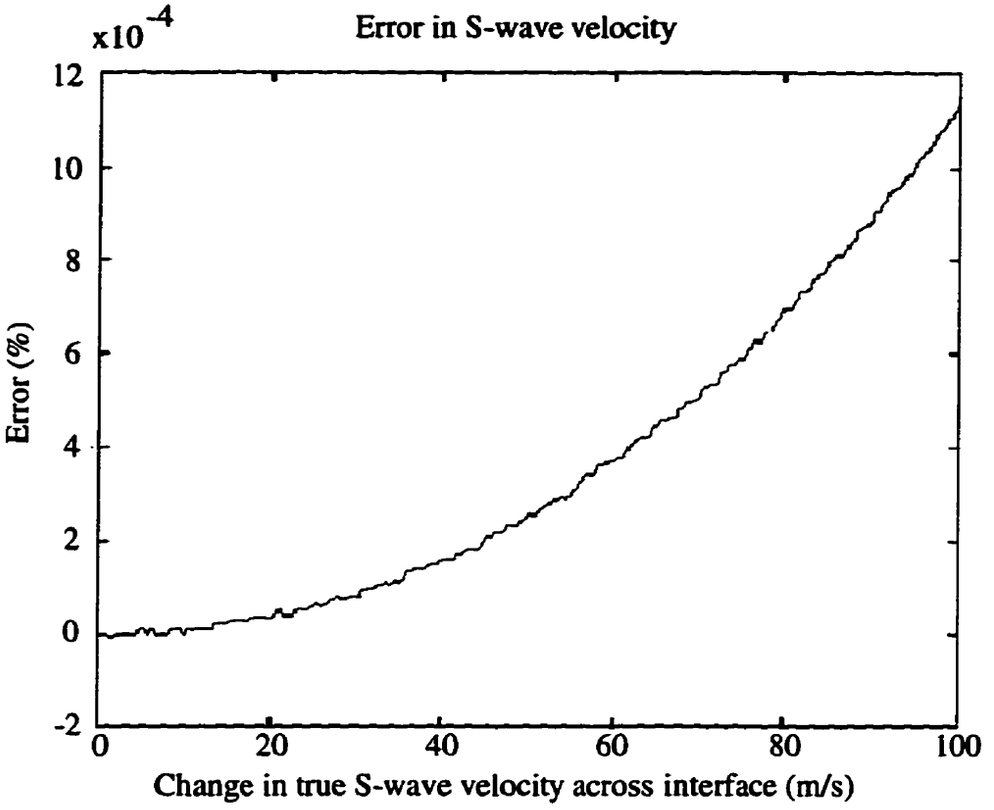

Figure 2.11. Error due to the change in β across z = 1000m in Figure 2.10. As the value of Δβ increases, the error increases exponentially. Error is small for small Δβ.

The single reflection amplitude computed for the geometry of Figure 2.10 was converted to Δβ/β using equation 2.17 and a number of different background α and β values. The errors in these background velocities ranged from +/- 762.5 m/s for β and +/- 1525.0 m/s for α, or +/- 50 % for each. The resulting Δβ/β stacks were then inverted using the recursive method of equation 2.22. The correct value for β_1 (= 1500 m/s) was used to initiate each recursive inversion. Figure 2.12 plots the percent error in the resulting β estimates as a function of percent error in background α and β. Note that, with zero reflection error and no band-limiting, and using the correct β_1 to initiate the recursion, the β estimates were quite robust. For example, a 50 % error in background α was found to

result in a 20 % error in the estimated β. As Figure 2.12 shows, the error in estimated β is small when error is a function of background β only. The slope of the error surface in Figure 2.12 is much steeper in the direction of the P-wave axis than the S-wave, indicating a greater dependence on accuracy in P-wave background than S-wave (or ρ if equation 2.15 is used).

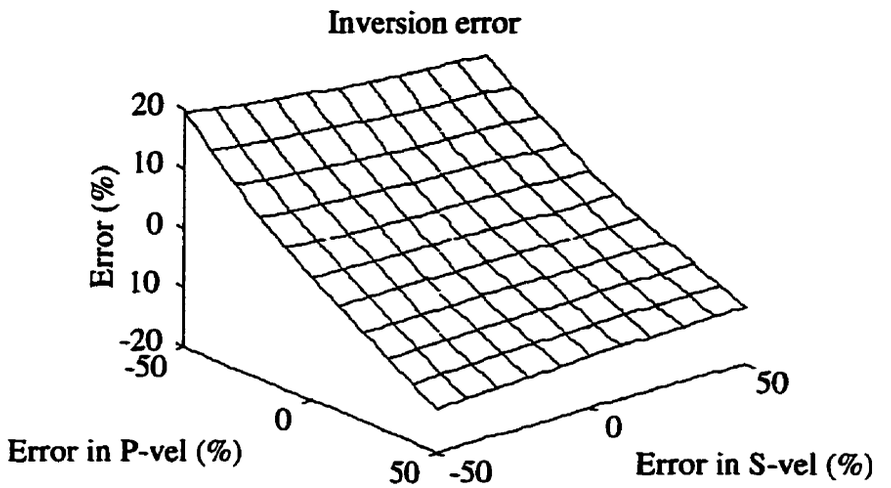

Figure 2.12. Error in estimated β due to error in background α and β. Note largest error due to α (or ρ if an α - ρ relationship is not assumed).

2.4.2 Blocked log model

To test the performance of the P-S inversion in the presence of more realistic data (with band-limitation and distorted-phase data), a model based on blocked sonic logs was constructed (Figure 2.13a). A synthetic CCP gather was generated for the model of Figure 2.13a using Zoeppritz equations, and again assuming a Gardner relationship between α and ρ. The ratio between the α and β logs was time-variant. The resulting seismic gather is shown in Figure 2.13b and a stack of this gather is given in Figure 2.13c.

To establish a 'best' β estimate the CCP gather of Figure 2.13a was converted to a $\Delta\beta/\beta$ trace using equation 2.17 and inverted using equation 2.22. This was done with exact parameters to establish a best β estimate. The stacked trace of Figure 2.13c was inverted

using equation 2.22 to compare to the best estimate. Figure 2.14 shows that there is good correlation between the P-S inversion β and the log until the velocity jump at 1.13 seconds. At this velocity jump, the S-velocity is overestimated by 250 m/s. The large error at 1.13 seconds is mainly due to violation of the small changes in rock properties assumption. The smaller errors at the remaining interfaces are mainly due to the approximation of the incident angles required by equations 2.10 and 2.11. These smaller errors could be reduced by using an iterative ray-tracing algorithm to provide better estimates of ray parameters in time. Simply inverting the unweighted stacked trace results in much larger error.

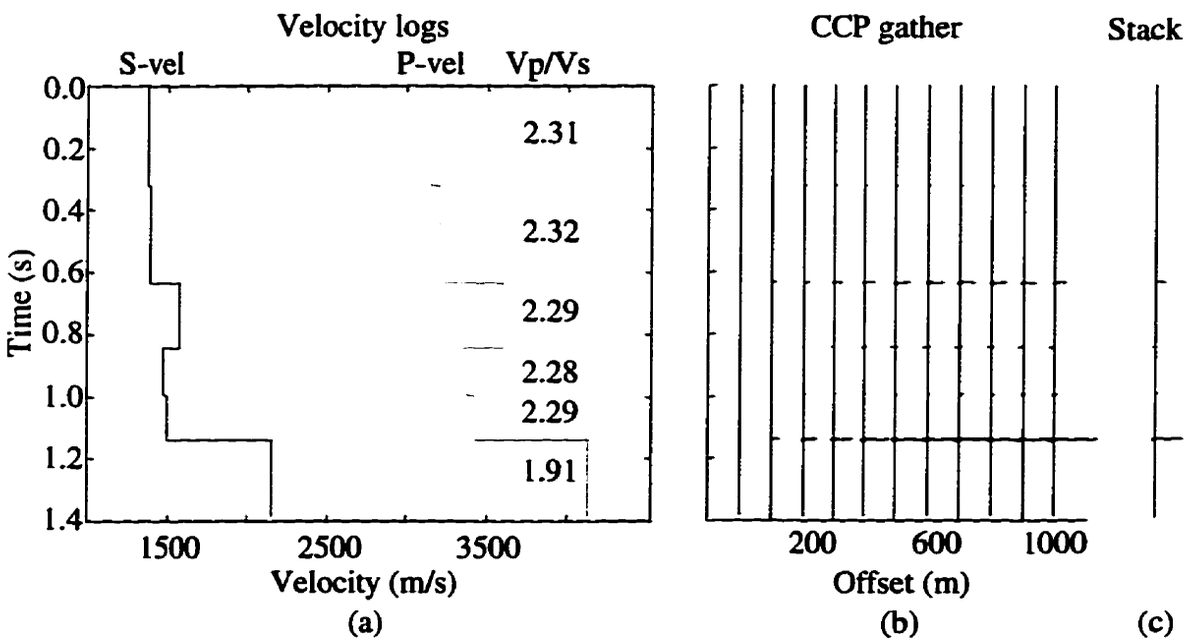

Figure 2.13. Blocked-log model. The α and β logs of plot (a) were used to generate a synthetic P-S gather plot (b) for P-S inversion. The trace (c) is a conventional stack of (b).

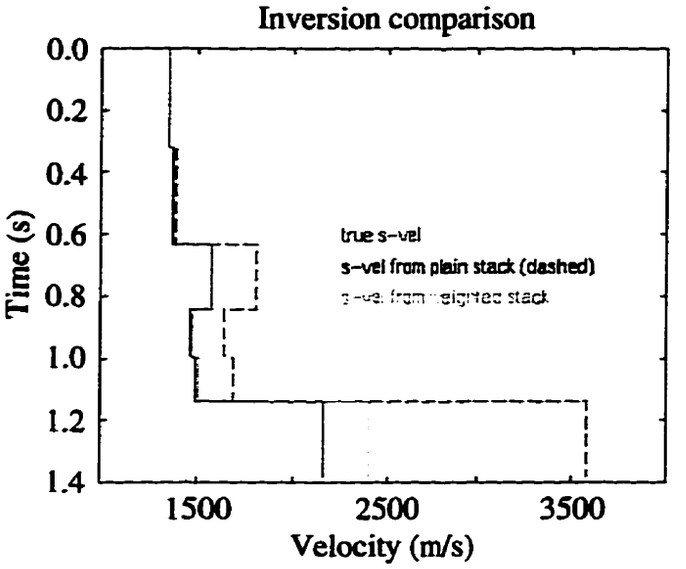

Figure 2.14. Comparison of inversion derived β to true β. The dashed line is β from the inversion of the trace of Figure 2.13c. The darkest line is the true β and the lightest line is the P-S inversion derived β. Note the good correlation between the true β and the P-S inversion estimate compared to the inversion of the stacked trace.

2.4.3 Error due to limited frequency-band

The CCP gather of Figure 2.13b was converted to a $\Delta\beta/\beta$ trace and then filtered with a number of high and low-cut filters. The inversion accuracy was found to be quite insensitive to the applied high-cut, until about 50 Hz where the error began to increase. Figure 2.15a is an example of the $\Delta\beta/\beta$ trace that has been high-cut filtered at 50 Hz and Figure 2.15b is the resulting velocity estimate. Error is pronounced at velocity boundaries, an effect that will impact high frequency velocity variations.

The data were then filtered with different low-cut filters as shown in Figure 2.16. Error increased dramatically from 0 - 10 Hz where it leveled off at a maximum RMS error of ~ 680 m/s.

Figure 2.17a is an example of the trace with a 5 Hz low-cut, and Figure 2.17b is the resulting velocity estimate. Note the sharpness of the interfaces due to high frequency

content (< 150 Hz), and also note the severe curvature in velocity where the estimate should be a constant value.

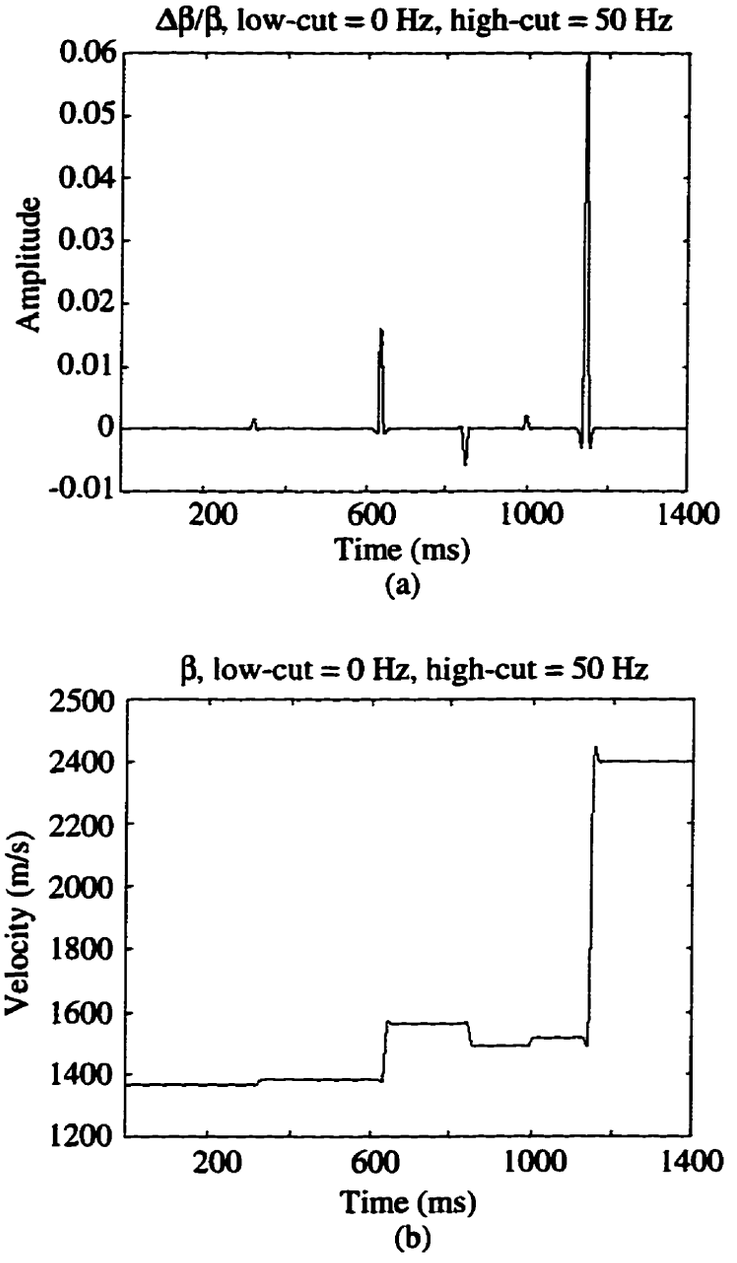

Figure 2.15. Example of inversion of high-cut filtered P-S gather. Plot (a) is the P-S gather of Figure 2.13b filtered with a 50 Hz high-cut and converted to a Δβ/β trace. Plot (b) shows the P-S inversion output is a stable estimate of the true β.

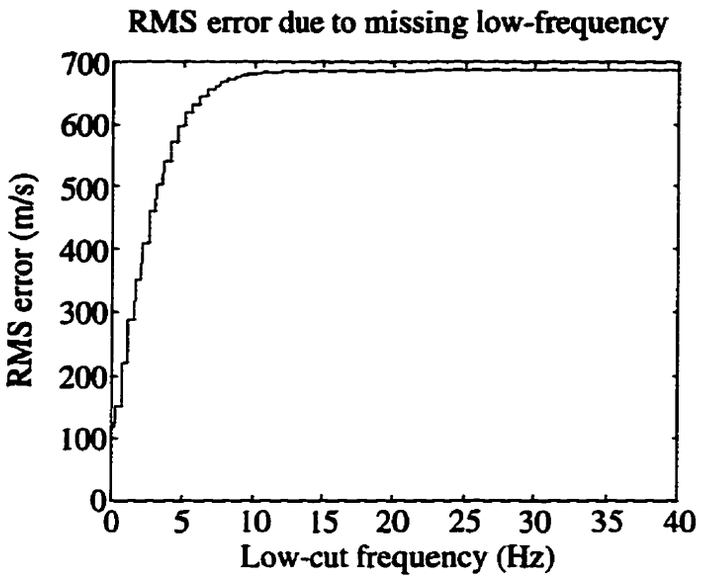

Figure 2.16. RMS error due to low-cut filter. After 12.5 Hz the RMS error has reached a maximum.

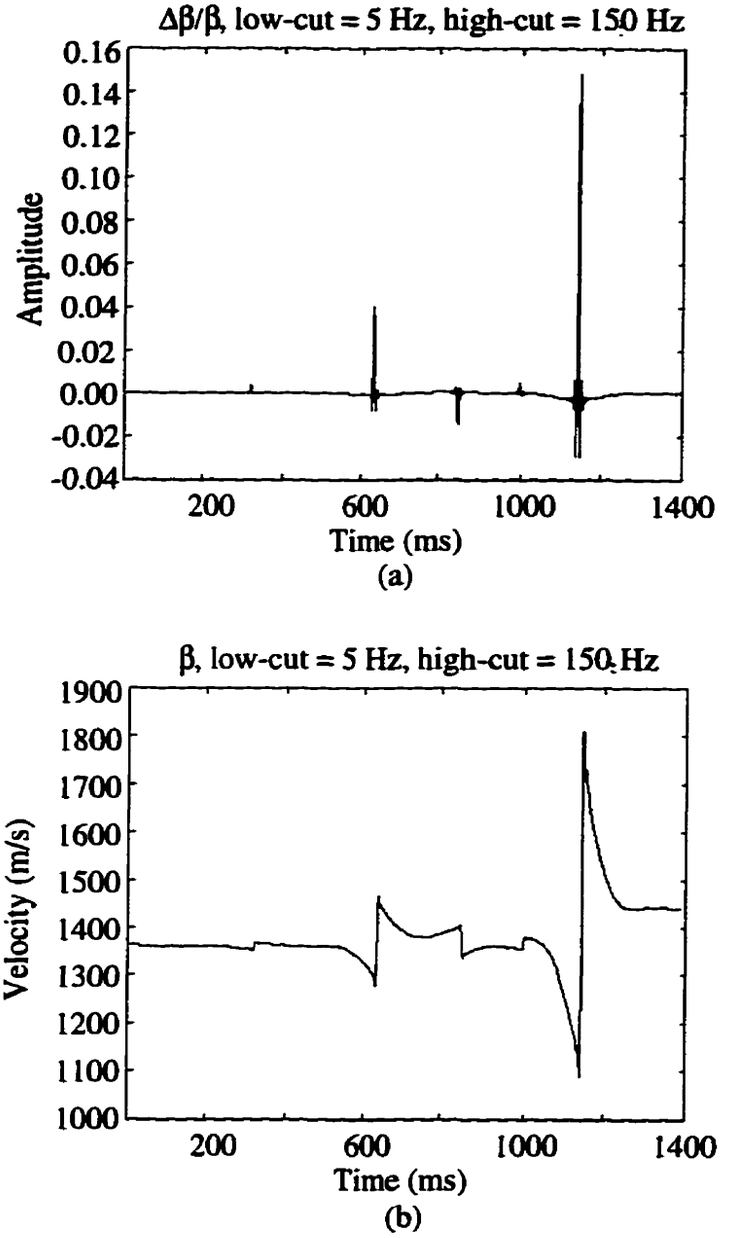

Figure 2.17. Example of inversion of band-pass filtered P-S gather. Plot (a) is the P-S gather of Figure 2.13b band-pass filtered with a 5 Hz low-cut and a 150 Hz high-cut and converted to a $\Delta\beta/\beta$ trace. Plot (b) shows that inversion of (a) results in a very distorted β estimate.

Because common practice in the acquisition of seismic data is to record with 10 to 14 Hz low-cuts it can be seen that, according to Figure 2.16, much of the important velocity information is not recorded. In the next chapter two P-S inversion schemes will be

presented which attempt to compensate for the band-limited nature of seismic data, especially at low-frequency. The alternative is to record lower frequency (Stewart et al., 1996).

2.4.4 Error due to non-zero phase

The next experiment was to test the performance of the P-S inversion in the face of phase errors in the seismic traces. The synthetic gather of Figure 2.13b had various phase rotations applied and the resulting RMS error responses are given in Figure 2.18. The largest RMS error occurred, near 180 degrees - centered at 215 degrees. There are two locations of low phase error, one of which has a lower RMS error than that at 0 degrees. These phase errors were at 70 and 344 degrees. Figures 2.19a and 2.19b show the trace rotated 220 degrees and resulting S-wave estimate. Note the very poor inversion result with the velocity decreasing rapidly with time. Figures 2.20a and 2.20b show the trace rotated 344 degrees and resulting S-wave estimate. The anomalously low error at 344 degrees could be due to systematic error in the $\Delta\beta/\beta$ estimates, resulting in an RMS error that is less than the error at 0 degrees.

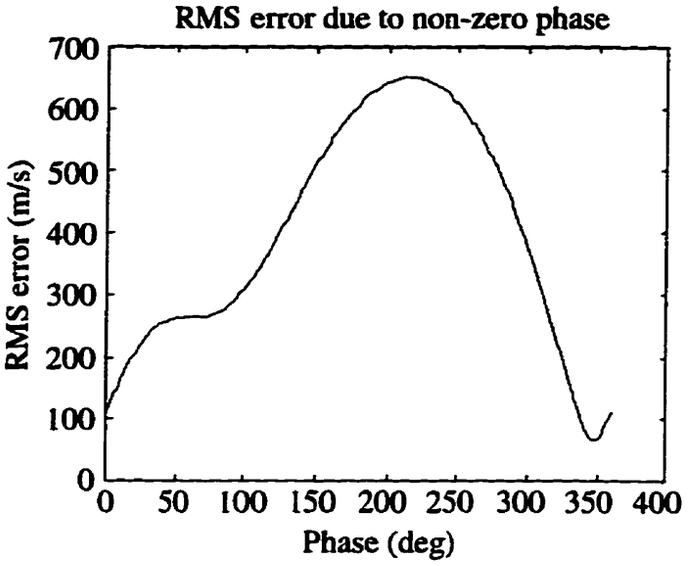

Figure 2.18. RMS error due to phase. Error increases to around 180 degrees out of phase and then decreases back to zero phase. Largest error at 220 degrees (Figure 2.19). Anomalously low error at 344 degrees (Figure 2.20).

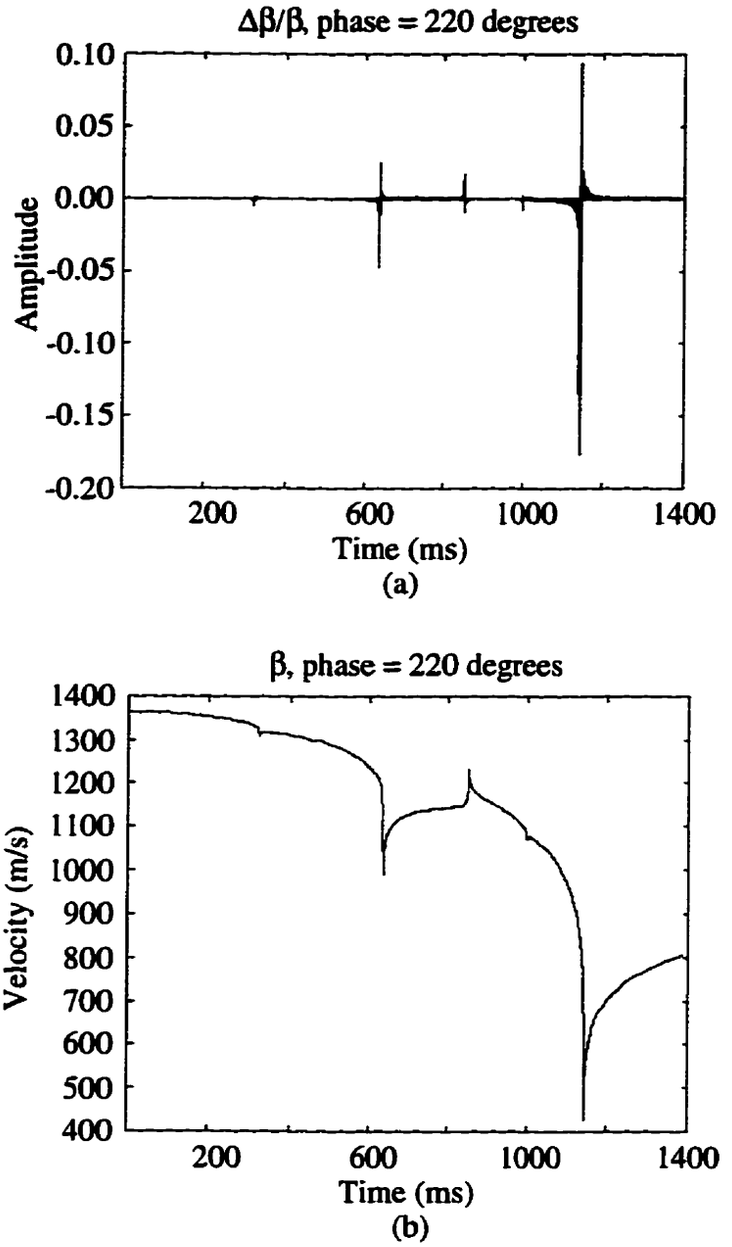

Figure 2.19. Example of inversion of phase-rotated P-S gather. Plot (a) is the P-S gather of Figure 2.13b phase-rotated to 220 degrees and converted to a $\Delta\beta/\beta$ trace. Plot (b) shows that inversion of (a) results in major distortion of the β estimate.

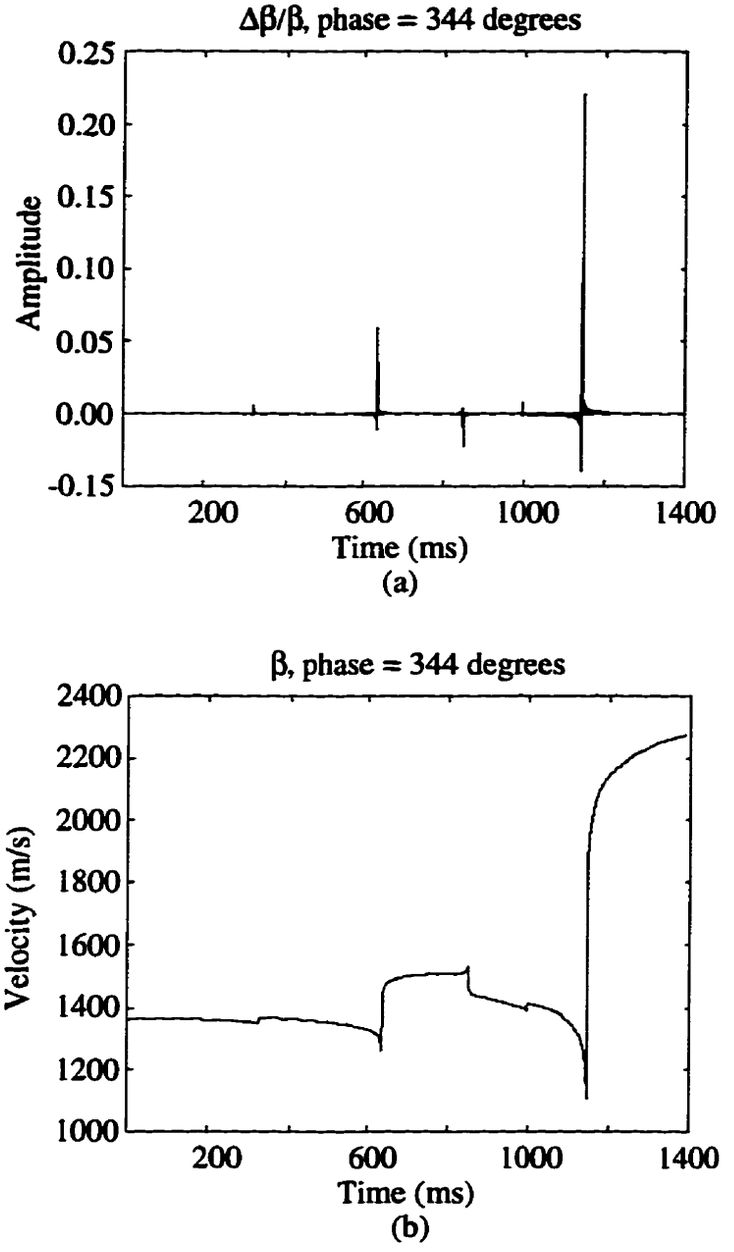

Figure 2.20. Example of inversion of phase-rotated P-S gather. Plot (a) is the P-S gather of Figure 2.13b phase-rotated to 344 degrees and converted to a $\Delta\beta/\beta$ trace. Plot (b) shows that inversion of (a) results in a phase-distorted β estimate yet the RMS error is lower than that for zero phase.

The preceding examples show that seismic data must be processed to zero phase to return reliable β estimates using this inversion method.

2.5 Chapter summary

The previous Sections have described two methods by which P-S data can be inverted to provide estimates of S-wave velocity (β). By knowing the converted-wave traveltimes bounding a lithologic unit, and the converted-wave stacking velocity, a direct computation of β was shown to be possible. The estimate's reliability would be increased if a shifted hyperbolic velocity analysis were used, or if offset / depth ratios are kept below about 1.0.

The relationship between P-S reflection data and $\Delta\beta/\beta$ inversion is shown to provide an estimate of β. However, such an estimate can be compromised by frequency-band limiting and by phase distortion. Phase distortion, can usually be compensated for in seismic processing. Phase compensation is discussed in Chapter 4.

The problem of frequency-band limiting is an acquisition problem. Current seismic surveys typically do not record low-frequency data (<10 Hz). Because it has been shown that low-frequency data is an important component of seismic inversion, some kind of compensation must be done. Two methods are examined in Chapter 3 by which low-frequency compensation can be applied to P-S seismic data.

Chapter 3 LOW-FREQUENCY COMPENSATION FOR P-S INVERSION

3.1 Introduction

Two methods are presented which restore low-frequency trends to the inversion of band-limited P-S data. The first is an extension of an inversion method described by Waters (1978). Waters' method (SAIL -Seismic Approximate Impedance Log) was derived as a simple approach to estimating impedance values from P-P seismic data. By making some modifications a form of the SAIL method can be used to estimate S-wave velocity from P-S weighted stacks.

P-S seismic data from the Blackfoot broad-band 3C-2D seismic survey were obtained, and a single 10 Hz trace was inverted and compared to an S-wave log which tied the line. This result was then compared to the inversion of the equivalent 2 Hz trace. The modified SAIL method of P-S inversion was found to provide reliable S-wave velocity estimates.

Constrained linear inversion (CLI) was also modified to invert P-S weighted stacks. In common practice this method is used to invert P-P data using linear programming techniques (Cooke and Schneider, 1983). The modified CLI method was used to provide S-wave velocity estimates from synthetic P-S data. Further development of the algorithm was found to be required due to solution instability beyond small numbers of data points.

3.2 Frequency domain inversion

A simple P-P inversion is the (SAIL) method described by Waters (1978). This method uses an impedance estimate, derived from well logs or stacking velocities, to provide the low-frequency trend commonly missing in seismic data. Thus, detailed

impedance values are provided by [redacted]

provided by the impedance log. The n[redacted]

1) Obtain an impedance estim[redacted]

and tie it to the seismic section

2) Integrate then exponentiate

3) Fourier transform the impe[redacted]

4) Scale the amplitude spectra

estimate.

5) High-cut filter the impedanc[redacted]

the integrated seismic traces.

6) Inverse Fourier transform t[redacted]

dictated by the lowest reliable s[redacted]

The above process, with som[redacted]

'BLIMP' (Band Limited IMPedance) [redacted]

requires a minimum of user input.

BLIMP can be used to invert P[redacted]

wave velocity and the P-S weighted

instead of an impedance estimate.

3.2.1 Method

Define the jth sample of a P-[redacted]

velocity across the jth interface (Aki ar[redacted]

$$\frac{1}{2}\frac{\Delta\beta}{\beta} = \frac{\beta_{j+1} - \beta_j}{\beta_{j+1} + \beta_j} = r_j ,$$

where β is the S-wave velocity.

Solve (3.1) for β_{j+1},

$$\beta_{j+1} = \beta_j\left(1 + \frac{2r_j}{1-r_j}\right) = \beta_j\left(\frac{1+r_j}{1-r_j}\right) = \beta_1\left(\frac{1+r_1}{1-r_1}\right)\left(\frac{1+r_2}{1-r_2}\right)\cdots\left(\frac{1+r_j}{1-r_j}\right)$$

$$\Rightarrow \beta_{j+1} = \beta_1\prod_{k=1}^{j}\frac{1+r_k}{1-r_k}. \tag{3.2}$$

Divide (3.2) by β_1 and take the logarithm,

$$\ln\left(\frac{\beta_{j+1}}{\beta_j}\right) = \sum_{k=1}^{j}\ln\left(\frac{1+r_k}{1-r_k}\right) \approx 2\sum_{k=1}^{j} r_k. \tag{3.3}$$

The right hand side of equation 3.3 follows from an approximation for the *ln* term (see Jeffrey (1995), pg. 122) which is valid for small r ($r^2 < 1$). Solve (3.3) for β_{j+1}:

$$\beta_{j+1} = \beta_1\exp\left(2\sum_{k=1}^{j} r_k\right). \tag{3.4}$$

An alternative derivation of equation 3.4 is as follows. From equation 3.1 let,

$$r_j \approx \frac{1}{2}\Delta\ln(\beta_j) \approx \frac{1}{2}\left(\ln(\beta_{j+1}) - \ln(\beta_j)\right) \approx \frac{1}{2}\ln\left(\frac{\beta_{j+1}}{\beta_j}\right). \tag{3.5}$$

Summing both sides and reducing gives,

$$2\sum_{k=1}^{j} r_k = \sum_{k=1}^{j}\ln\left(\frac{\beta_{k+1}}{\beta_k}\right) = \ln\left(\frac{\beta_{k+1}}{\beta_k}\frac{\beta_k}{\beta_{k-1}}\cdots\frac{\beta_2}{\beta_1}\right)$$

$$\Rightarrow 2\sum_{k=1}^{j} r_k = \ln\left(\frac{\beta_{j+1}}{\beta_1}\right). \tag{3.6}$$

Solve for $\ln(\beta_{j+1})$,

$$\ln(\beta_{j+1}) = \ln(\beta_1) + 2\sum_{k=1}^{j} r_k \tag{3.7}$$

Exponentiation of equation 3.7 gives,

$$\beta_{j+1} = \beta_1\exp\left(2\sum_{k=1}^{j} r_k\right), \tag{3.8}$$

which is identical to equation 3.4.

Model the P-S weighted stack as scaled r (to account for the unknown scale of recorded data),

$$S_k = \frac{2r_k}{\gamma}, \tag{3.9}$$

then equation 3.4 becomes:

$$\beta_{j+1} = \beta_1 \exp\left(\gamma \sum_{k=1}^{j} S_k\right). \tag{3.10}$$

Equation 3.10 integrates the P-S weighted stack and exponentiates the result to provide an S-wave velocity trace. Equation 3.10 is the P-S equivalent to step 2 of Waters' impedance inversion. BLIMP can be used to invert P-S seismic traces in the same manner as Waters (1978), but it has some modifications related to the pre-conditioning of the required S-wave velocity (Vs) estimate and the scaling of the seismic data.

The following is a step by step description of the BLIMP method as applied to P-S inversion (Ferguson and Margrave, 1996):

1) Compute the linear trend of the Vs estimate.

2) Subtract the linear trend from the Vs estimate (this reduces edge effects during subsequent frequency domain operations).

3) Compute the Fourier spectrum of step (2).

4) Apply a band-limited integration filter to each seismic trace and exponentiate the result.

5) Compute the Fourier spectra of (4).

6) Determine a scalar to match the mean magnitude of (5) and (3) over the seismic signal band.

7) Multiply the spectra of (5) by the scalar from (6).

8) Low-pass filter (3) and add to (7).

9) Inverse Fourier transform (8).

10) Add the low-frequency trend from (1) to (9).

The required filters in steps (2), (6) and (8) are designed using the same user specified Gaussian rolloff at high and low frequencies.

3.2.2 Examples

The data of Figure 3.1 were obtained from the Blackfoot Broad-Band 3C-2D seismic survey. A well-log 14-09-23-23W4, which tied the line (Figure 3.2), was obtained, and used to provide the required low-frequency Vs estimate.

To illustrate the need to compensate for missing low-frequency, a recursive inversion was computed using the 10 Hz trace at the well location (Figure 3.1a). This was done using the following equation:

$$\beta_{j+1} = \beta_j \frac{\left(1 + r_j\right)}{\left(1 - r_j\right)} \tag{3.11}$$

The resulting Vs was compared to the log-Vs (Figure 3.3). Note how, for low-frequency (0 - 10 Hz), the recursive inversion has failed to give an accurate Vs estimate. However, for mid- to high-frequency (10 - 90 Hz) the log and the inversion estimate have much the same character. This result implies that, for mid-high frequency, seismic data may resolve small changes in Vs but requires a low-frequency trend to complete the estimate.

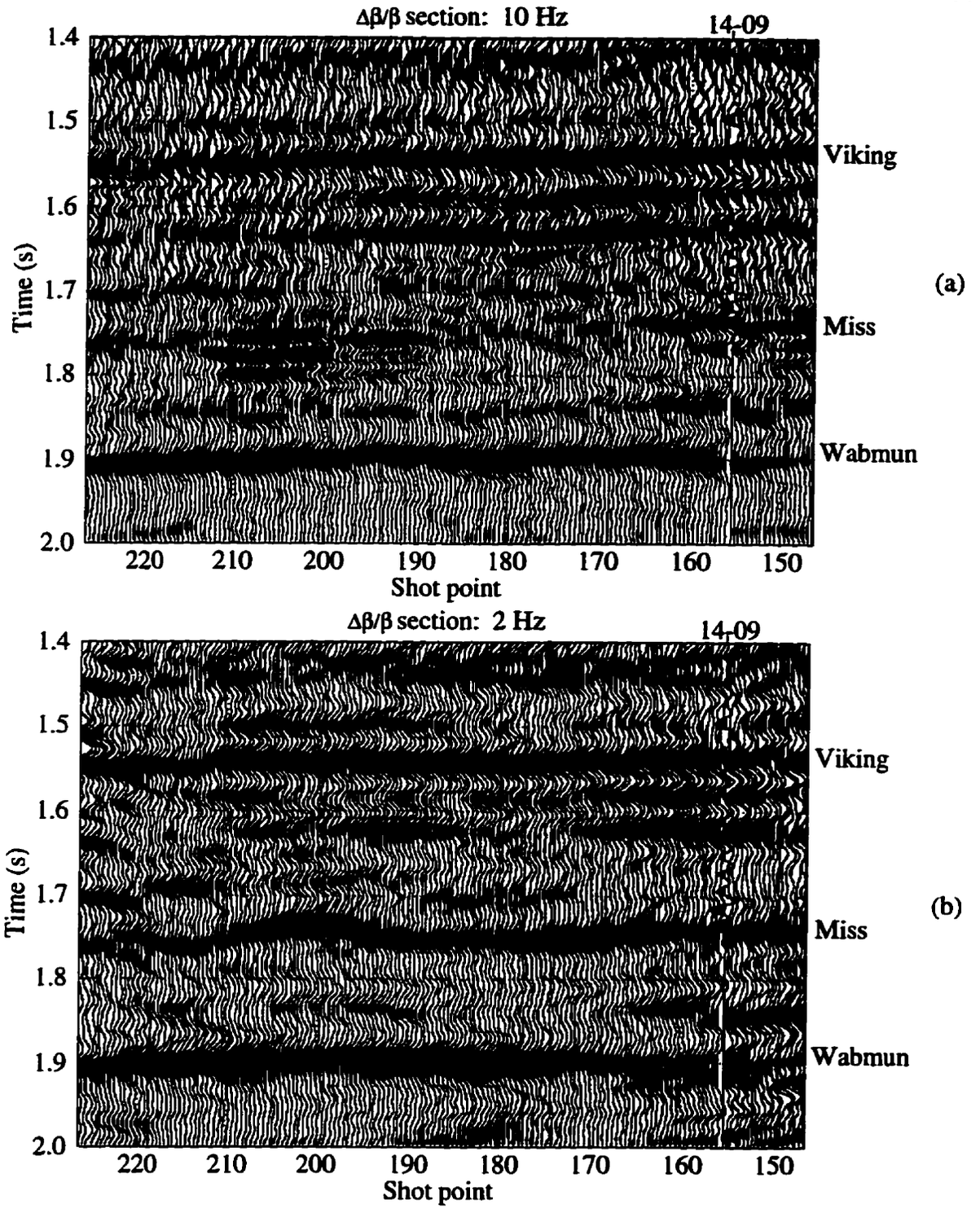

Figure 3.1. P-S weighted stack sections. The 10 Hz (a) and 2 Hz (b) data are shown with AGC applied. Inversions were computed without AGC. Synthetic P-S traces overplot the seismic at the well locations. The real P-S traces at the well locations were used as inversion examples.

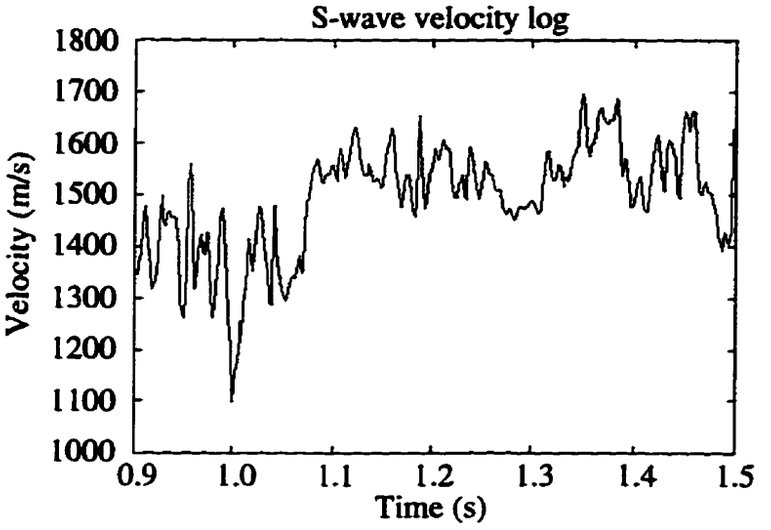

Figure 3.2. Vs log from well 14-09-23-23W4.

The 10 Hz trace was then inverted using BLIMP. Figures 3.4 and 3.5 are step-by-step illustrations of the inversion process. Figures 3.4a, b and c illustrate how the log-Vs is conditioned by removing a linear Vs trend. Figures 3.4d, e and f show frequency spectra of the conditioned log, a 10 Hz high-cut filter, and the application of the filter. Figures 3.5 a, b and c show the spectra of the filtered log combined with the scaled spectrum of the integrated trace. Figures 3.5d, e and f show the inverse Fourier transform of the result and the restoration of the linear trend to form the final Vs (Figure 3.5f). Figure 3.6 shows a comparison of the log, recursive and band-limited inversion results.

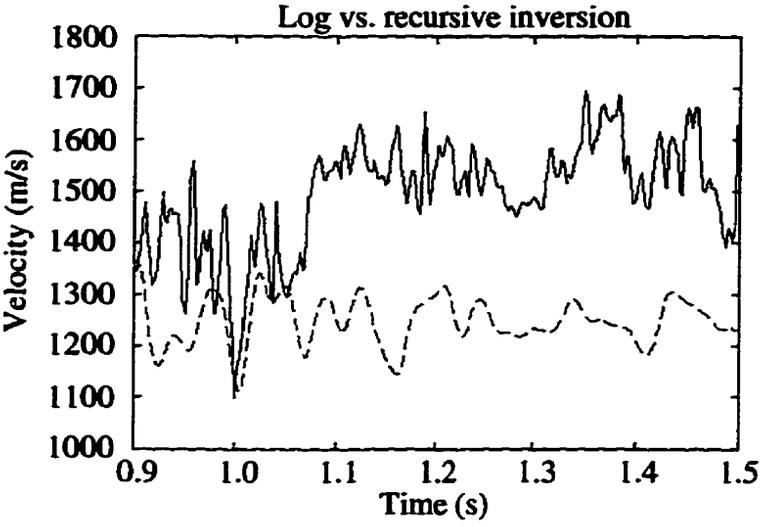

Figure 3.3. Comparison between Vs derived from the 10 Hz trace by recursive inversion (dashed curve) and the true log Vs (solid curve). There is good correlation of values in a mid- to high-frequency sense (10 - 90 Hz), and poor low-frequency (0 - 10 Hz) correlation due to seismic band-limiting.

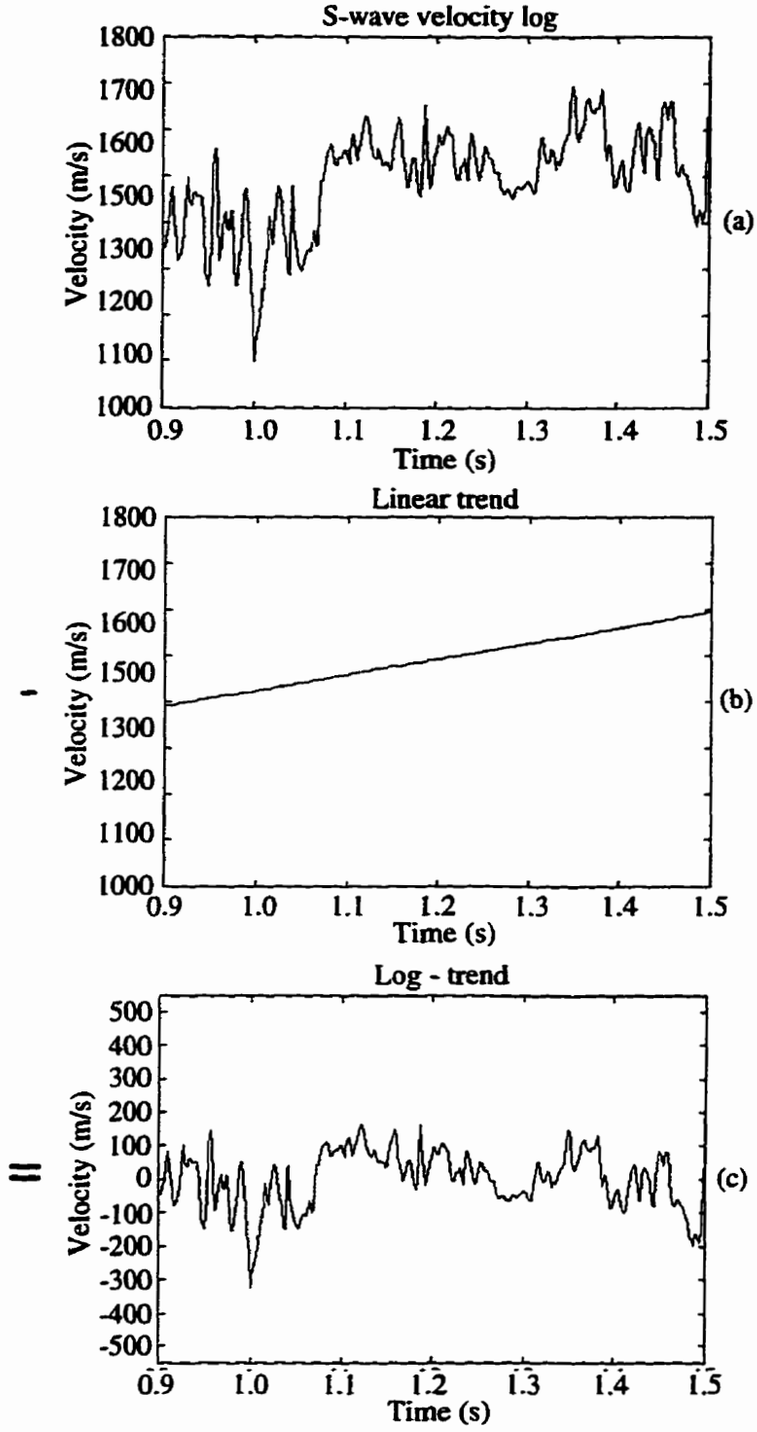

Figure 3.4. Conditioning of the Vs log prior to inversion. The Vs log (a) has a linear trend (b) removed to leave a mid- to high-frequency log (c). The amplitude spectrum (d) (continued next page) of the log is high-cut filtered (e), to provide low-frequency (f) (0 - 10 Hz in this example).

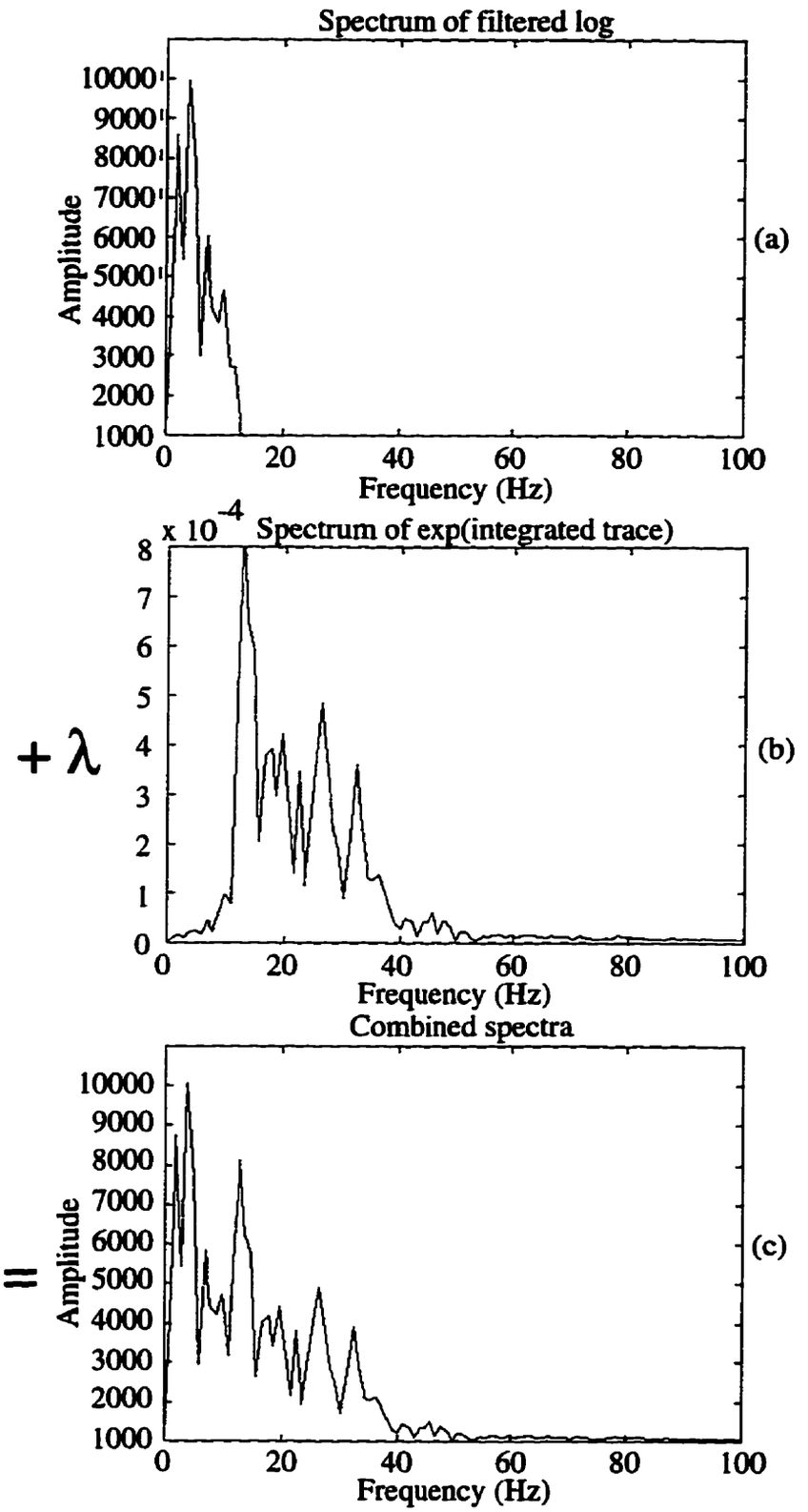

Figure 3.5. Computation of Vs. The spectrum of the low-frequency trend from the log (a) is added to the scaled spectrum of the integrated trace (b). λ is a numerically estimated

scale factor. The combined spectra (c) is inverse Fourier transformed (d) (continued next page) and the linear trend (e) is restored. Figure (f) is the resulting Vs.

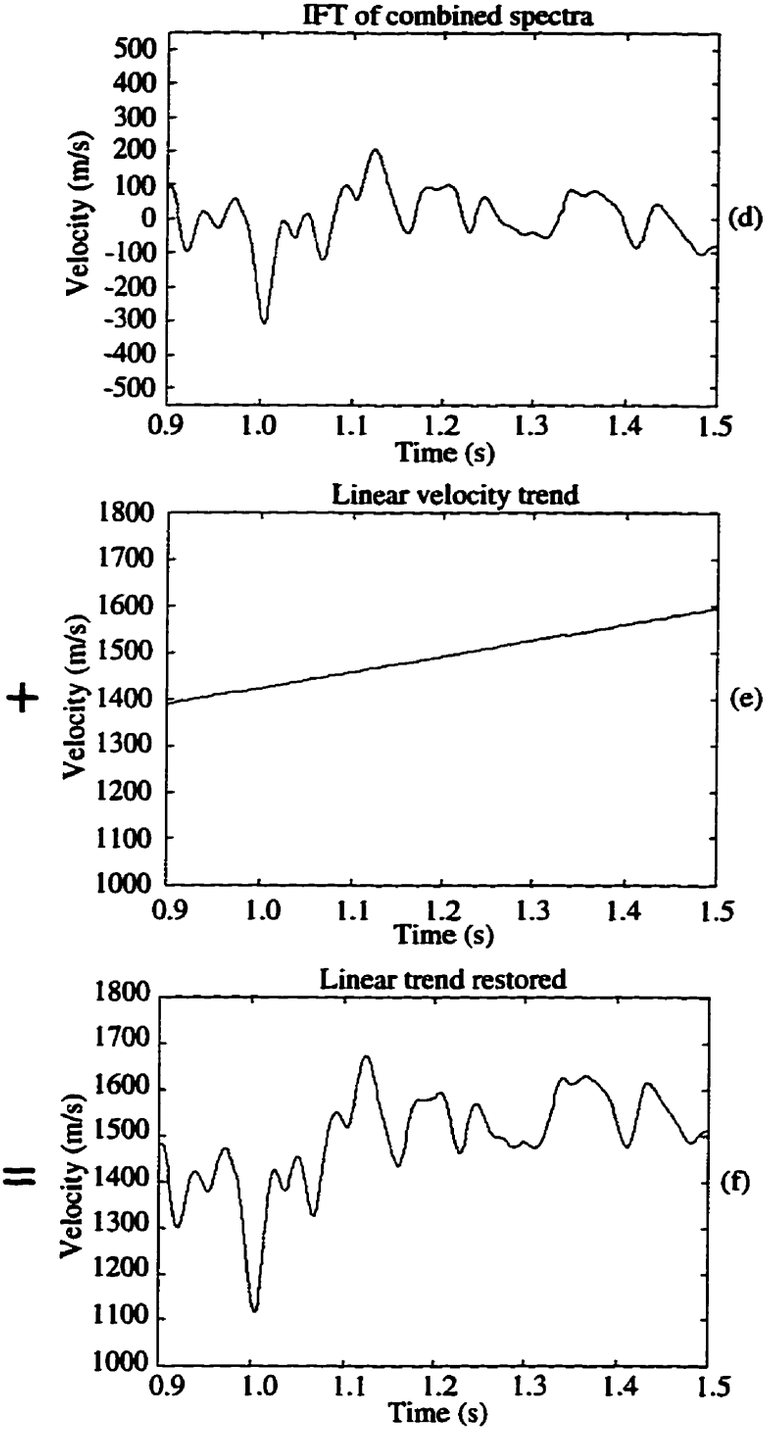

Figure 3.5. Continued from previous page.

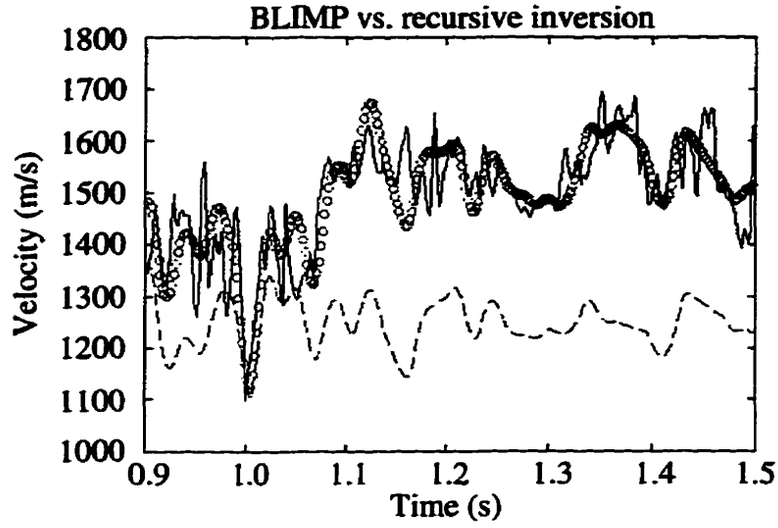

Figure 3.6. Comparison of the log-Vs and inversion Vs' for the 10 Hz trace. Note the very good correlation of the BLIMP estimate (circle curve), with the true Vs (darkest curve) compared to the recursive Vs (dashed curve).

Examination of Figure 3.6 shows how BLIMP has improved the Vs estimate of the 10 Hz data over the recursive inversion. The mid- to high-frequencies of the trace derived Vs (circle curve) are still present, and direct comparisons to the log-Vs (darkest curve) are now possible (the curves overlay each other). Additionally, the BLIMP procedure is virtually insensitive to the overall scale of the seismic data while recursion is not.

Figure 3.7 shows the Vs estimates from the equivalent 2 Hz trace. The correlation of the recursive inversion (dashed curve) to the log-Vs (solid curve) is much improved, especially the Vs jump at 1.08 seconds. This high quality of correlation is due to the reliability of the recorded low-frequency, in other words, usable data has been recorded down to 2 Hz. The band-limited inversion therefore, adds very little log-Vs information (0 - 2 Hz) to the inversion result. The inversion result has very little bias, compared to the 10 Hz trace, to the log-Vs.

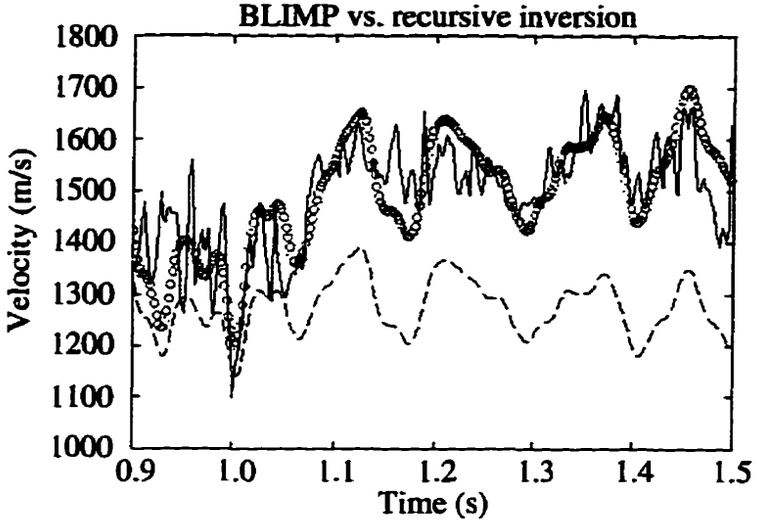

Figure 3.7. Comparison of the log-Vs and inversion Vs' for the 2 Hz trace. Note the very good correlation of both the BLIMP Vs (circle curve) and the recursive Vs (dashed curve) to the true Vs (solid curve). The high quality of the recursive estimate is due to the recording of reliable low-frequency.

3.3 Constrained linear inversion

Velocity estimates from P-P seismic inversion have often been compromised by a lack of low-frequency information in typical seismic data (Hendrick and Hearn, 1993). That is, velocity estimates exhibit low-frequency instability. In the P-P case, linear inversion can be stabilized by constraining the impedance solution to be close to an initial guess (Russell and Hampson, 1991). The result is that impedance information not resolved by the data is provided by the initial velocity estimate. Similarly, a constrained algorithm can be used to estimate Vs from the P-S weighted stacks. Rewriting equation 3.5 replacing r with equation 3.1, gives:

$$\frac{\Delta\beta}{\beta}_i = \ln\left(\beta_{i+1}\right) - \ln\left(\beta_i\right) \tag{3.12}$$

Let,

$$\theta_i = \ln\left(\beta_i\right), \tag{3.13}$$

then equation 3.12 becomes:

$$\frac{\Delta\beta}{\beta}_i = \theta_{i+1} - \theta_i \tag{3.14}$$

In vector form Equation 3.14 can be represented by the following first-order Taylor expansion (Lines and Treitel, 1984),

$$\frac{\overrightarrow{\Delta\beta}}{\beta} = \frac{\overrightarrow{\Delta\beta}}{\beta}_0 + Z\left(\vec{\theta} - \vec{\theta}_o\right), \tag{3.15}$$

where vectors $\Delta\beta/\beta o$ and θo are derived as functions of an initial guess βo, and Z is an n x n+1 matrix of the partial derivatives of equation 3.14,

$$Z = \begin{bmatrix} -1\ 1\ 0 \ldots\ldots 0 \\ 0\ -1\ 1\ 0 \ldots\ldots 0 \\ \vdots \\ 0 \ldots\ldots 0\ -1\ 1 \end{bmatrix}, \tag{3.16}$$

where a single element of Z is (again using equation 3.14):

$$Z_{ij} = \frac{\partial \frac{\Delta\beta}{\beta}_i}{\partial\theta_j}, \tag{3.17}$$

and j goes from 1 to n+1. Let

$$\vec{\delta} = \vec{\theta} - \vec{\theta}_o, \tag{3.18}$$

then equation 3.15 becomes,

$$\frac{\overrightarrow{\Delta\beta}}{\beta} = \frac{\overrightarrow{\Delta\beta}}{\beta}_0 + Z\vec{\delta} \tag{3.19}$$

Let error vector ε represent the difference between equation 3.19 and the P-S weighted stack computed from seismic data,

$$\vec{\varepsilon} = \frac{\overrightarrow{\Delta\beta}}{\beta_w} - \frac{\overrightarrow{\Delta\beta}}{\beta_0} - \mathbf{Z}\vec{\delta} \tag{3.20}$$

The sum of the squares of (3.16) is,

$$\vec{\varepsilon}^T\vec{\varepsilon} = \left(\frac{\overrightarrow{\Delta\beta}}{\beta_w} - \frac{\overrightarrow{\Delta\beta}}{\beta_0} - \mathbf{Z}\vec{\delta}\right)^T\left(\frac{\overrightarrow{\Delta\beta}}{\beta_w} - \frac{\overrightarrow{\Delta\beta}}{\beta_0} - \mathbf{Z}\vec{\delta}\right) \tag{3.21}$$

At this point a constraint λ is introduced to the squared error function in the form of a Lagrange multiplier problem (Lines and Treitel, 1984).

$$\vec{S} = \vec{\varepsilon}^T\vec{\varepsilon} + \lambda\left(\vec{\delta}^T\vec{\delta} - \delta_0^2\right) \tag{3.22}$$

where the S vector is minimized subject to the constraint that the absolute value of vector δ is constant (Lines and Treitel, 1984).

The use of λ has a twofold effect. Singularities in matrix inversion are avoided, and the resulting Vs estimates are constrained to be close to an initial guess (Lines and Treitel, 1984). Differentiating the S vector with respect to vector δ, and setting the result equal to zero, gives a modified form of the least-squares error,

$$\frac{\partial\vec{S}}{\partial\vec{\delta}} = 0. \tag{3.23}$$

Solving for vector δ

$$\vec{\delta} = \left(\mathbf{Z}^T\mathbf{Z} + \lambda\vec{\mathbf{I}}\right)^{-1}\mathbf{Z}^T\left(\frac{\overrightarrow{\Delta\beta}}{\beta_w} - \frac{\overrightarrow{\Delta\beta}}{\beta_0}\right). \tag{3.24}$$

Replacing vector δ with equation 3.18 and solving for vector θ,

$$\vec{\theta} = \left(\mathbf{Z}^T\mathbf{Z} + \lambda\mathbf{I}\right)^{-1}\mathbf{Z}^T\left(\frac{\overrightarrow{\Delta\beta}}{\beta_w} - \frac{\overrightarrow{\Delta\beta}}{\beta_0}\right) + \vec{\theta}_o. \tag{3.25}$$

Thus, exponentiation of equation 3.25 and substitution using equation 3.13 provides an S-wave velocity estimate for the P-S weighted stack. It ensures that the initial guess provides as much velocity information as the user thinks is required. Control of the inversion can be achieved through an iterative process - beginning with a large value for λ (Lines and Treitel, 1984). For each iteration, the value of λ was can be decreased by perhaps 50% and an RMS error calculated between the Vs estimate and the initial guess. Iteration of the inversion ceases when the RMS error has increased to a percentage of the RMS velocity of the initial guess. This percentage would be supplied by the user.

3.3.1 Examples

A model consisting of a band-limited P-S gather was constructed to test the CLI method. This model was based on the well logs of Figure 2.2 and the unfiltered gather of Figure 2.4. The gather was low-cut filtered to 2 Hz and high-cut filtered to 60 Hz. It was found that convergence to a predetermined RMS error percentage was possible over only a limited number of data points.

For comparison to the CLI estimates to follow, Figure 3.8 shows the model Vs overlain by the Vs derived from recursive inversion of the P-S gather. The recursive inversion was initiated at 1.285 seconds with the correct velocity and thus, over this short log range, the correlation is quite good. Figure 3.9a shows the Vs from CLI with the allowable RMS error set to 0%. The initial-guess velocity used for this inversion was taken from an unrelated well log. The inversion Vs was found to reproduce the initial guess. As the RMS error was allowed to increase to 20% (Figure 2.9b), the inversion Vs was found to more closely approximate the true Vs. As the RMS error was increased to 50% (Figure 3.9c), the inversion Vs tended even more towards the true Vs. As the RMS error was allowed to increase further, the inversion Vs began to equal the Vs from recursive inversion.

The inversion Vs values of Figures 3.10a, b and c were created using the true Vs as the initial guess. It was found that the inversion was much less sensitive to the imposed RMS error, and as the RMS error increased from 0% (Figure 3.10a), through 20% (Figure 3.10b) to 50% (Figure 3.10c) the inversion Vs improved with little discernible improvement beyond 50%.

Further development of the constrained limited inversion, as coded here, was found to be necessary. The algorithm was unable to converge to reasonable error bounds with large numbers of samples. The limit for synthetic examples tended to be about 51 samples. Experiments with real seismic data showed that convergence was possible with less than 20 samples. Note that, an alternative - non iterative solution to the constrained linear inversion exists, and future work should include this implementation.

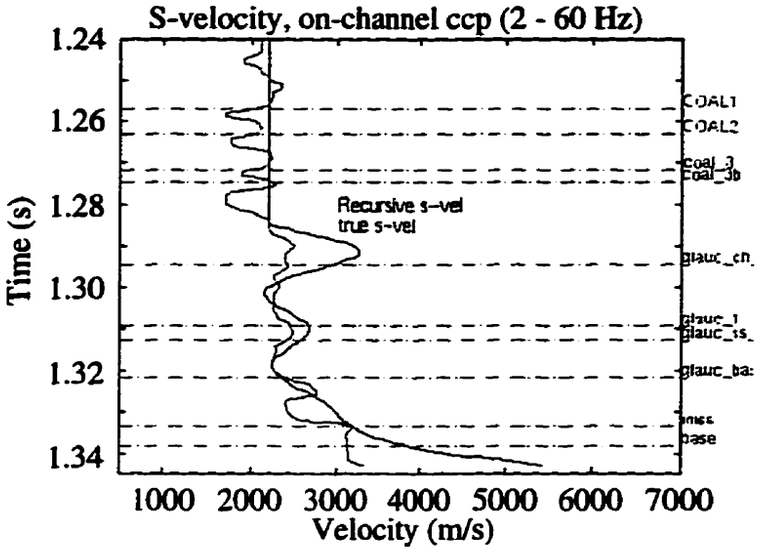

Figure 3.8. Recursive inversion (darkest velocity trace) of synthetic data.

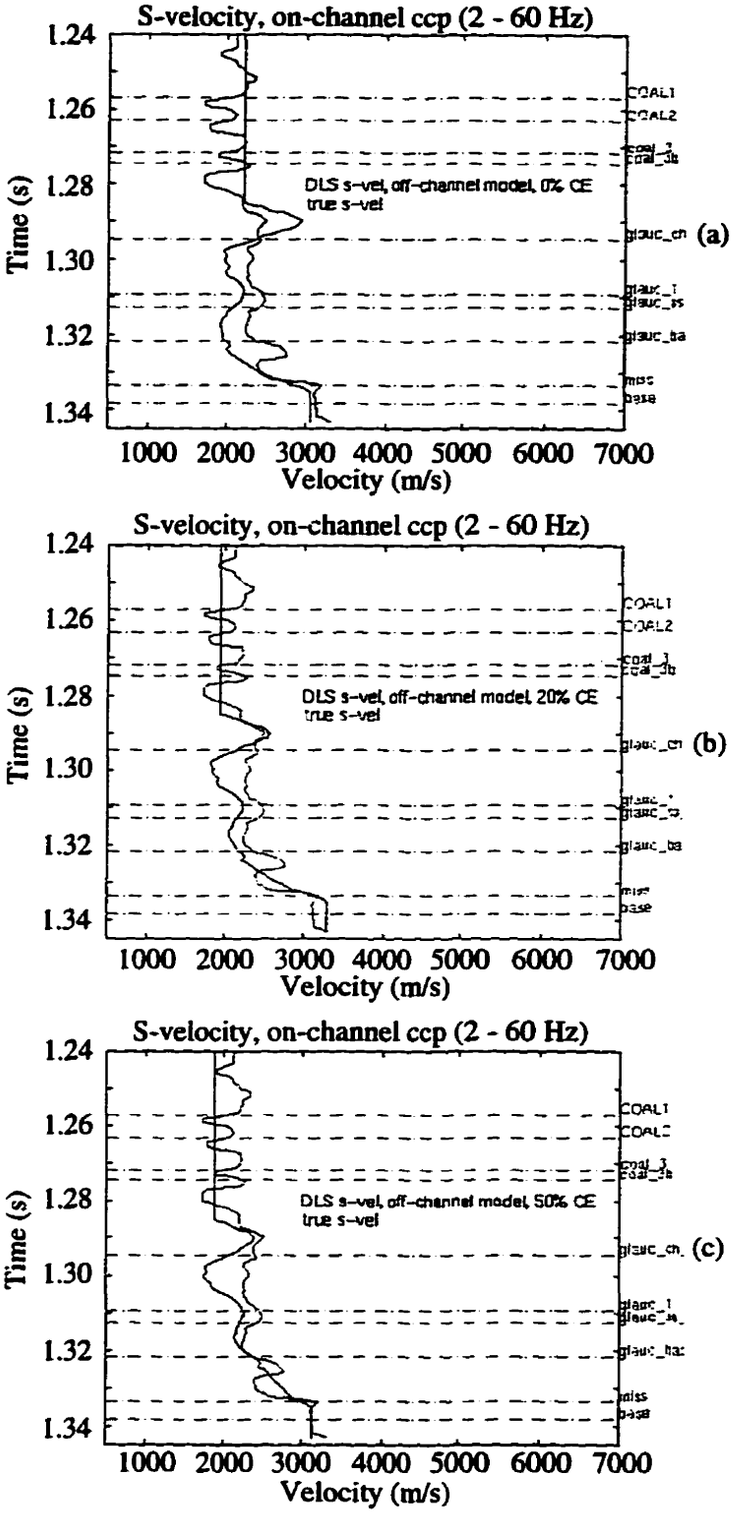

Figure 3.9. Constrained linear inversion, an unrelated well log (ligtest velocity trace) was used as an initial guess.

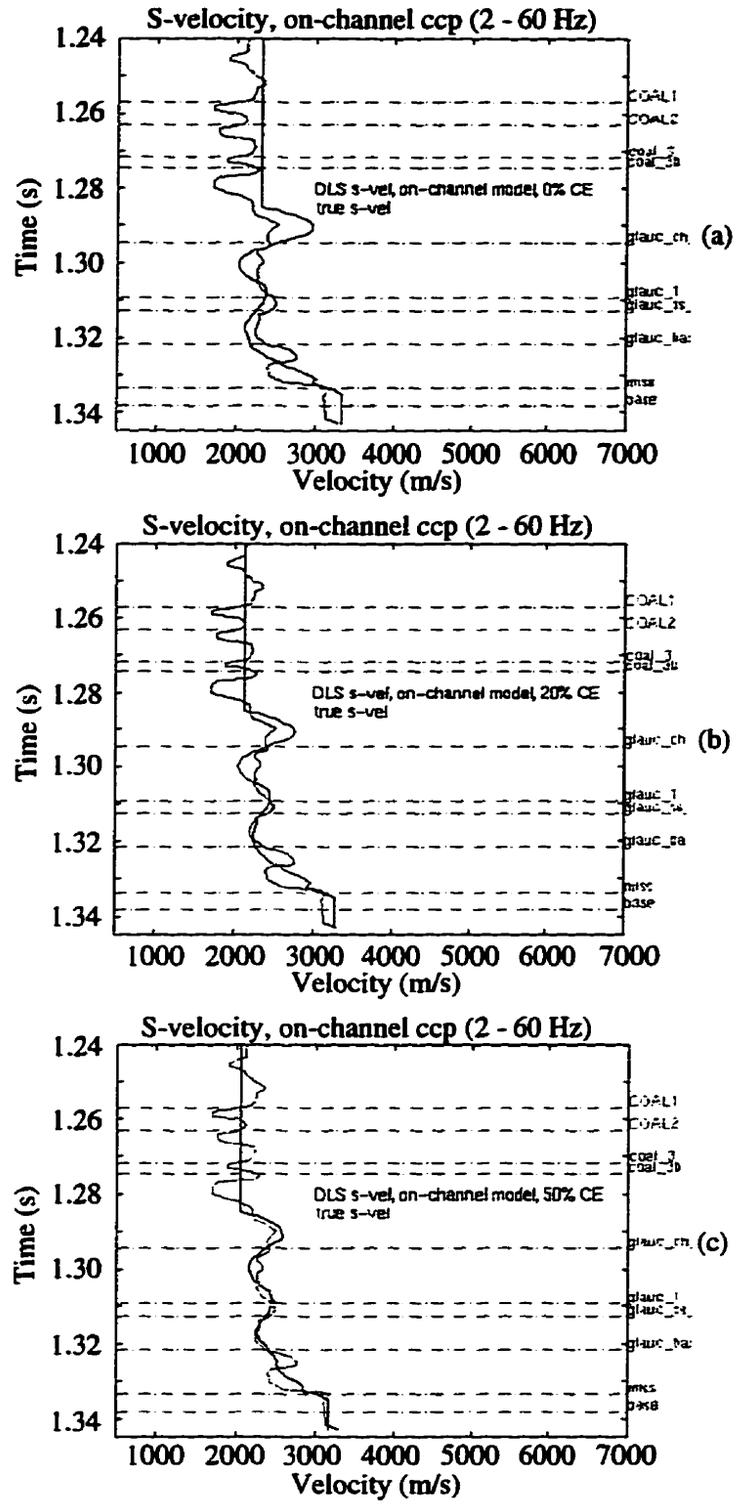

Figure 3.10. Constrained linear inversion, the model well log (lightest velocity trace) was used as an initial guess.

3.4 Chapter summary

Two methods were presented whereby Vs could be estimated using band-limited P-S data. Both inversions can be used to provide low-frequency to P-S inversion using well logs, or other Vs measurements. The first method, BLIMP, combines the low-frequency trend of a Vs log, with the band-limited Vs estimate from a P-S weighted stack, all in the frequency domain. BLIMP was used to estimate Vs for a single 10 Hz trace. The result was compared to a Vs log which tied the line. The Vs log was then compared to the inversion of a single 2 Hz trace. BLIMP was found to provide reliable Vs estimates for both the 10 Hz and 2 Hz traces.

Inversion by constrained linear inversion was also presented. It was shown that the method could be used to invert P-S weighted stacked data, but, further development of the constrained limited inversion was found to be required. Large numbers of trace samples were found to prevent convergence to reasonable Vs values. The limit for synthetic examples was about 51 samples, the limit for real seismic data was less than 20 samples.

Chapter 4 THE BROAD-BAND BLACKFOOT 3C-2D.

4.1 Introduction

Chapter 3 presented two methods by which band-limited P-S data could be inverted to provide broad-band S-wave velocity estimates. In this chapter, the P-S weighted stack of Section 2.3 and the band-limited inversion method of Section 3.2 were used to predict S-wave velocity (Vs) and the ratio of P-wave velocity (Vp) to Vs (Vp/Vs) for the Broad-Band Blackfoot 3C-2D seismic data. This work was also undertaken to demonstrate the effect of recorded low frequency in improving both P-P and P-S seismic inversion.

The Broad-band Blackfoot 3C-2D survey was acquired during the summer of 1995 (Section 1.3.2 provides a detailed description of the acquisition). The dataset was unusual in that four sets of geophones, three of them multicomponent - all with different fundamental frequencies, were used to simultaneously record a seismic survey. This chapter will examine the three multicomponent data sets representing the P-P and P-S wave fields as recorded by 2 Hz, 4.5 Hz and 10 Hz geophones. First, a series of seismic models are examined. These models were constructed to represent oil productive and non-oil productive geology, and synthetic seismic data were computed to represent data recorded over these two geologic conditions. The data were low-cut filtered and inverted to examine whether recording down to 2 Hz would result in better Vp and Vs inversions compared to conventional 10 Hz recordings. It was found that, because the synthetic data were not sufficiently long in time, filter performance was impacted at 2 Hz.

Processing of the Blackfoot data will then be presented. Examples of seismic sections and frequency spectra will be provided as comparisons between the 2 Hz and 10 Hz recordings. Inversion of the P-P ad P-S data will be presented along with the Vp/Vs estimates for the 2 Hz and 10 Hz frequency ranges. The inversion velocities and Vp/Vs

will then be examined in terms of rock properties, and a lithologic interpretation of the inversion results will be provided.

4.2 The target geology of the Blackfoot Field

The target geology of the Blackfoot prospect are oil producing channel-sands of the lower Cretaceous, and are the result of infilling of incised river valleys. The regional geology from which we distinguish these sands are mainly shales. A detailed summary of the Blackfoot geology can be found in Miller et al.(1995). The effect these sands have on the propagation of seismic waves is to increase Vs to about 2400 m/s from about 2200 m/s, and decrease Vp to 4000 m/s from about 4050 m/s. There is, therefore a net decrease of the Vp/Vs from 1.89 to 1.67 when oil-producing sands are encountered.

4.3 Modeling

A synthetic experiment, based on well logs, was constructed to provide a set of inversion examples for the broad-band Blackfoot seismic experiment. Synthetic P-P and P-S seismic gathers were computed incorporating Vp, Vs and density information from two sets of well logs representing oil productive and non-oil productive geologic regimes. P-P inversion and P-S inversion were used to estimate Vp, Vs and Vp/Vs for the 2 Hz and 10 Hz low-frequency ranges. Inversion modeling was performed to predict whether inversion could differentiate between oil productive and non oil productive locations, and which low-frequency ranges were capable of doing so.

4.3.1 Generation of synthetic data

Two sets of well logs were obtained near the seismic line. The first, 14-09-23-23 (Figure 4.1a), provided a P-wave sonic log and a density log which were used to represent a non-oil productive well placement. The second well, 08-08-23-23, was a productive well providing P-wave sonic and density logs as well as an S-wave sonic log which was recorded over a short range. These logs were modified in the following way. Using a

depth varying Vp/Vs at the location of 14-09-23-23 (Miller et al., 1995) a Vs log was derived by scaling the Vp log with these depth varying ratios. Then, in order to simplify the comparison, the Vp, Vs and density logs from 08-08-23-23 were clipped at the top of the zone of interest (Figure 4.1b) and grafted on to copies of the 14-09-23-23 logs, yielding two sets of Vp, Vs and density logs. The logs were identical except for the last 50 m thus providing a model of the regional geology and a model of the target geology. Figures 4.2a and 4.2b show the logs at the zone of interest.

Seismic gathers were then computed for the on- and off-channel models using SYNTH, a Zoeppritz modeling algorithm developed by Dr. Don Lawton and Dr. Ed Krebes of the University of Calgary. Figures 4.3 and 4.4 are comparisons of the unfiltered P-P and P-S gathers for the off-channel and on-channel models. Figures 4.5 through 4.8 show gathers that have been filtered to represent 2 Hz and 10 Hz acquisition.

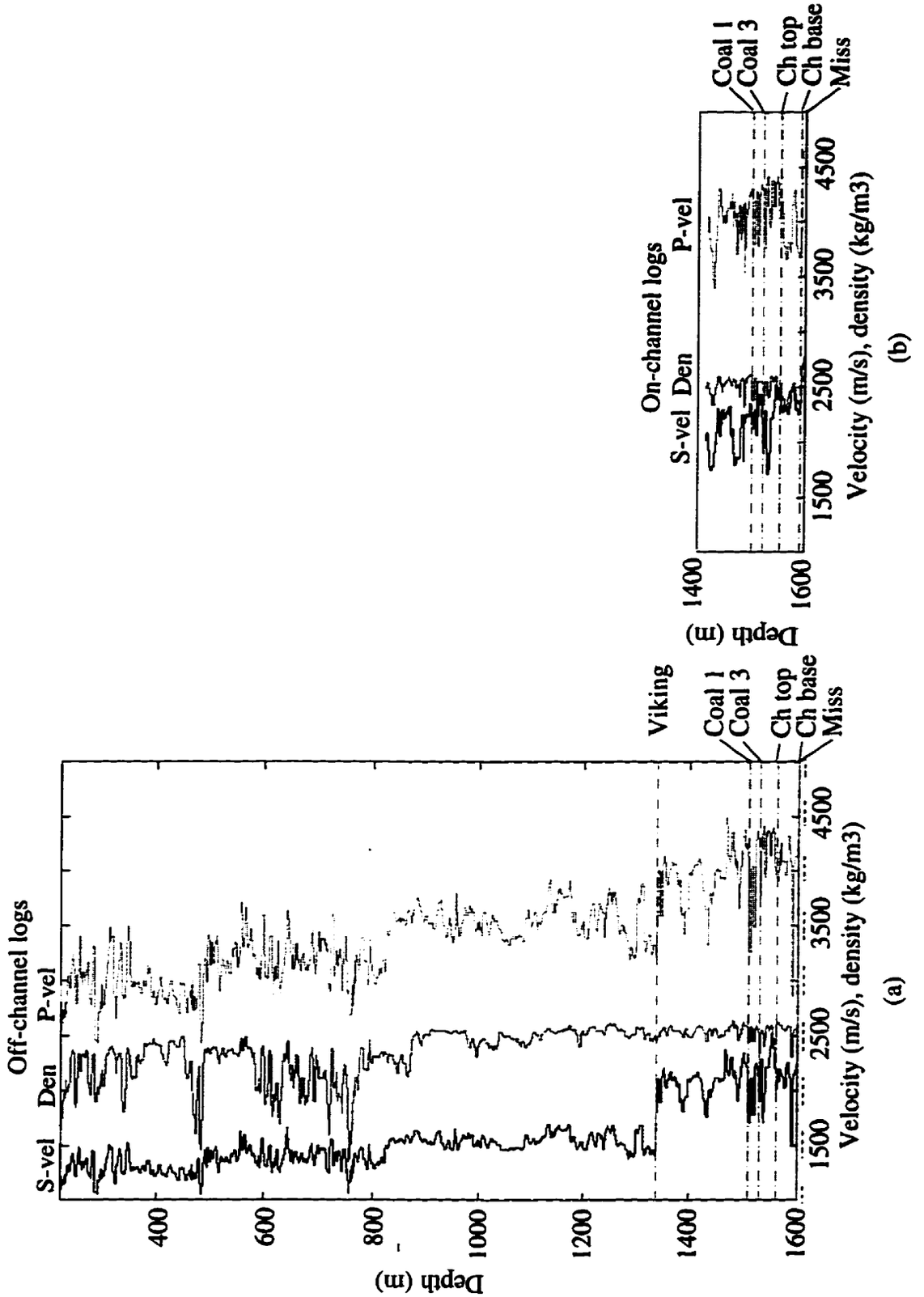

Figure 4.1. Logs used for seismic models. Potential oil production from the Ch top - Miss. Figure (a) represents shale in this zone, (b) represents oil-productive sand.

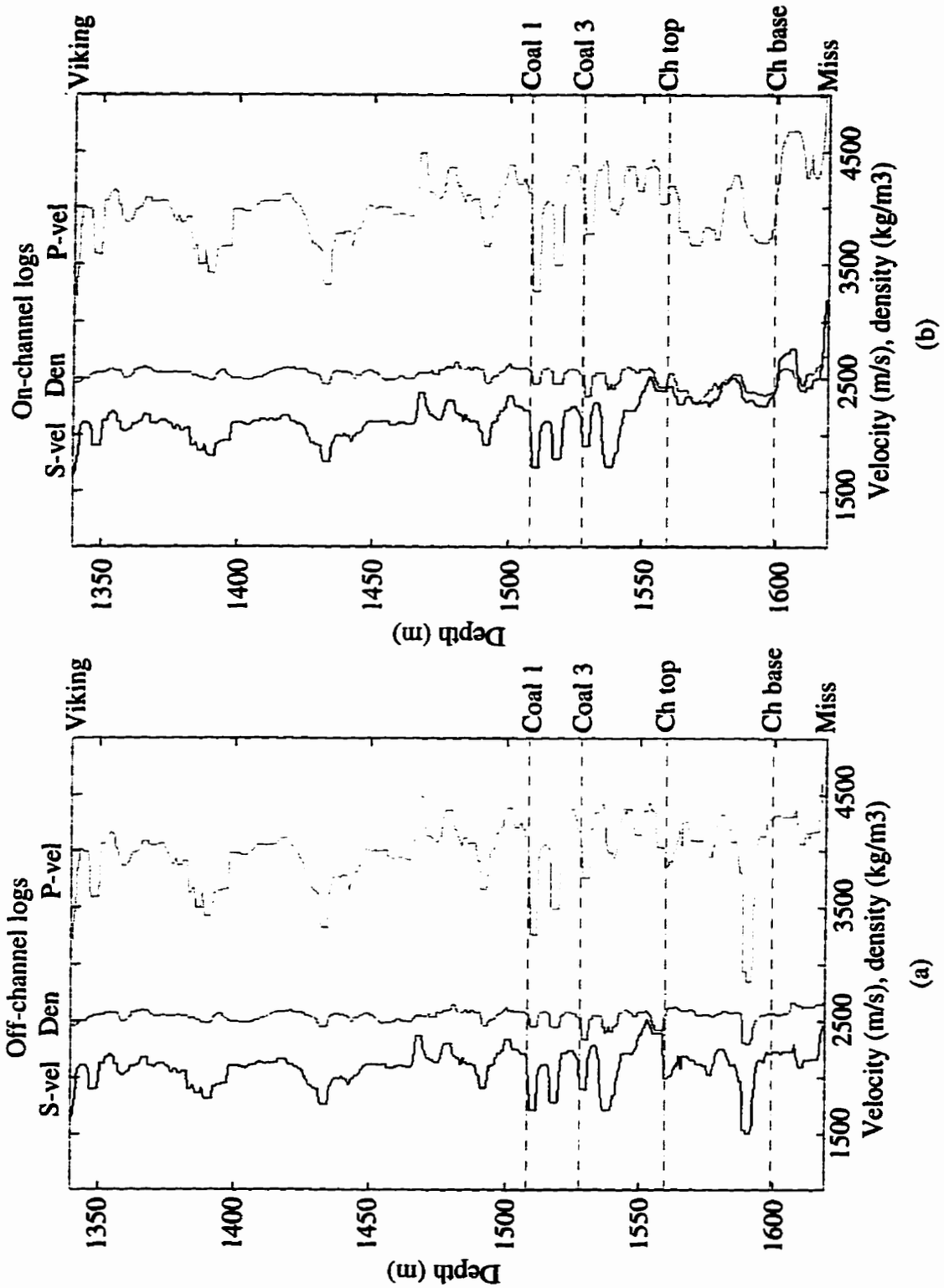

Figure 4.2. Close up of log models. The last 50m of Figure 4.1b was spliced onto a copy of Figure 4.1a. Note the 200 m/s increase in Vs between the off- and on-channel locations.

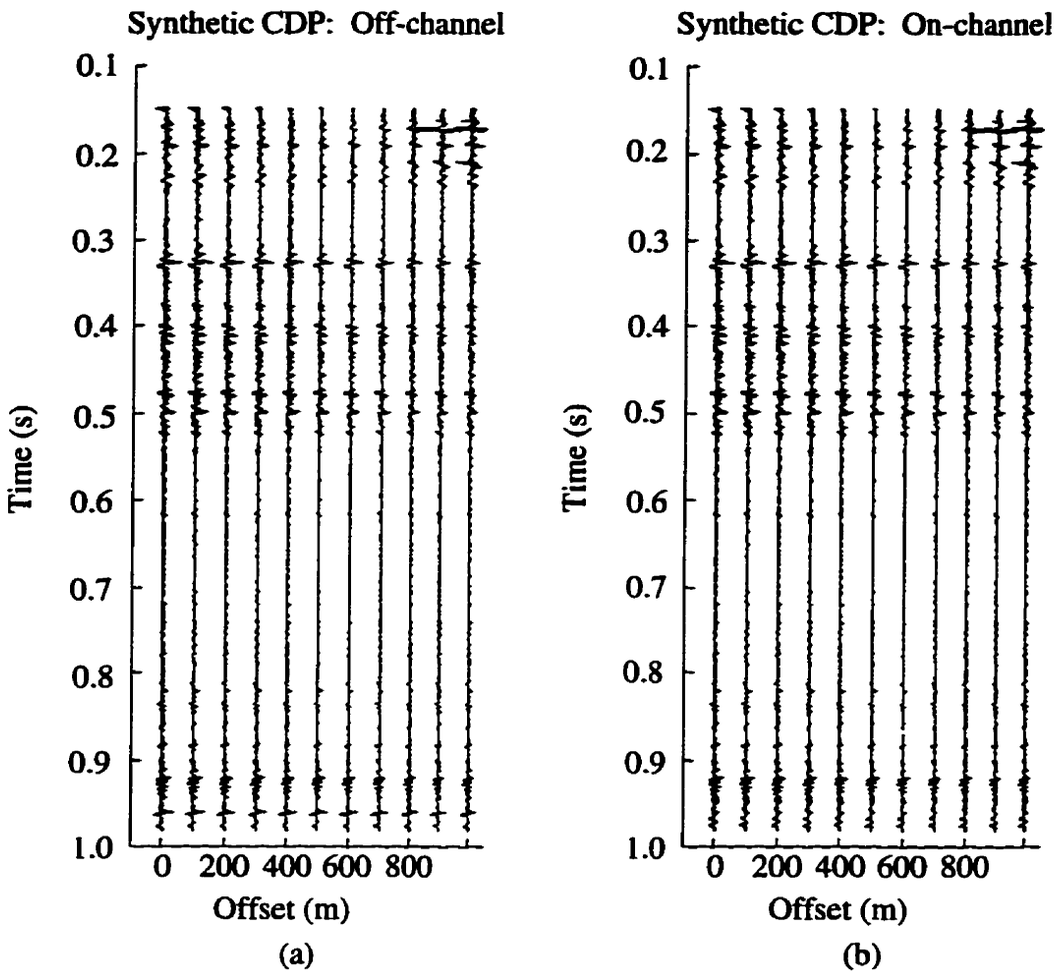

Figure 4.3. Comparison of synthetic CDP seismic gathers (NMO has been applied). The data is shown unfiltered. Figure (a) was computed based on the off-channel model, Figure (b) was computed using the on-channel model.

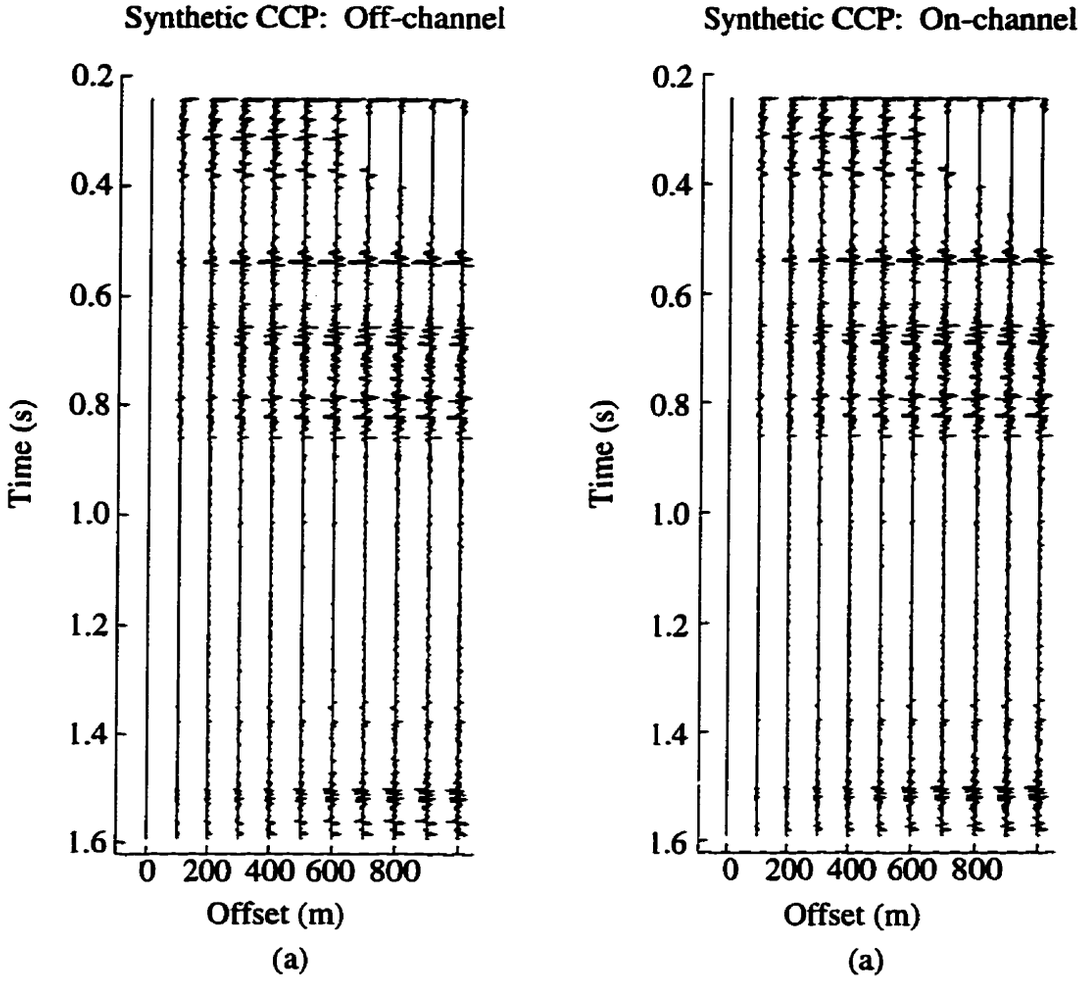

Figure 4.4. Comparison of synthetic CCP seismic gathers (NMO has been applied). The data is shown unfiltered. Figure (a) was computed based on the off-channel model, Figure (b) was computed using the on-channel model.

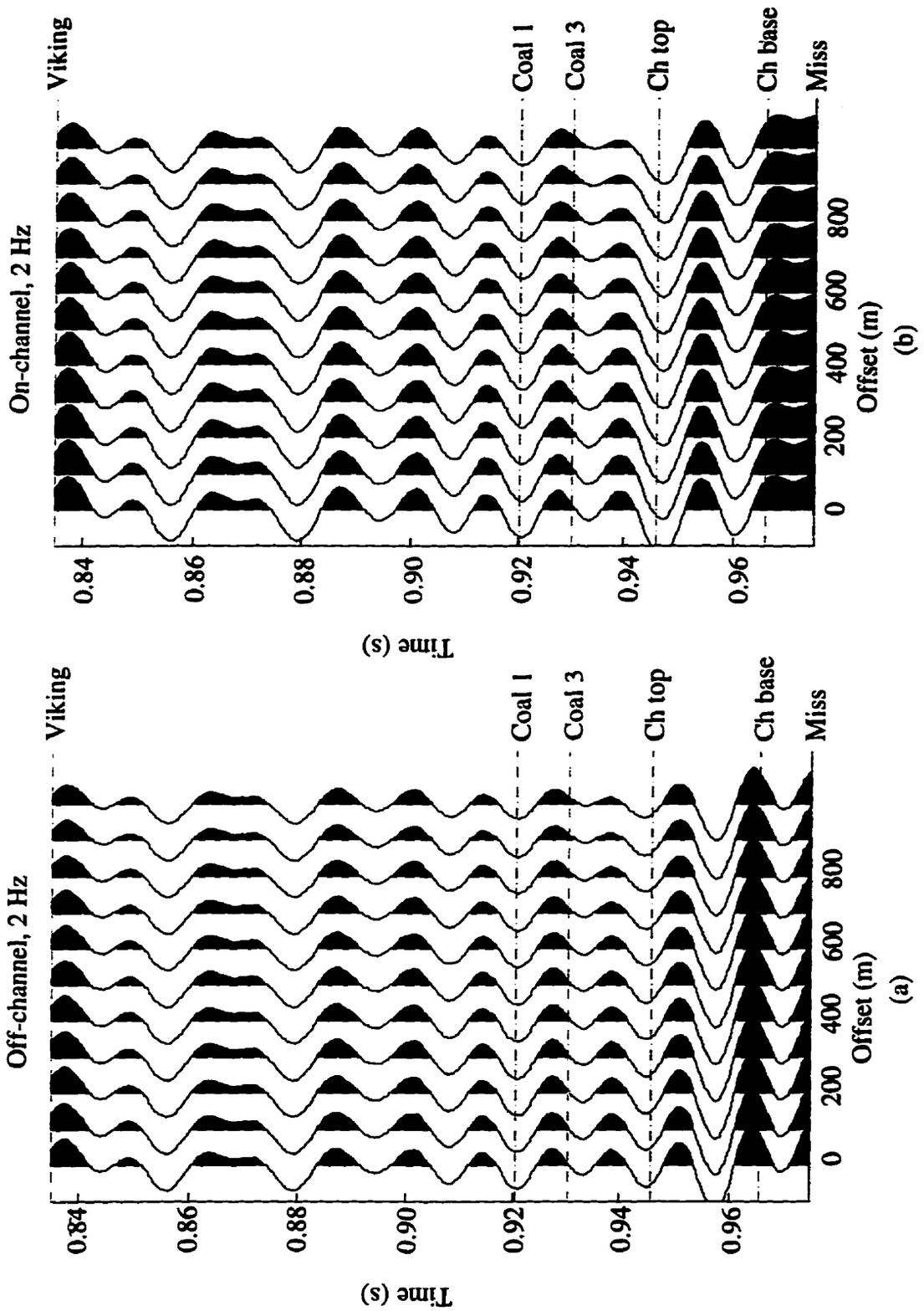

Figure 4.5. Close up view of the 2 Hz CDP gathers. Shown are the Off-channel (a) and on-channel (b) models. Applied filters are 2 Hz low-cut and 90 Hz high-cut.

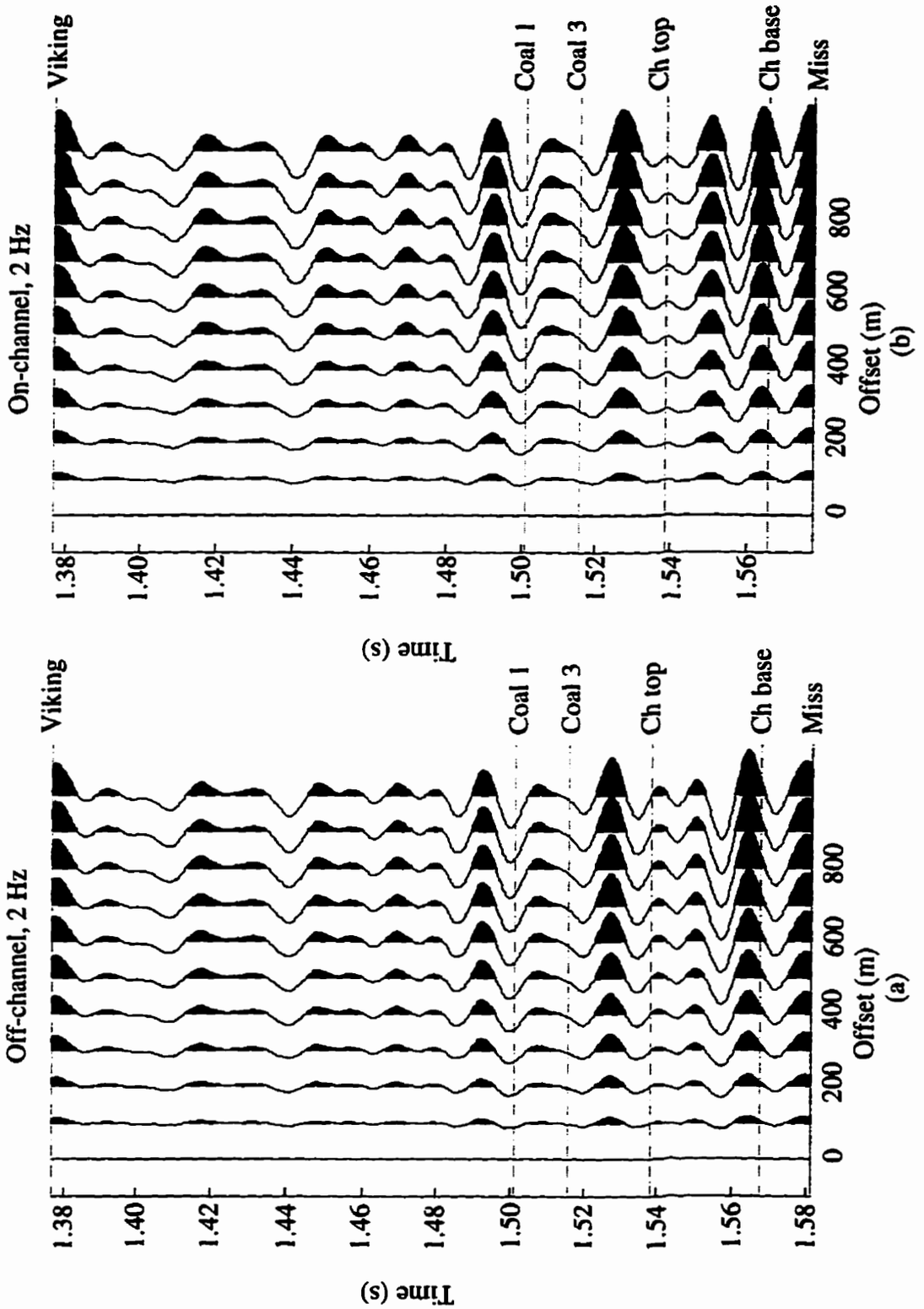

Figure 4.6. Close up view of the 2 Hz CCP gathers. Shown are the Off-channel (a) and on-channel (b) models. Applied filters are 2 Hz low-cut and 60 Hz high-cut.

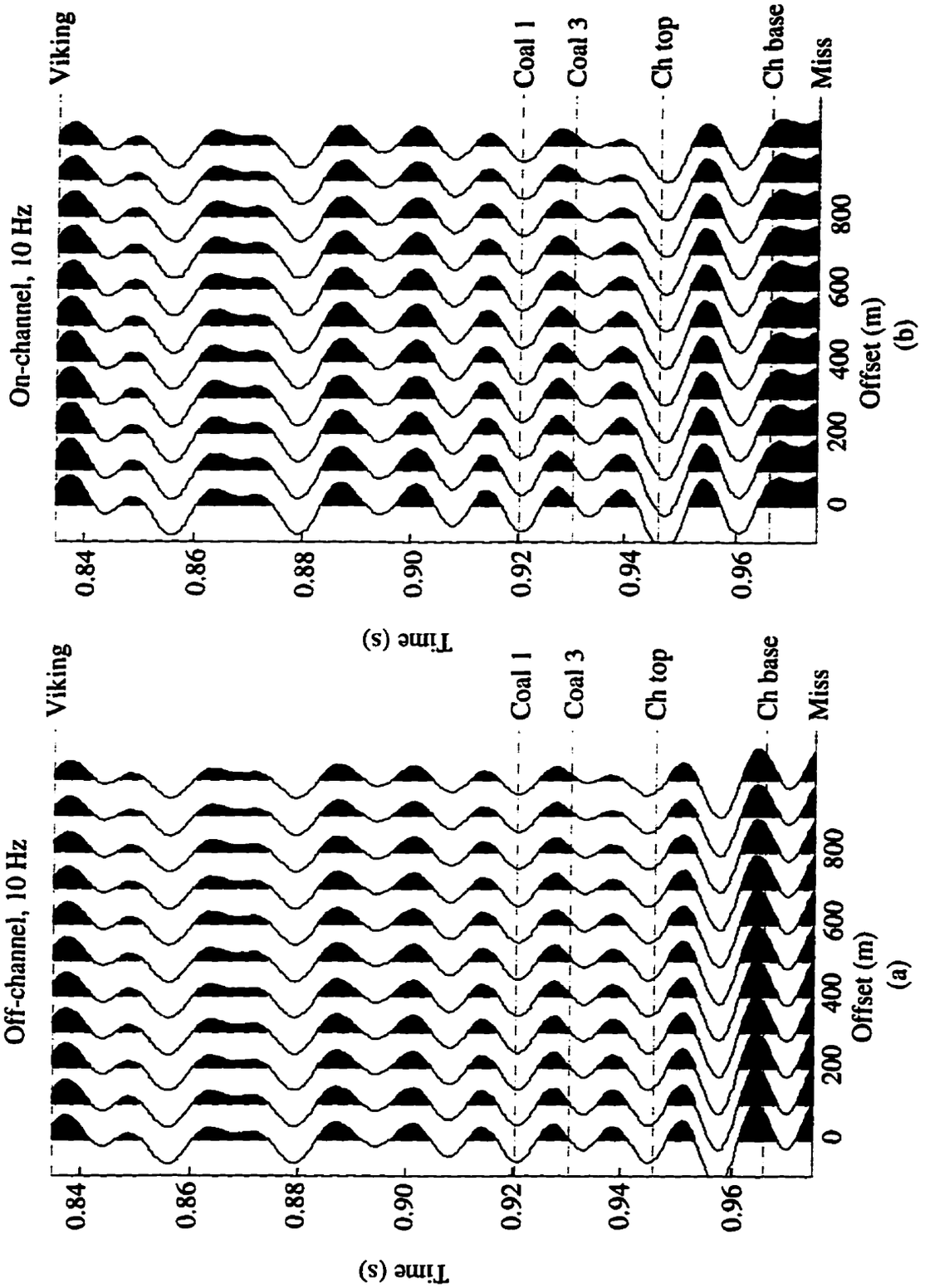

Figure 4.7. Close up view of the 10 Hz CDP gathers. Shown are the Off-channel (a) and on-channel (b) models. Applied filters are 10 Hz low-cut and 90 Hz high-cut.

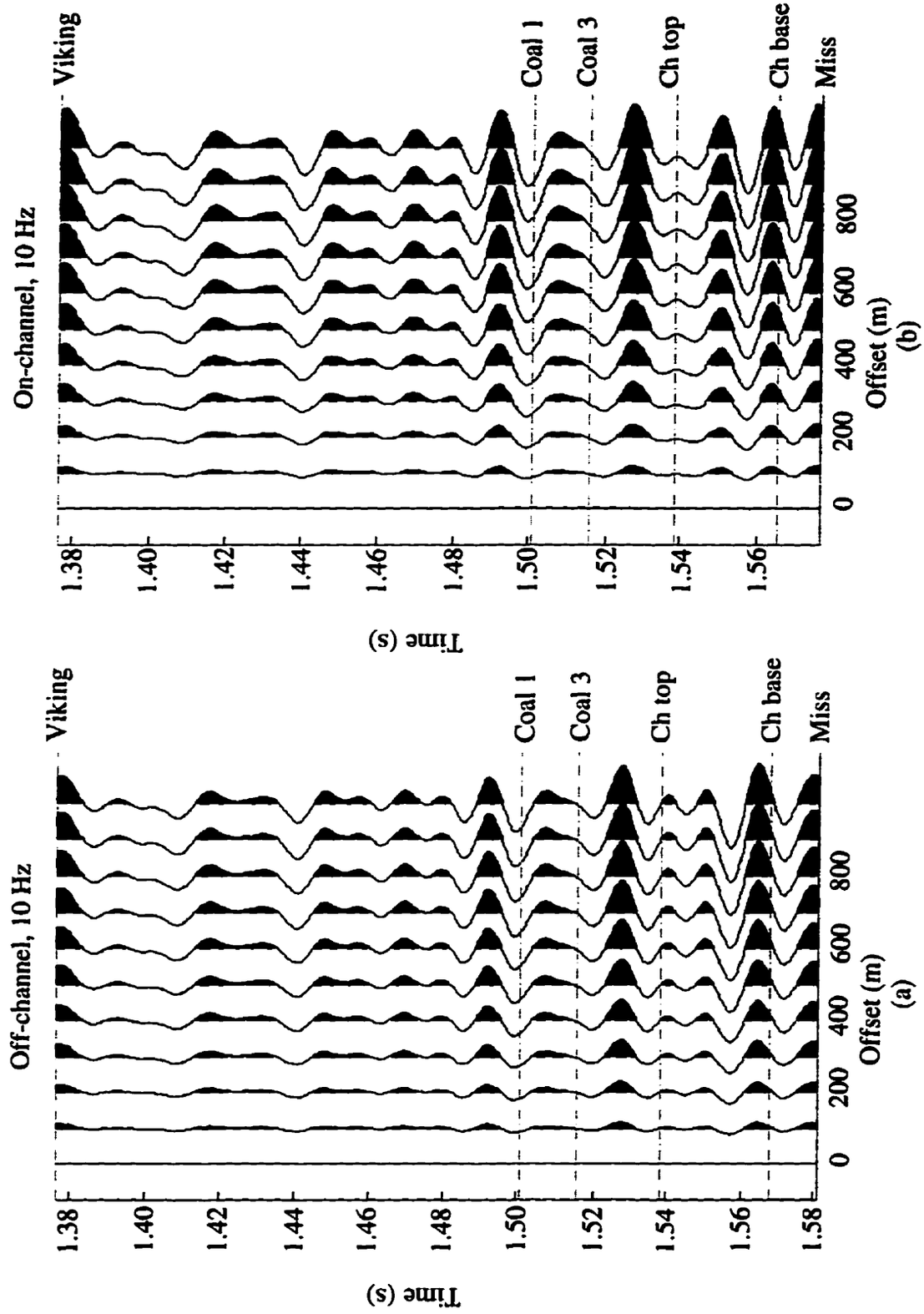

Figure 4.8. Close up view of the 10 Hz CCP gathers. Shown are the Off-channel (a) and on-channel (b) models. Applied filters are 10 Hz low-cut and 60 Hz high-cut.

4.3.2 Inversion of synthetic data

Inversion of the synthetic P-P data was done using the BLIMP method which is described in detail in Section 3.2. The impedance estimate required by BLIMP was obtained from the off-channel model (Figure 4.1a) by converting the Vp and density logs from depth to P-P time and multiplying them together. Figure 4.9 shows the regional logs converted to P-P time and their band-limited counterparts, 4.9a has the 2 Hz high-cut applied and 4.9b 10 Hz. The off- and on-channel gathers of Figure 4.3 were stacked and input to the BLIMP inversion with the off-channel impedance estimate. Two inversions were then computed for each model, one with the frequency split at 2 Hz and the other at 10 Hz. The impedance estimates from BLIMP inversion were then converted to Vp using a best-fit velocity-density relationship (Gardener et al., 1974). The Gardner constants were found using the 08-08-23-23 logs.

Inversion of the synthetic P-S data was done by first stacking the data using the P-S weighted stack of Section 2.3, and then inverting the result using BLIMP. The Vs estimate required for both the weighted stack and the inversion, was obtained from the regional model (Figure 4.1a), by converting the Vs log from depth to P-S time. Figure 4.10 shows the regional logs converted to P-S time and their band-limited counterparts. The Gardner relationship derived for the P-P inversion was assumed for the P-S weighted stack. Two inversions were then computed for each model, one with the frequency split at 2 Hz and the other at 10 Hz.

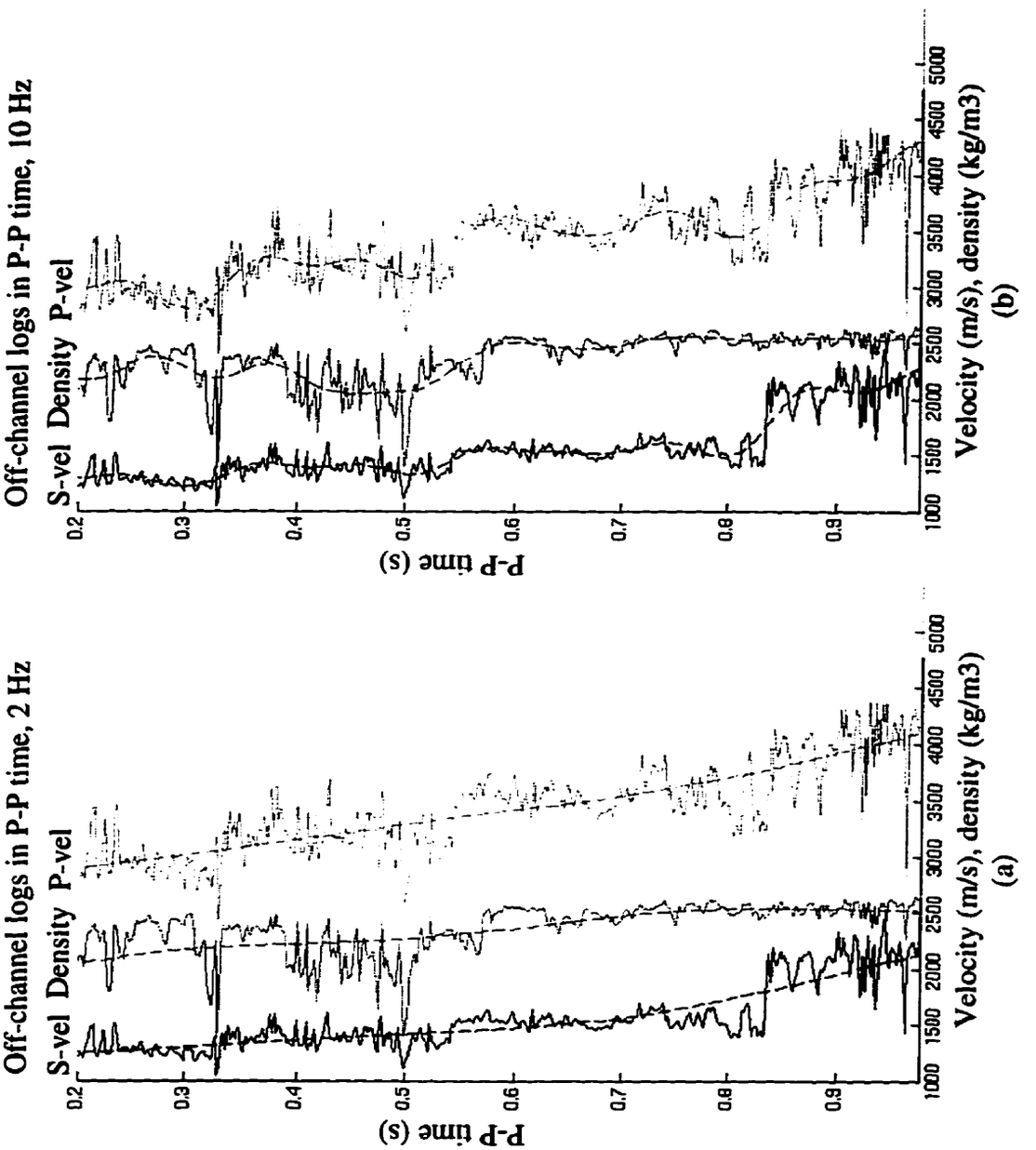

Figure 4.9. Log input to BLIMP inversions for the P-P synthetic data. Figure (a) shows the Vp, Vs and density logs (solid curves) plotted with 0 - 2 Hz pass-filtered logs (dashed curves). Similarly, Figure (b) shows the 0 - 10 Hz pass-filtered logs.

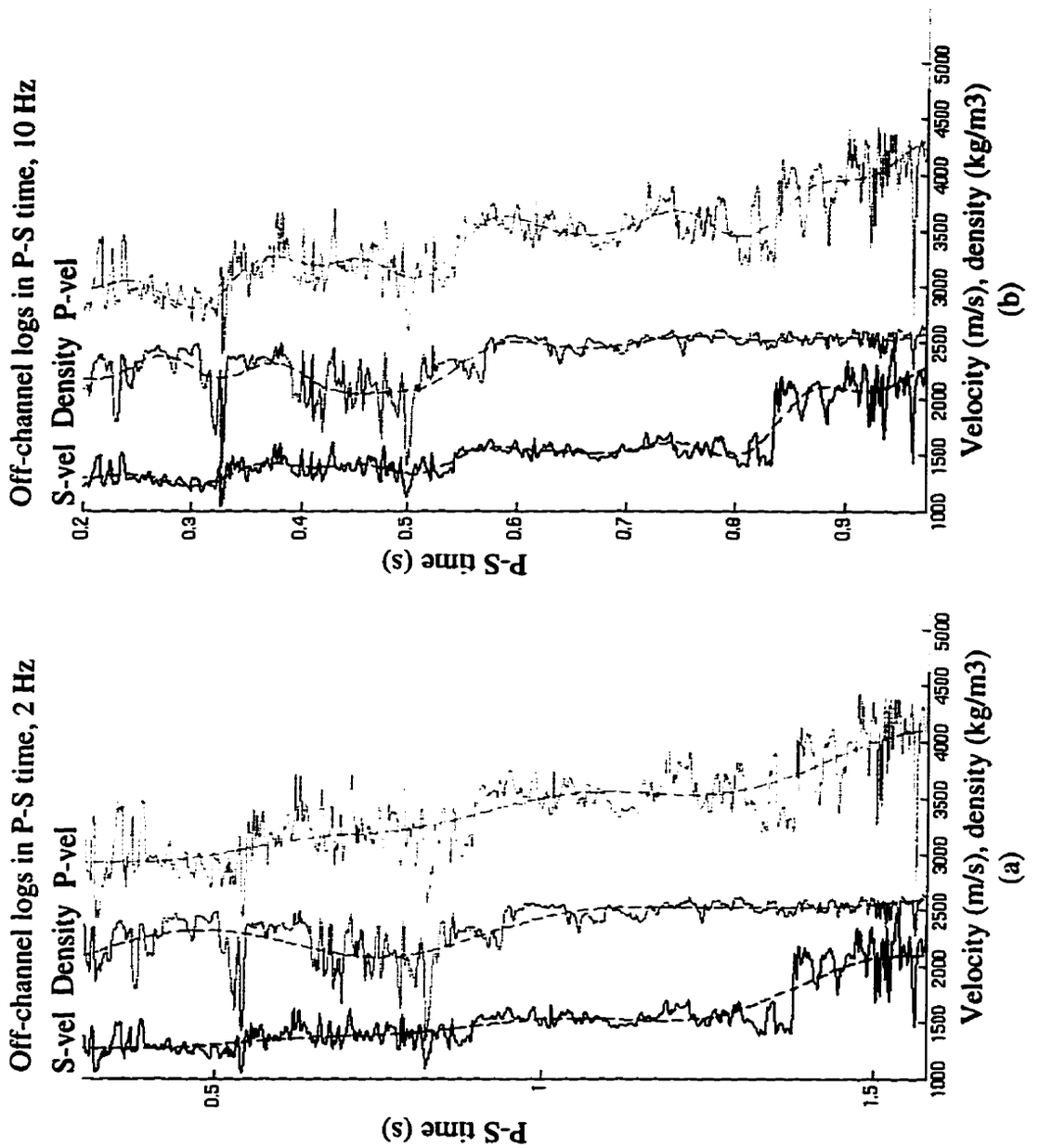

Figure 4.10. Log input to BLIMP inversions for the P-S synthetic data. Figure (a) shows the Vp, Vs and density logs (solid curves) plotted with 0 - 2 Hz pass-filtered logs (dashed curves). Similarly, Figure (b) shows the 0 - 10 Hz pass-filtered logs.

4.3.3 S-wave velocity

Figures 4.11a and b are composite plots of the Vs inversion results for the off- and on-channel models. Of interest is the comparison of the 2 Hz and 10 Hz inversions to the log. Figure 4.11a shows that both the 10 and 2 Hz inversions have resolved the off-

channel Vs quite well. Differences between them indicate that filter performance at 2 Hz may be different than at 10 Hz (the true Vs log was used to provide the low-frequency in the estimate hence, the results should be very close). A solution may be to build models which provide data that extends well below the zone of interest. This would generate a greatly extended reflectivity sequence which would provide more 2 Hz frequency samples for filtering. Fortunately, in the real data case to follow, the record lengths extend to more than twice the time of the zone of interest, thus filter performance should be less of a concern.

The on-channel comparison shows that both the 2 Hz and 10 Hz inversions are not quite able to image the velocity increase in the on-channel model relative to the off-channel model. The difference is an underestimate of about 200 m/s.

4.3.4 P-wave velocity

Figures 4.12a and b are composite plots of the Vp inversion results for the off- and on-channel models. Again of interest is the comparison of the 2 Hz and 10 Hz inversions to the log Vp. Figure 4.12a shows that both the 10 and 2 Hz inversions have resolved the off-channel Vp quite well, with differences possibility due to poor filter performance at 2 Hz relative to 10 Hz.

The on-channel comparison shows that the 2 Hz inversion is not quite able to image the velocity decrease in the on-channel model relative to the off-channel model.

4.3.5 Vp/Vs

The inversion results for the above models were used to generate Vp/Vs estimates for the two models. Figures 4.13a and b are the resulting estimates. The off-channel Vp/Vs has been resolved by both the 2 Hz and 10 Hz data. The on-channel Vp/Vs has been resolved less well by inversion, but does show a decrease relative to off-channel.

Again, with longer records (the field data are twice as long) the Vp/Vs decrease should be distinct.

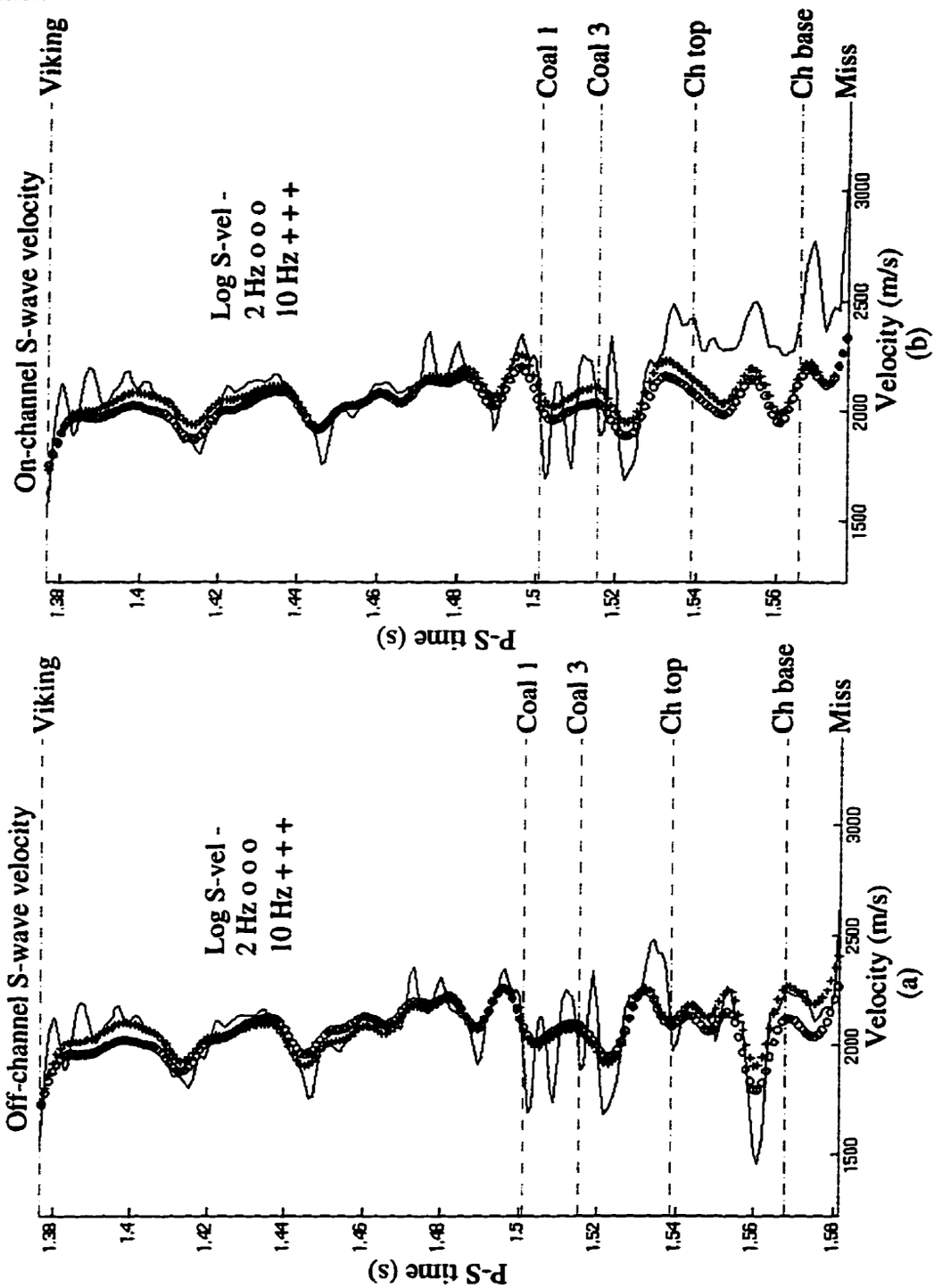

Figure 4.11. Comparison of inversion Vs to model Vs. The off-channel log was used as input for both off- and on-channel inversions. Good recovery of off-channel Vs by both 2 Hz and 10 Hz inversion. Less well resolved is the on-channel Vs.

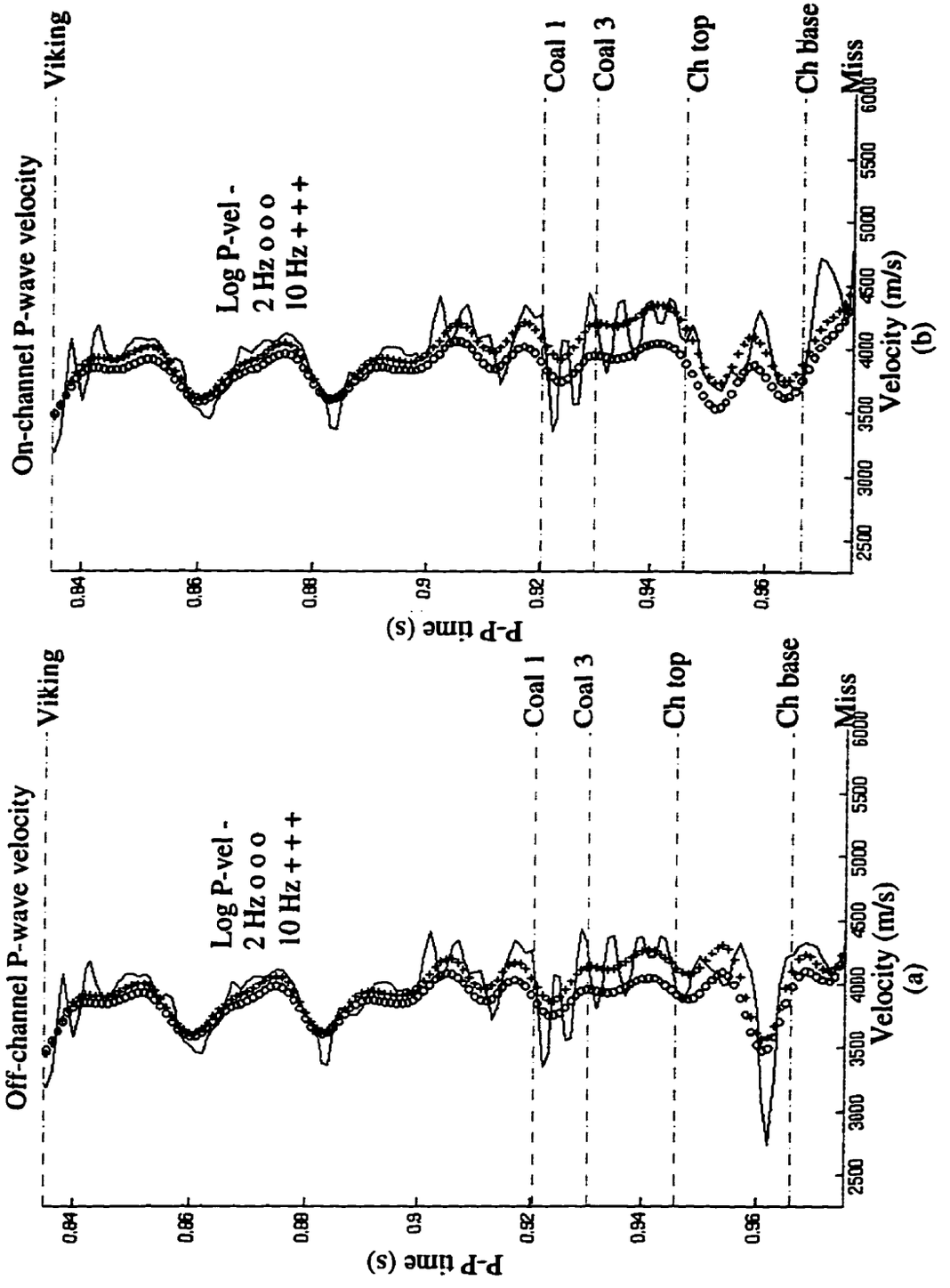

Figure 4.12. Comparison of inversion Vp to model Vp. The off-channel log was used as input for both off- and on-channel inversions. Good recovery of off-channel Vp by both 2 Hz and 10 Hz inversion. Less well resolved is the on-channel Vp by the 2 Hz data.

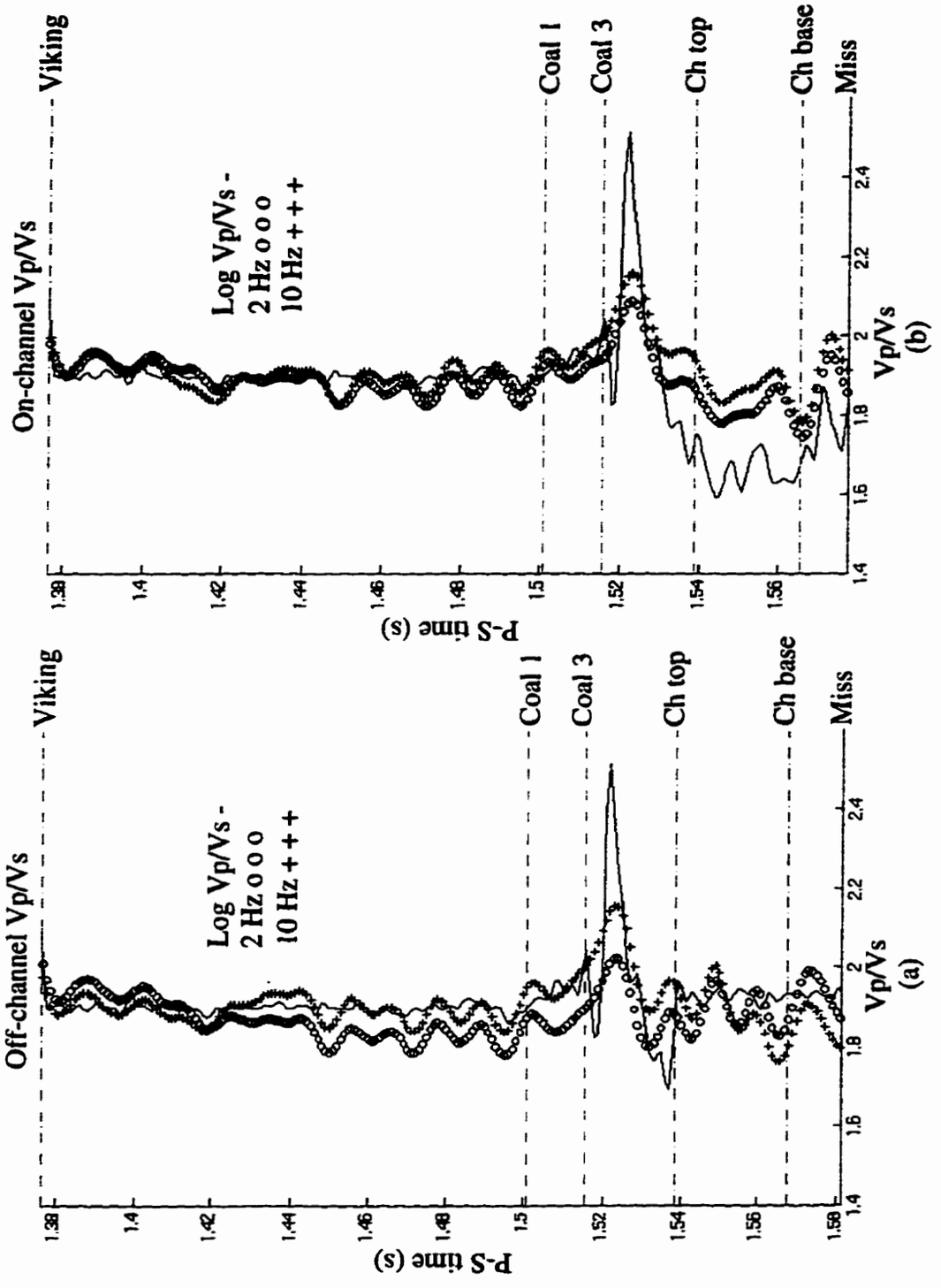

Figure 4.13. Comparison of inversion Vp/Vs to model Vp/Vs. The off-channel log was used as input for both off- and on-channel inversions. Good recovery of off-channel Vp/Vs by both 2 Hz and 10 Hz inversion. Less well resolved is the on-channel Vp/Vs by the 10 Hz data.

4.4 Processing of the Blackfoot survey

The seismic data from the Broad-band Blackfoot 3C-2D were processed, and all three frequency ranges of single geophone data were inverted. A detailed description of the Blackfoot survey can be found in Section 1.3.2. The goals of processing were to provide seismic data which represented true amplitude, with broad-band frequency range and zero phase. Inversions were computed for each data set and Vp/Vs ratios were calculated.

The geologic targets in the Blackfoot Field were the Glauconite channel-sands of the Lower Cretaceous. These sands are often difficult to resolve with conventional seismic recordings (Stewart, 1995). Stratigraphic interpretation of the 10 Hz P-P component data hinted at a possible oil-bearing sand beneath the traverse of the seismic line (Miller et al., 1995). Modeling using well-logs from the Blackfoot area indicated that Vp/Vs values should decrease in transition from the reservoir sands (Vp/Vs ~ 1.67) to regional shales (Vp/Vs ~ 1.89). Seismic modeling showed that inversion of band-limited seismic data might resolve Vp/Vs changes enough to provide a potential reservoir indicator. By recording low frequencies (< 10 Hz), the 4.5 Hz and 2 Hz seismic inversions depend less on a-priori velocities and hence, were expected to return more accurate rock velocities compared to the 10 Hz data.

4.4.1 Preliminary processing

The goals of seismic processing were to achieve the optimal data sets for velocity inversion in terms of true amplitude, broad-band frequency and zero phase. The preliminary data sets were obtained from Sensor Geophysical of Calgary, Alberta with the following processing applied:

a) Geometry Assignment (Asymptotic binning for P-S component, Vp/Vs =2.2)

b) Trace Edits

c) Shot-mode FK Filter

d) Spherical Divergence correction

e) Surface-Consistent Spiking-Decon

f) Time Variant Spectral Whitening

g) Statics

h) Normal moveout correction

At no point in the above processing flow were automatic gain control or trace to trace equalization applied.

4.4.2 Processing for inversion

The goals of the next processing stage were to remove noise in the data, as well as remove any residual wavelet. This was done using F-X deconvolution and spiking deconvolution. The data were then phase-shift migrated. The P-P data were processed using the following processing flow:

a) Trace edits

b) Surface Consistent Amplitude Correction

c) CDP Stack

d) F-X Decon

e) Spiking Decon (zero phase)

f) High-cut filter

g) Phase Shift Migration

h) Phase correction

i) Band-limited inversion

k) Conversion of impedance to P-wave velocity

The three low-end frequency ranges for the P-S component data were processed using the following flow:

a) Trace edits

b) Surface Consistent Amplitude Correction

c) Common Offset Binning: Bin width = 40m

d) F-X Decon of Common Offset Planes

e) Spiking Decon (zero phase) of Common Offset Planes

f) High-cut filter

g) Phase Shift Migration of Common Offset Planes

h) P-S weighted stack

i) Phase correction

j) Band-limited inversion

Because P-S inversion requires a weighted P-S stack the data were processed in common-offset gathers.

The next Sections will describe in detail the processing of the 2 Hz an 10 Hz data sets.

4.4.3 Surface consistent amplitude correction

Many factors influence the quality of data recorded during a seismic survey leading to incorrect representation of reflectivity information. A number of these factors are charge energy, the coupling of the charge to the ground, geophone response, geophone coupling to the ground, channel to channel differences in the recorder, shot to receiver offset and ray-path in the subsurface. Of the previous list all but the last two can be considered as seismic noise. Surface consistent amplitude correction is a process by which this seismic noise is removed. Amplitudes are broken down into their contributing components in a surface consistent manner, and then amplitude corrections are applied to each trace. The result is, idealy, a seismic dataset that is free from trace to trace amplitude variations that are not directly the result of impedance contrasts in the subsurface.

The full suite of surface consistent amplitude corrections were computed and applied to the P-P data. Because the inversion of the P-S data requires AVO information, the surface consistent offset component was included in the computations but was not applied to the traces.

The zero offset stacks and frequency spectra of the 2 Hz and 10 Hz P-P data are given in Figures 4.14 and 4.15. The stacked sections (Figures 4.14a and b) appear quite similar with the 2 Hz data having more peak to trough amplitude, especially between 1050 ms and 1100 ms and shotpoints 161 and 201. The 2 Hz data has coherent noise through the section between shotpoints 191 to 211. The frequency spectra (Figures 415a and b) are quite similar, large differences being confined to the sub-10 Hz range, the 2 Hz data having an average three decibels (dB) more than the 10 Hz data between 2 Hz and 10 Hz. Both datasets appear to have useable frequency, assuming a background noise level of -30 dB, up to about 85 Hz.

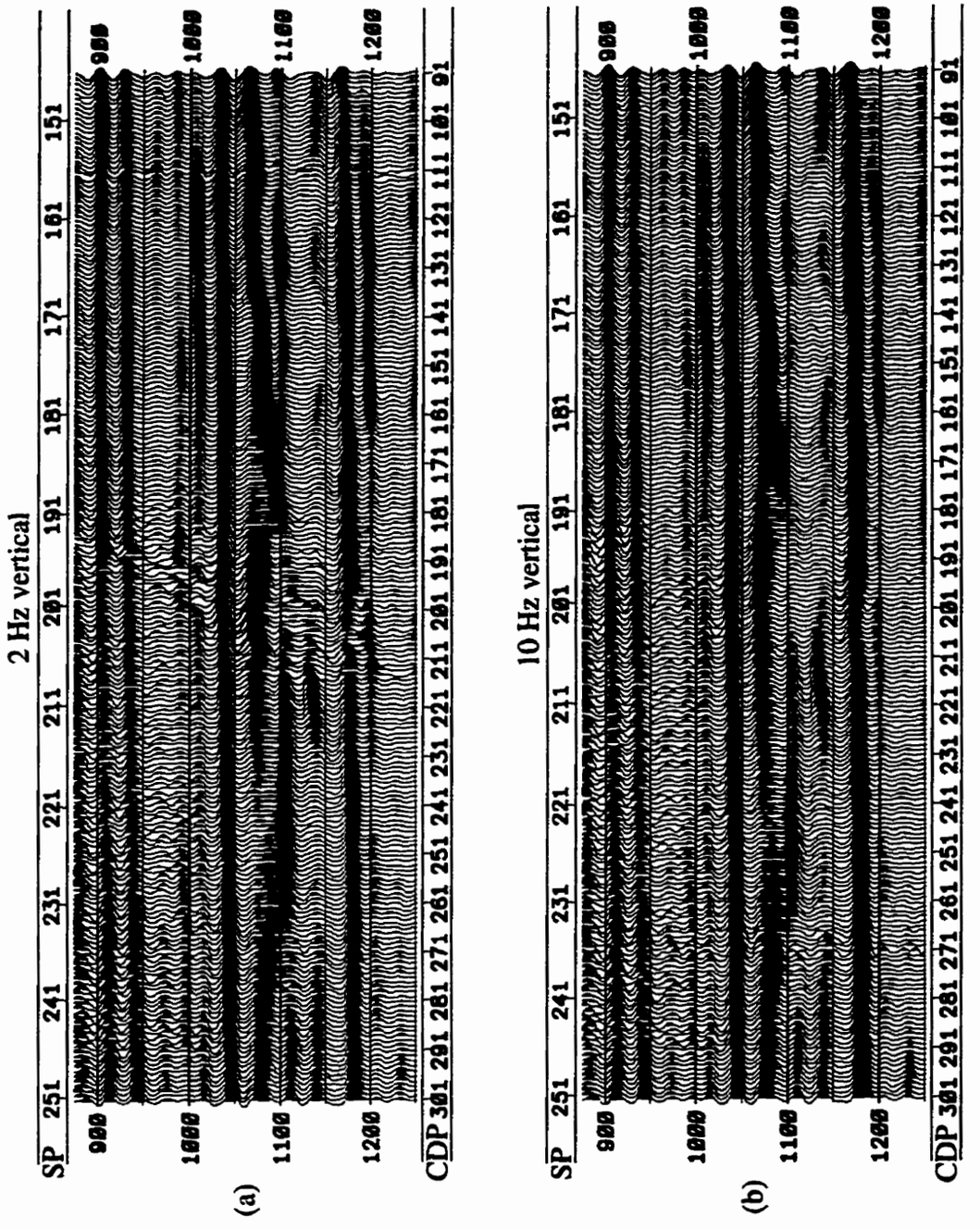

Figure 4.14. Stacked sections, (a) 2 Hz vertical and (b) 10 Hz vertical.

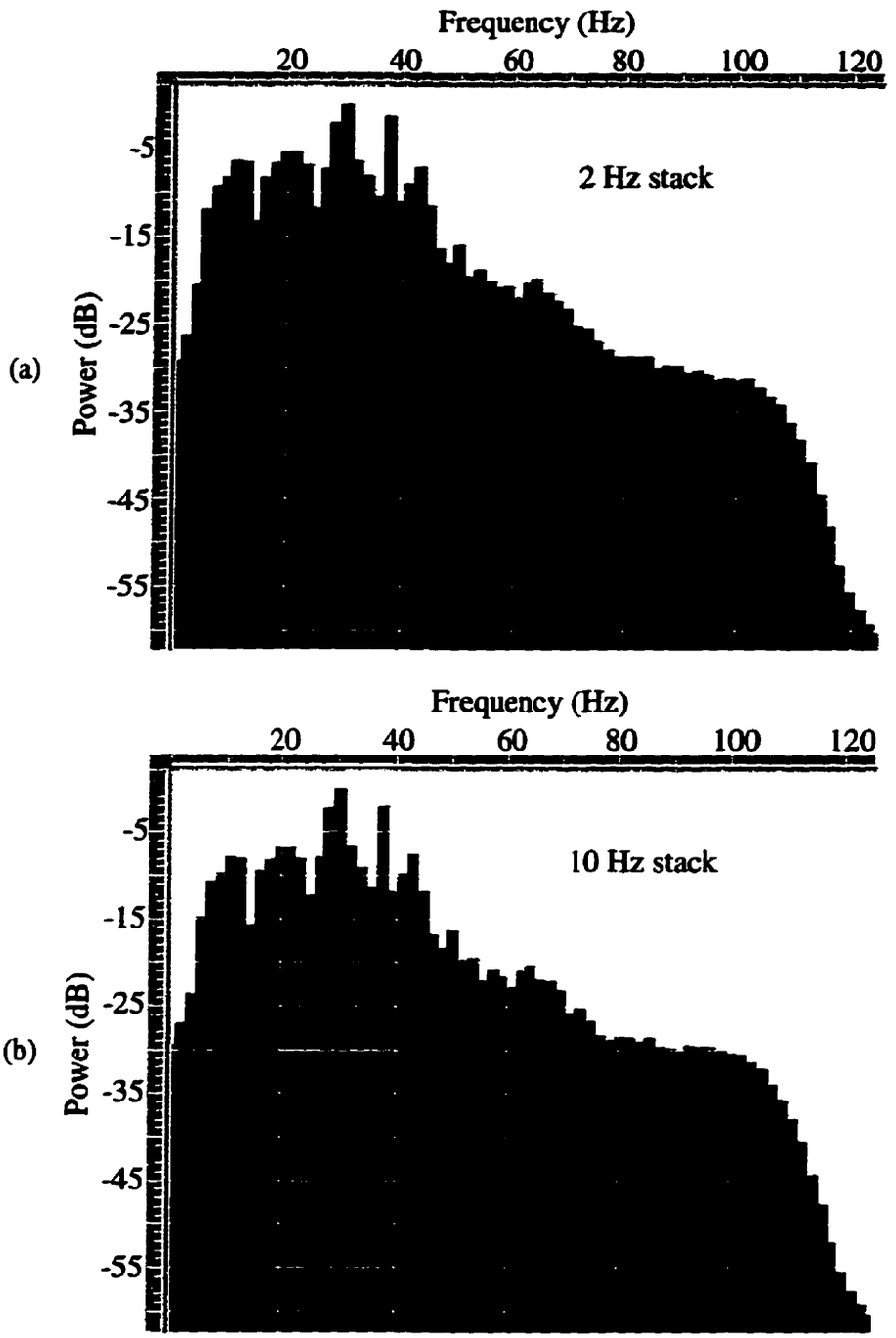

Figure 4.15. Frequency spectra of stacked sections, (a) 2 Hz vertical and (b) 10 Hz vertical. The 2 Hz spectra shows an average 3 dB more power between 2 and 10 Hz.

4.4.4 Common offset binning and stacking of P-S data

P-S inversion required processing of the P-S data to be applied prior to stack. To facilitate this the P-S data were grouped into common conversion point gathers. Each trace within a gather was assigned an offset bin based on absolute value of offset and a bin width of 40 meters. These bins were then stacked into single traces. The result was first, the number of traces was reduced by a factor of two and second, pre-stack processing could be accomplished by grouping the data into panels of common offset and applying each processing step one panel at a time.

CCP stacks and frequency spectra for the 2 Hz and 10 Hz P-S data are given in Figures 4.16 and 4.17. The stacked sections were computed by stacking the offset sections into a single trace plane. The 2 Hz radial line was shorter than the rest of the lines in the survey due to limited numbers of 2 Hz geophones. Comparison between Figures 4.16a and 4.16b shows the 2 Hz data to be noisier than the 10 Hz data. A peak occurring between shotpoints 161 and 181 and 1650 ms and 1700 ms on the 2 Hz data has larger amplitude than the corresponding peak on the 10 Hz data. The frequency spectra are quite similar, large differences being confined to the sub-10 Hz range, the 2 Hz data having an extra six dB between 2 and 6 Hz. Both datasets appear to have useable frequency, assuming a background noise level of -20 dB, up to about 70 Hz.

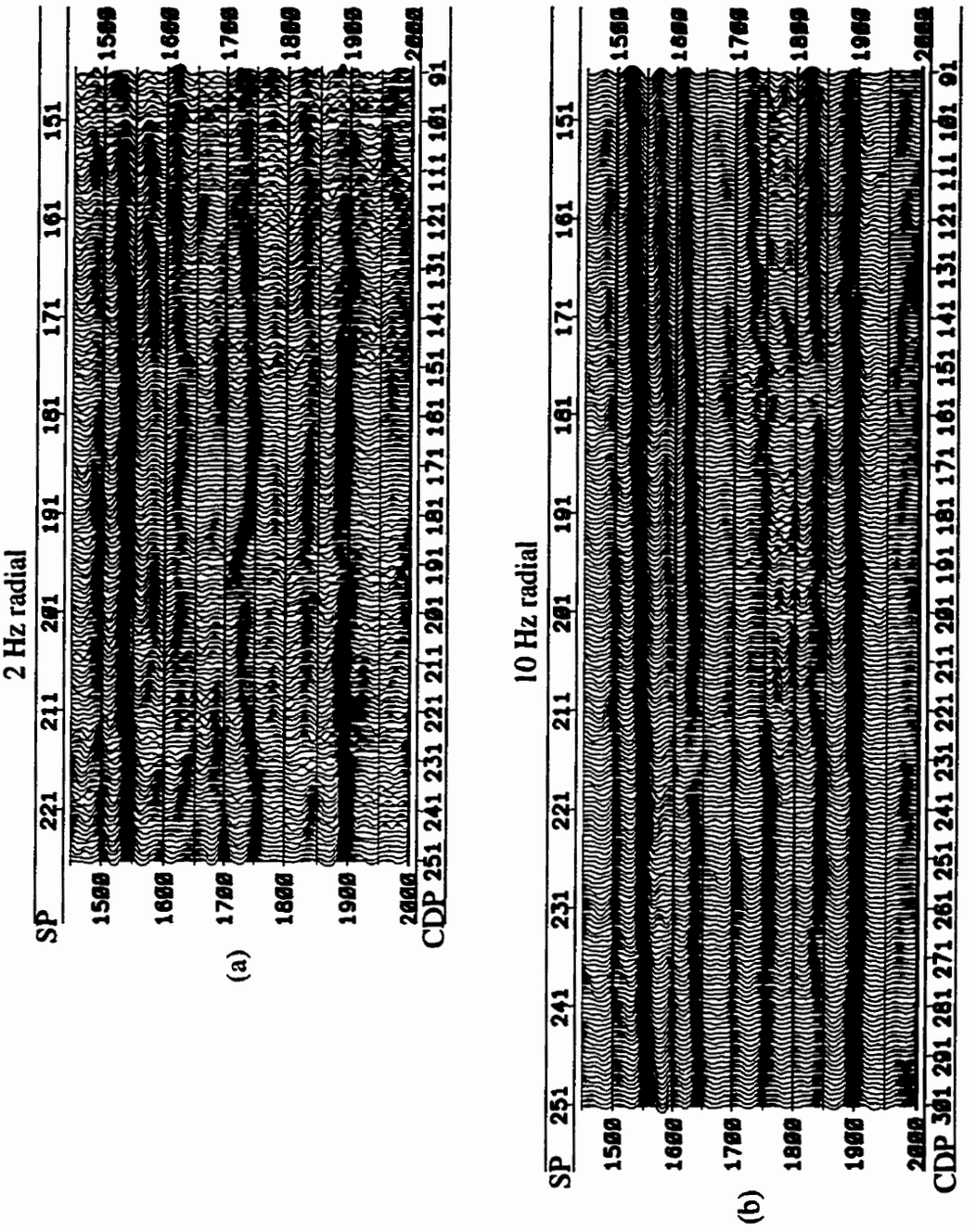

Figure 4.16. Stacked sections, (a) 2 Hz radial and (b) 10 Hz radial. The 2 Hz line has fewer CDPs due to shorter surface acquisition.

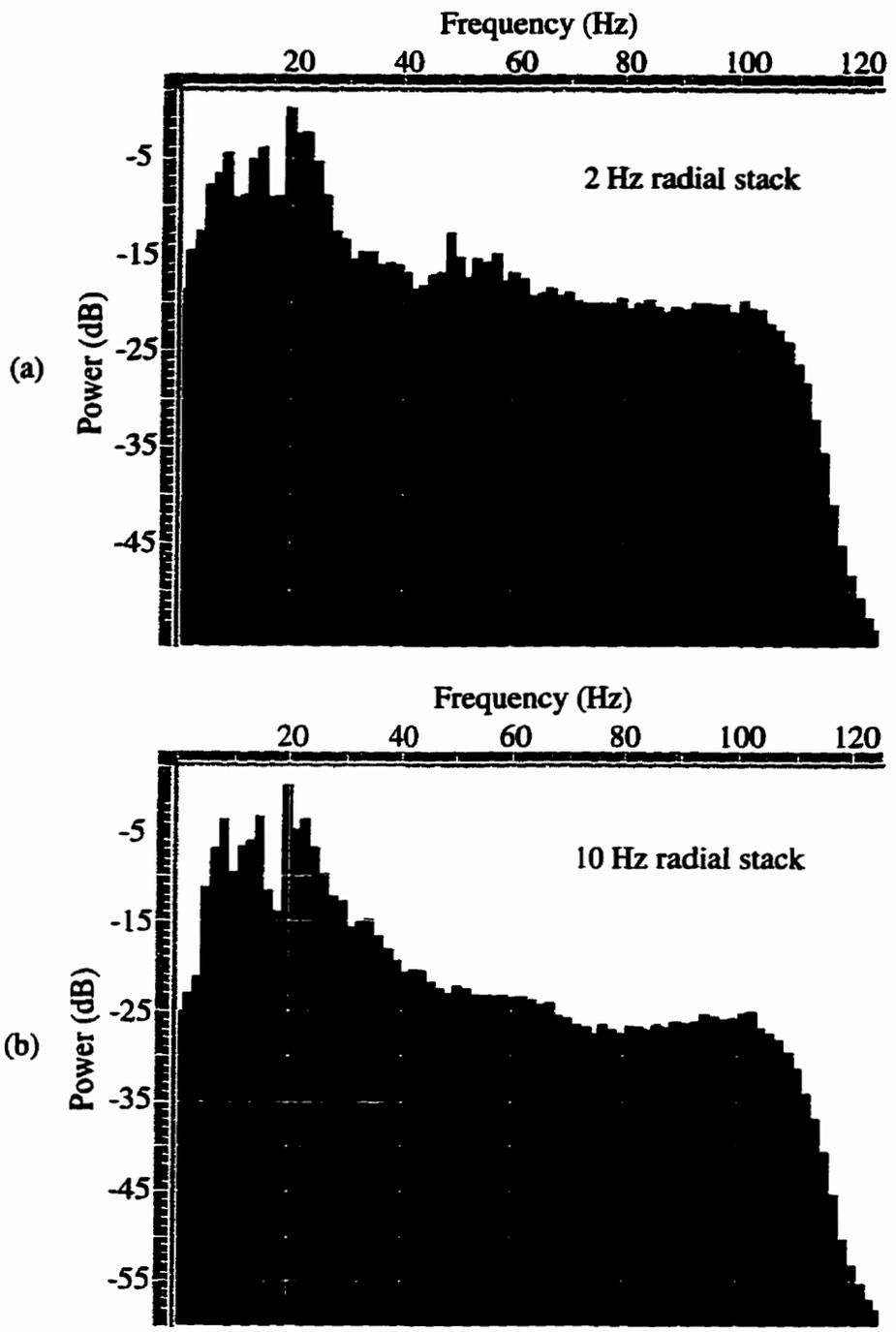

Figure 4.17. Frequency spectra of stacked sections, (a) 2 Hz radial and (b) 10 Hz radial. The 2 Hz data have an average of 6 dB more power between 2 Hz and 10 Hz than the 10 Hz data.

4.4.5 Noise reduction

The data from Blackfoot broad-band survey used in this study were expected to be especially susceptible to seismic noise because they were recorded without surface arrays. F-X decon was used for noise reduction due to its robust performance and simplicity of design. It is a process by which coherency filters are computed and applied in the F-X domain, with the aim of reducing random noise (Gulunay, 1986). It was assumed that any coherent noise had been removed by Sensor Geophysical during the shot-mode FK step of the preliminary processing.

After application of F-X decon to the P-P data it was found that the higher frequencies (75 - 85 Hz) in the useable range were attenuated relative to the background noise. The three dB of extra low-frequency was preserved on the 2 Hz data relative to the 10 Hz data. A coherent noise train was enhanced by F-X decon on the 2 Hz data between shotpoints 191 and 211. It was found that trace to trace equalization applied pre-stack eliminated this event. However, such a process was found to reduce trace to trace amplitude changes indicative of lithologic changes. Therefore, equalization was not applied.

Application of F-X decon to the P-S data was found to attenuate useable frequencies between 30 and 70 Hz relative to the background noise. This range of frequency attenuation was large compared to the P-P data suggesting that these higher frequencies may not be reliable. Indeed, the two P-S sections were found to be similar only in a low-frequency sense. The six extra dB of low-frequency were preserved on the 2 Hz data relative to the 10 Hz data. The next step in processing was to attempt to restore the attenuated high-frequency and to remove any residual wavelet energy using spiking deconvolution.

4.4.6 Spiking deconvolution

Spiking deconvolution (spiking decon) was applied to compensate for the filtering effect of F-X decon at higher frequencies and to remove any residual wavelet. Spiking decon is a process by which an inverse filter is derived which, in a least-squares sense, converts the auto correlation of a seismic trace to a zero lag spike (Yilmaz, 1987).

High-cut filters were applied after the application of spiking decon to the P-P data. Migration testing had shown that frequencies higher than about 80 Hz were causing migration artifacts. The spectra within this new frequency range show good spectrum flattening. The coherent noise train on the 2 Hz P-P data between shotpoints 191 and 211 was eliminated, it's origin remaining a mystery.

The P-S data were also high-cut filtered after application of spiking decon. Again due to high-frequency artifacts in migration. The spectra within this new frequency range showed good spectrum flattening.

4.4.7 Phase shift migration

Phase shift migration was applied to the data using stacking functions derived by Sensor Geophysical. For the P-P data this process was applied to the stacked data with F-X decon and spiking decon applied and a high-cut filter of 75-85 Hz to eliminate high-frequency artifacts.

The P-S data were migrated as common offset panels which in turn had F-X decon, Spiking decon and high-cut filters (50-60 Hz) applied. Migration of P-S data by the phase-shift method proceeded as described by Harrison (1992).

Figures 4.18 and 4.19 show the 2 Hz and 10 Hz P-P data after phase shift migration. Note the differences between the two stacked sections (Figures 4.18a and 4.18b) between 1050 and 1100 ms and shotpoints 161 and 191. Both sections show a structural low which might indicate an incised river channel. However, the 2 Hz data resolve two extra amplitude events, one at about 1060 ms between shotpoints 166 and 182,

and the other at about 1075 ms between shotpoints 171 and 179. The lower of the two events was interpreted to be the top of the Mississippian.

The frequency spectra of Figures 4.19a and 4.19b are very similar except below 10 Hz where the 2 Hz data gained four dB over the 10 Hz data

Figure 4.20 and 4.21 show the 2 Hz and 10 Hz P-S data after phase shift migration. Note the differences between the two stacked sections at the zone of interest between 1650 and 1750 ms and shotpoints 161 and 191. Significant differences between the two P-S sections are numerable, however the most notable difference occurs in the zone of interest. The 2 Hz data resolve a strong increase in amplitude at 1700 ms between shotpoints 171 and 184. The same location on the 10 Hz data also shows an amplitude increase but it is not distinct from the background peak.

The frequency spectra of Figures 4.21a and 4.21b are very similar except below 10 Hz where the 2 Hz data have about two dB over the 10 Hz data

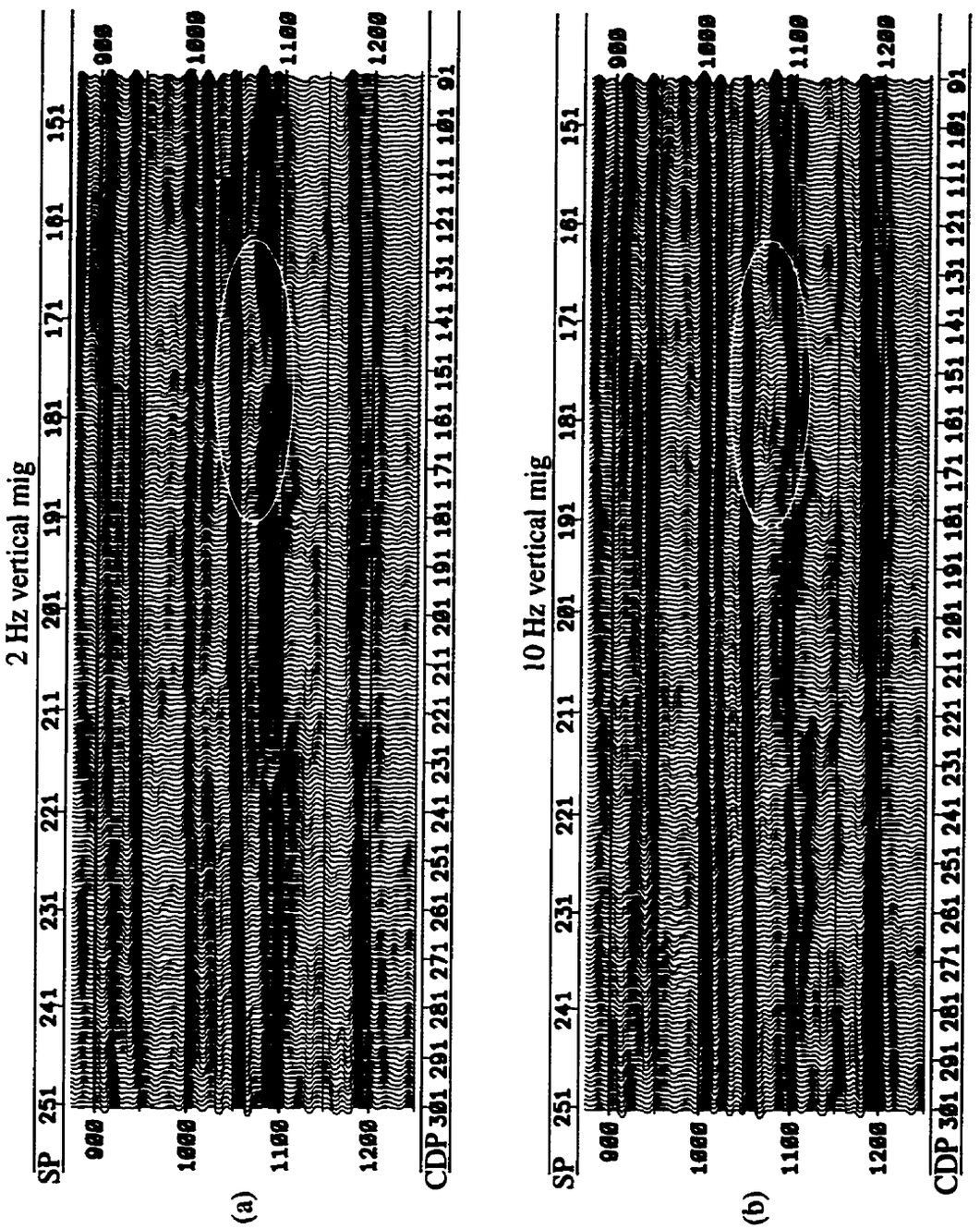

Figure 4.18. Migrated stacks, (a) 2 Hz vertical, (b) 10 Hz vertical. An interpreted Glauconite channel is circled. The 2 Hz data resolve two events in the channel structure. The lower of the two events is interpreted to be the top of the Mississippian.

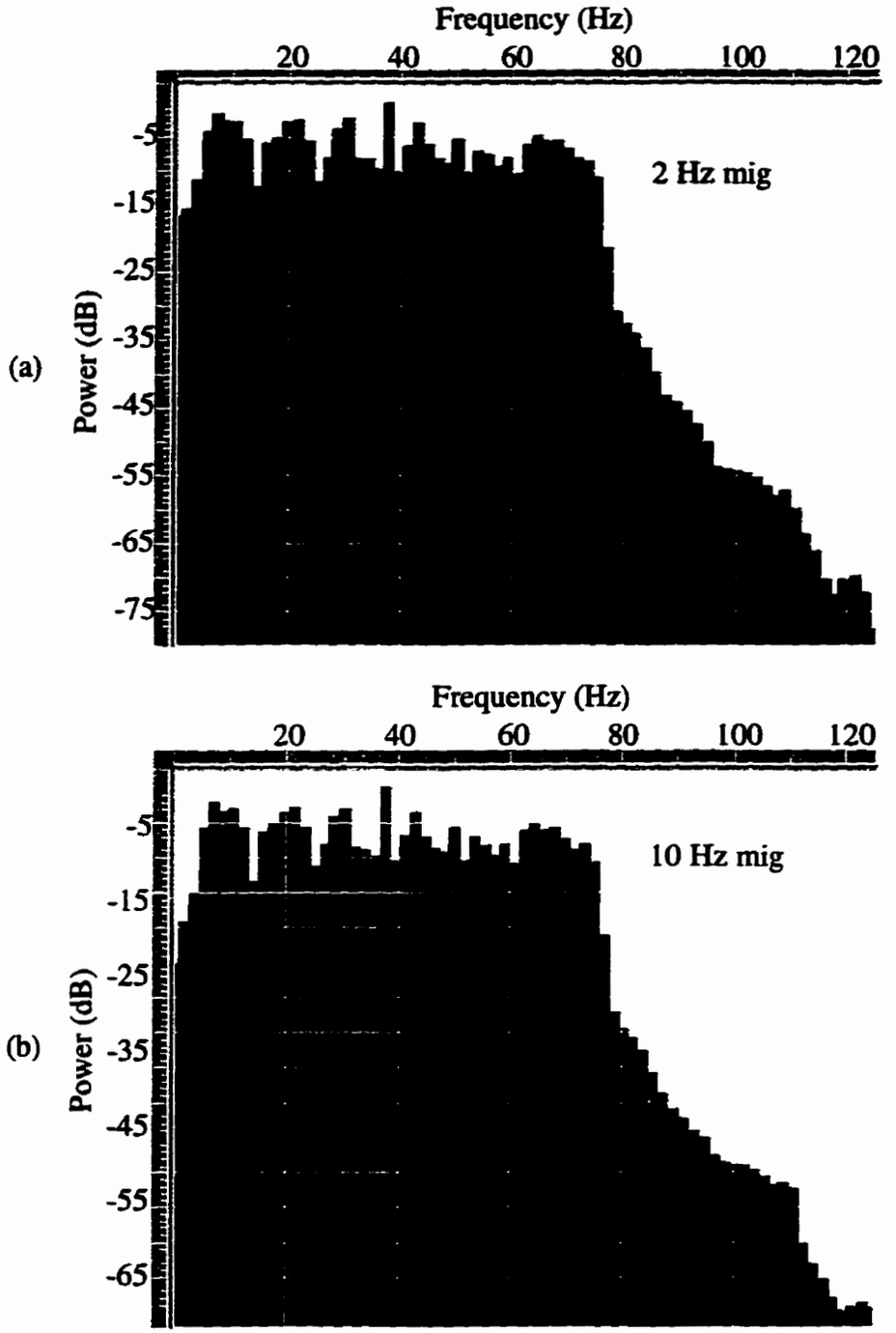

Figure 4.19. Frequency spectra of migrated sections, (a) 2 Hz vertical and (b) 10 Hz vertical. The 2 Hz spectra shows an average 4 dB more power between 2 and 10 Hz.

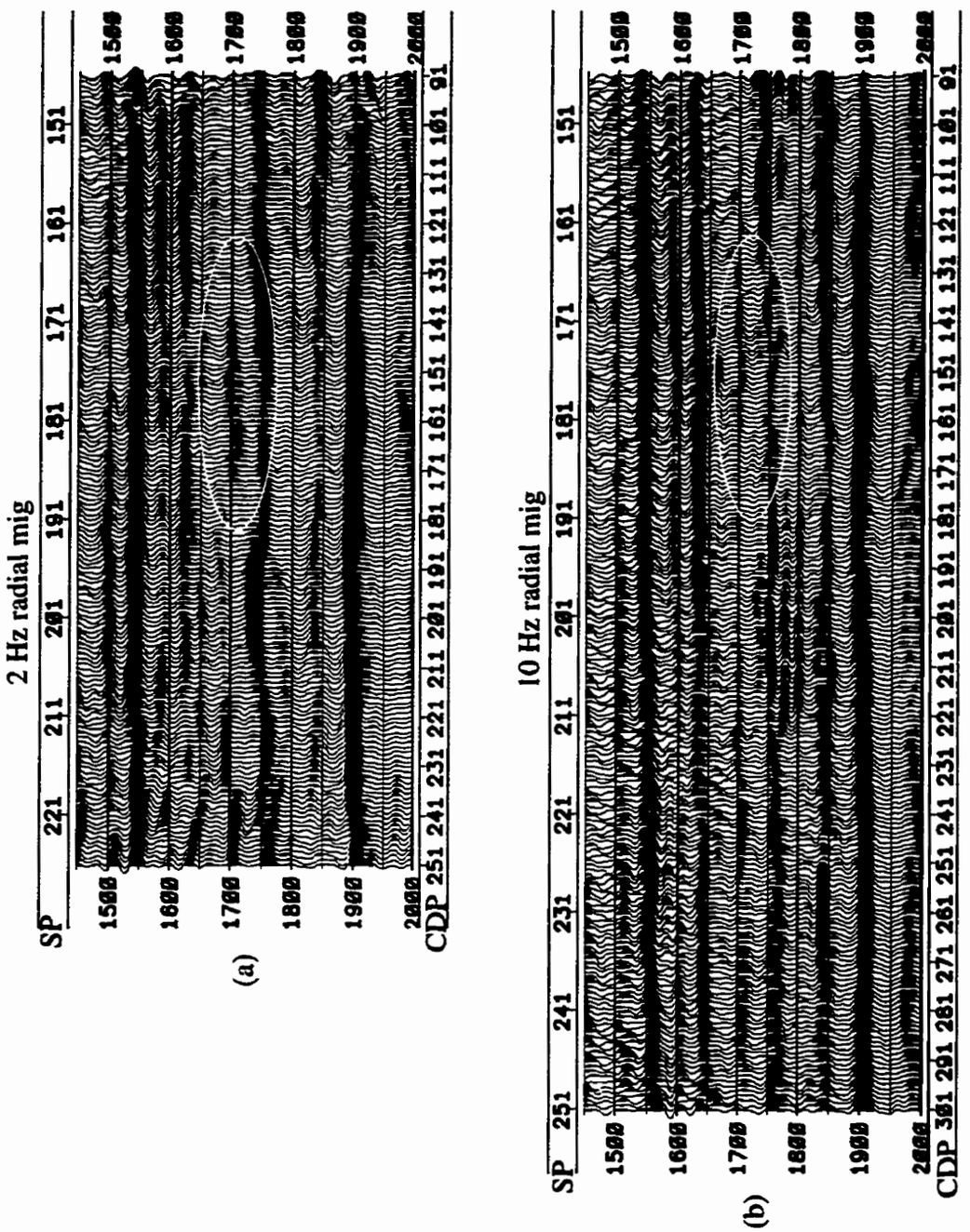

Figure 4.20. Migrated stacks, (a) 2 Hz radial, (b) 10 Hz radial. An interpreted Glauconite channel is circled. The 2 Hz data resolve a large peak in the channel structure.

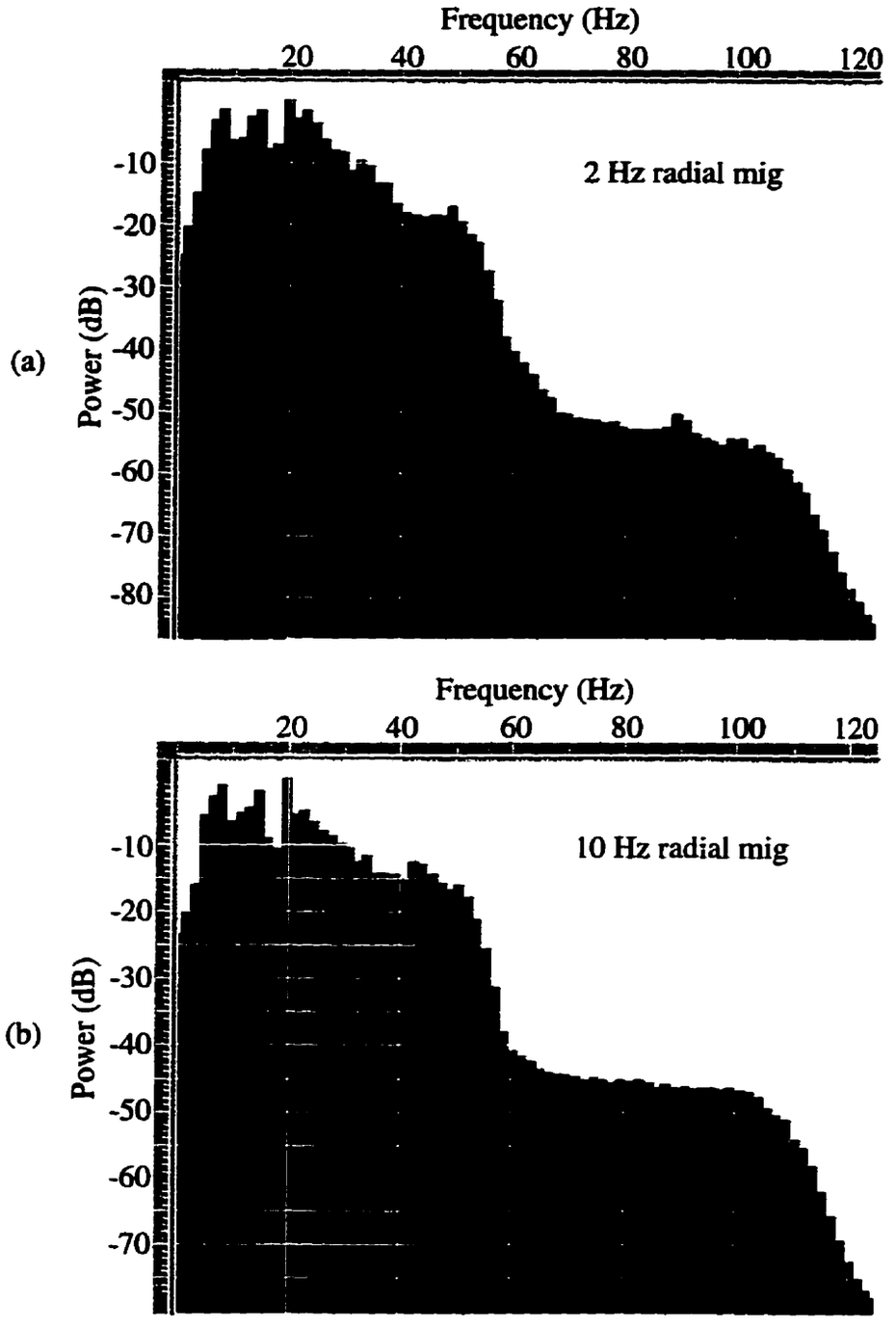

Figure 4.21. Frequency spectra of migrated sections, (a) 2 Hz radial and (b) 10 Hz radial. The 2 Hz spectra shows an average 2 dB more power between 2 and 10 Hz.

4.4.8 P-S weighted stack

The required background values for the P-S weighted stack were obtained from the regional log model of Figure 4.1a. Figure 4.22 shows the Vp and Vs models stretched to tie the P-S data. Care was taken to ensure that the log to seismic correlations were optimal for all three frequency ranges.

Because differences in overall scale of the input CCPs were found to cause error in the stacked results, the synthetic data of Figure 4.3b were used to estimate an optimum scale for each of the 2 Hz, 4.5 Hz and 10 Hz data. Filters were first applied to the synthetic CCP gather, a different low-cut filter for each frequency range (2 Hz, 4.5 Hz and 10 Hz). Then weighted stacks were computed and the RMS amplitude of each stack was noted, one value for each of the three frequencies. The 2 Hz, 4.5 Hz and 10 Hz filters were then applied to the corresponding Blackfoot data sets. The overall scale of each dataset was altered until the resulting weighted stacks provided roughly the same RMS value as the corresponding synthetic data. This scale result was then checked against a recursive inversion of the data. If the scale agreed with the synthetic RMS output, and the recursive inversion result was reasonable, then the chosen scale was considered to be approximately correct.

A final P-S weighted stack was then computed for each dataset and output. The density assumption, required by the method, was arrived at using an examination of the P-wave velocity and density logs of a near-by productive well (Section 4.22).

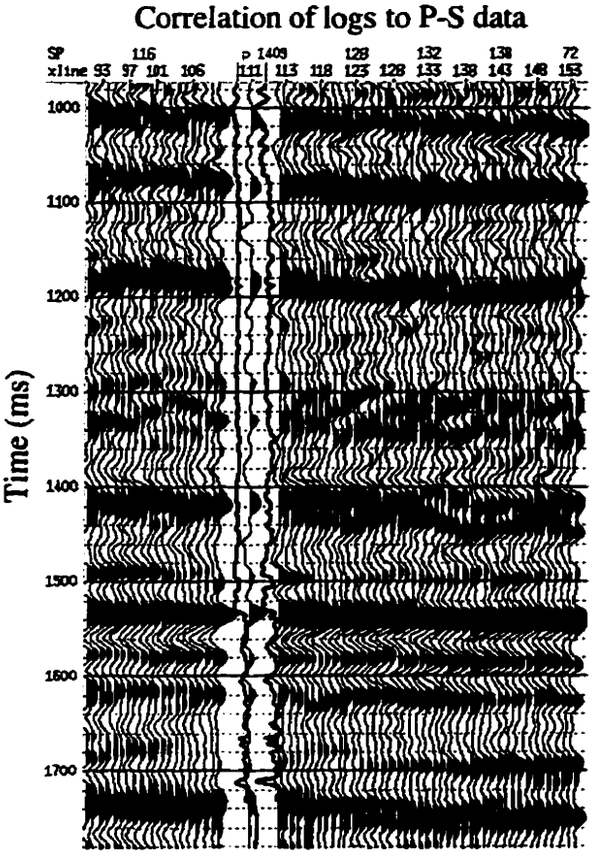

Figure 4.22. Correlation of the regional Vp and Vs logs to P-S time. The resulting correlated logs were used in computing P-S weighted stacks and inversions for the P-S data.

4.4.9 Phase correction

The migrated P-P sections and the P-S weighted stacks were phase corrected relative to the well log. It was found that the phase corrections were very sensitive to the range of frequencies input, and the time range over which the phase correction was computed. Due to this uncertainty, it was decided that each data set would have a single phase correction applied relative to the well log. The correction was computed on seismic data that had been band pass filtered to the ranges that were to be used during band limited inversion.

4.5 Inversion

The phase corrected migrations of the P-P seismic data and the phase corrected weighted stacks of the P-S data were inverted using BLIMP (Section 3.2.1). BLIMP was found to be a very simple inversion method to use, and was especially well suited to the comparison of the different low-end frequency ranges.

Inversion of the Blackfoot data set was also attempted using constrained linear inversion developed in Section 3.3. Noise and scale variations were found to prevent the damped least-squares method from converging to a reliable solution. It was found that convergence was only achievable over very small time windows of ~ 20 ms.

Recursive inversions were also computed as inversion quality control. Coherent trace-trace noise was found to contaminate the 2 Hz P-P data and was present on all components to a lesser degree. Trace equalization was found to reduce the presence of this noise, but the resulting recursive inversions were lacking in trace to trace velocity detail. It was found that a trade off between true-amplitude preservation and noise reduction by trace equalization had to be made in favor of true-amplitude preservation.

P-P inversion using BLIMP was done by first tying the regional density and Vs logs to the P-P data (Figure 4.23). Care was taken to ensure that the velocity to seismic correlations were optimal for all three data sets. An impedance log was then generated by multiplying each sample of the density log with each sample of the Vp log. The phase corrected P-P data were then inverted using the impedance log. The resulting inversion impedance's were converted to velocity estimates using Gardner's equation.

Figures 4.24 and 4.25 are the resulting Vp sections for the 2 Hz and 10 Hz data. The Vp from the well is overlain for comparison. The velocity estimates from the 2 Hz and 10 Hz data show similar values. Velocities in the zone of interest, just above the Mississippian level (annotated Miss) between shotpoint 161 and 191, average about 4000 m/s. A velocity decrease related to channel-sand was not resolved by either section.

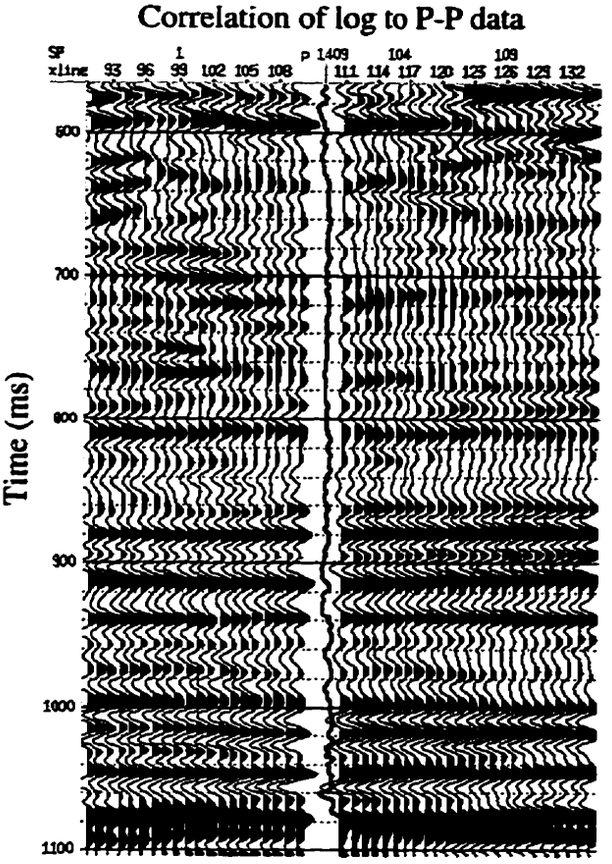

Figure 4.23. Correlation of the regional Vp logs to P-P time. The resulting correlated logs were used in computing P-P inversions.

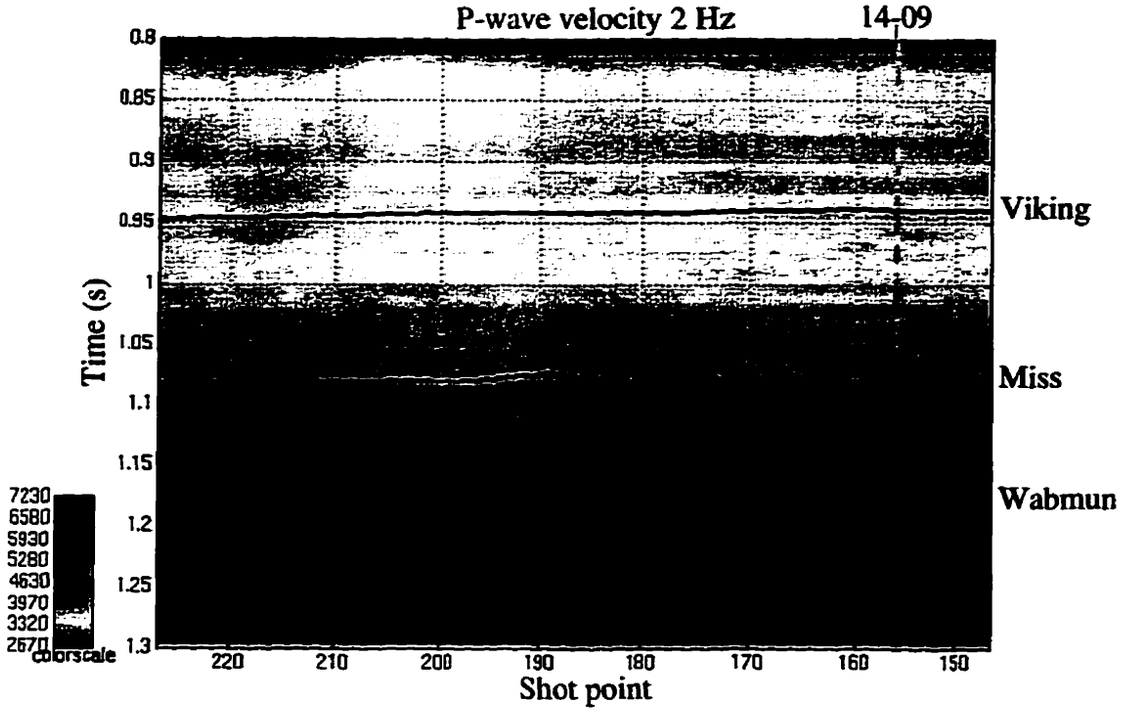

Figure 4.24. BLIMP inversion of the 2 Hz P-P data. The interpreted channel-sand lies between shotpoints 161 and 191, just above the Mississippian level. The expected 50 m/s decrease in Vp has not been resolved.

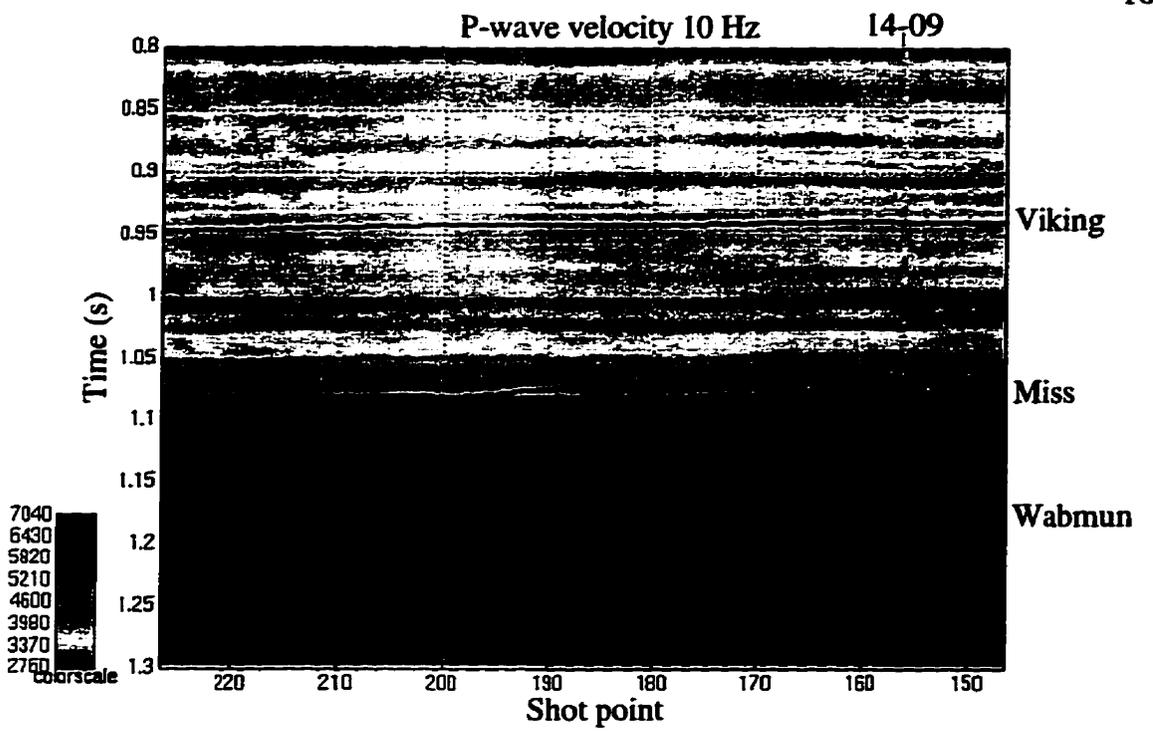

Figure 4.25. BLIMP inversion of the 10 Hz P-P data. The interpreted channel-sand lies between shotpoints 161 and 191, just above the Mississippian level. The expected 50 m/s decrease in Vp has not been resolved.

P-S inversion using BLIMP was done using the Vs log correlated to P-S time (Figure 4.22). Each frequency range was inverted using the correlated Vs log for low frequency velocity information. Figures 4.26 and 4.27 are the resulting Vs sections for the 2 Hz and 10 Hz data. The Vs velocity from the well is overlain for comparison. Values for Vs were expected to increase by 200 m/s from 2200 m/s to 2400 m/s when moving from a regional position to a channel position in this area. As Figure 4.26 indicates, the 2 Hz data resolved a significant Vs increase in the same location as the interpreted position of a possible channel, between shotpoints 170 and 191, just above the Mississippian level. The velocities vary from about 2400 m/s in the regional position to 2200 m/s in the on-channel position. On the left side of the section, the apparent velocity increase is most probably related to noise due to the low-fold of the line.

No velocity increase was apparent on the 10 Hz data and only a slight increase was found on the 4.5 Hz data.

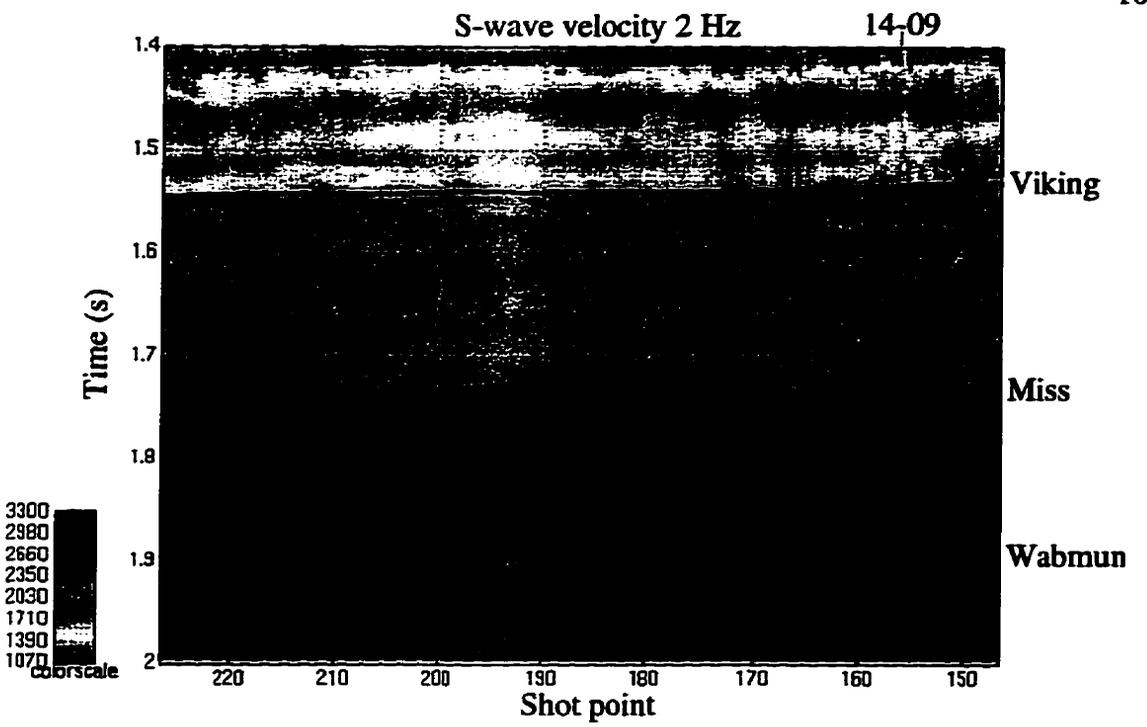

Figure 4.26. BLIMP inversion of 2 the Hz P-S data. The interpreted channel-sand lies between shotpoints 161 and 191, just above the Mississippian level. The expected 200 m/s increase in Vs has been resolved and is distinct between shotpoints 170 and 191. The velocities vary from about 2400 m/s in the regional position to 2200 m/s in the channel position.

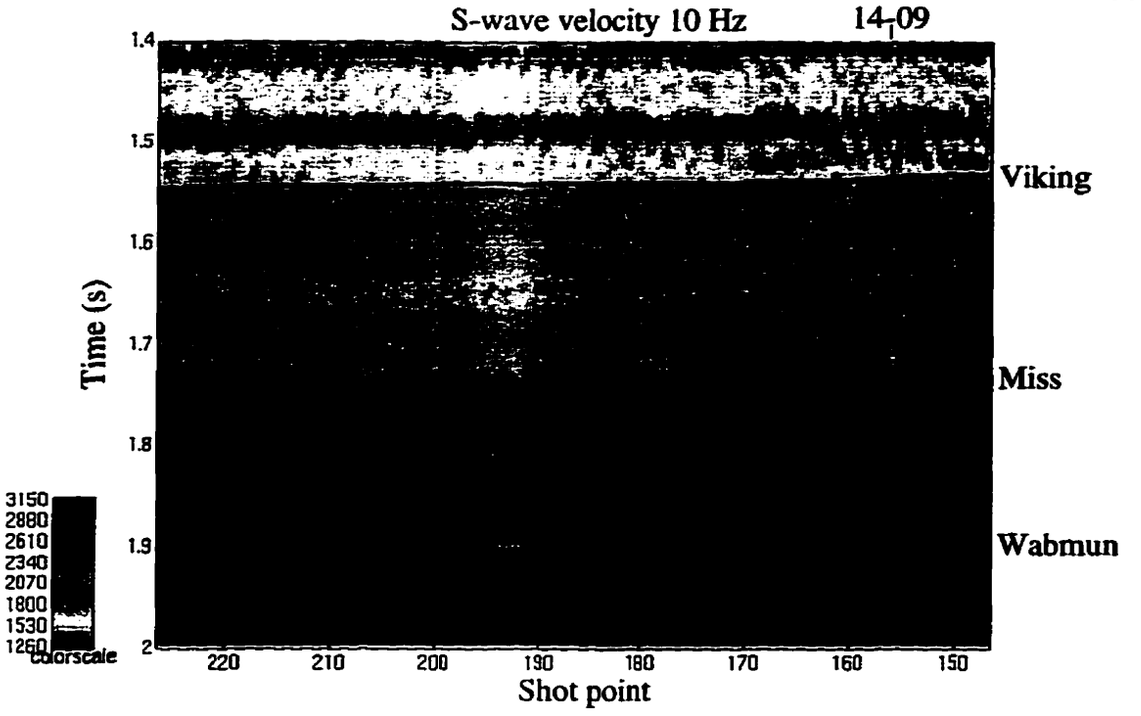

Figure 4.27. BLIMP inversion of the 10 Hz P-S data. The interpreted channel-sand lies between shotpoints 161 and 191, just above the Mississippian level. The expected 200 m/s increase in Vs has not been resolved through this zone. The velocity is constant at about 2500 m/s.

The Vp sections were then stretched to P-S time using the Viking, Mississippian and Wabmun horizons. A sinc function interpolator and an anti-alias filter were used to resample the stretched velocities. Division of the Vp sections by the Vs sections was done to yield Vp/Vs sections in P-S time.

The resulting Vp/Vs sections for the 2 Hz and 10 Hz data are given in Figure 4.28 and 4.29. The Vp/Vs change, when moving from a regional to a channel position, was expected to be a decrease to about 1.67 from about 1.89. The 2 Hz data show a decrease within the interpreted channel location of about 1.7 from about 1.9 which is consistent with the presence of sand.

The 10 Hz data show a weak Vp/Vs decrease which was spread over a larger number of shotpoints - from 152 to 195.

It was believed that the regional log was being imprinted in the 10 Hz inversions such that the Vp/Vs decrease was being masked. The 10 Hz data were then inverted using a frequency split of 2 Hz to extract as much low-frequency from the seismic as possible. Figure 4.30 shows the resulting Vp/Vs section. The Vp/Vs decrease over the zone of interest is better resolved relative to the background, however the results are noisy enough to negate independent interpretation.

In turn, the 4.5 Hz data were inverted using a 2 Hz frequency split. Figure 4.31 shows a Vp/Vs decrease which is consistent with the expected decrease for an on-channel position. The shape of the decrease is similar to that of the 2 Hz data.

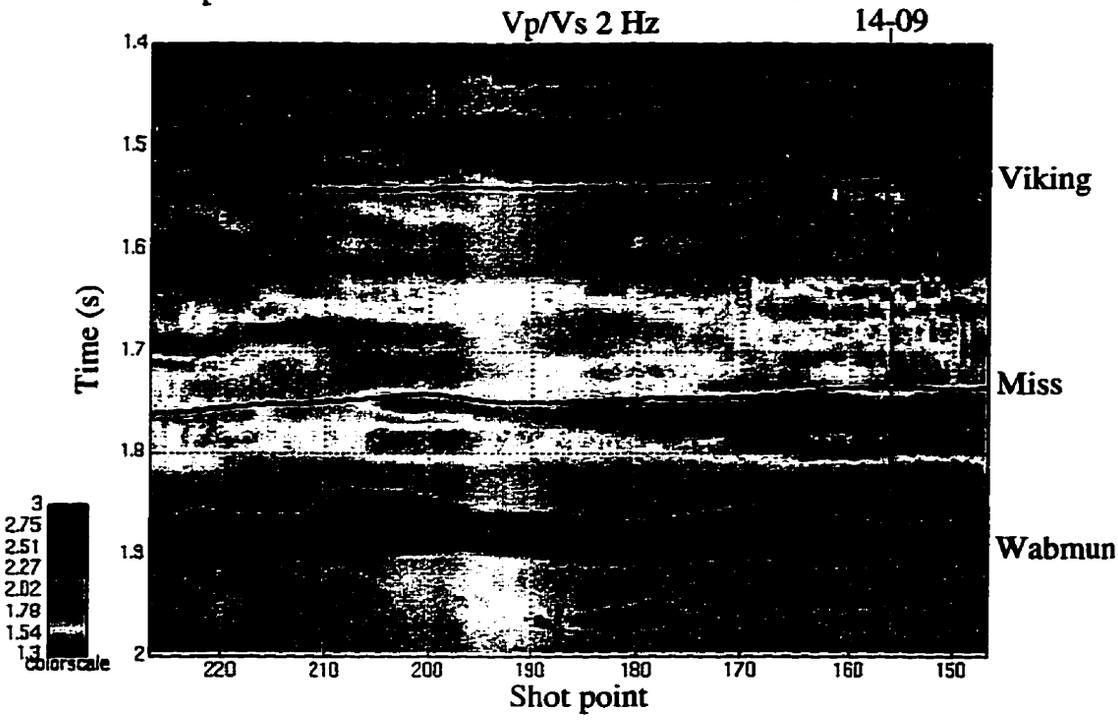

Figure 4.28. Vp/Vs section for the 2 Hz data. A Vp/Vs decrease (1.7 from 1.9), consistent with the presence of sand, is coincident with the interpreted channel position between shotpoints 170 and 187, just above the Mississippian marker.

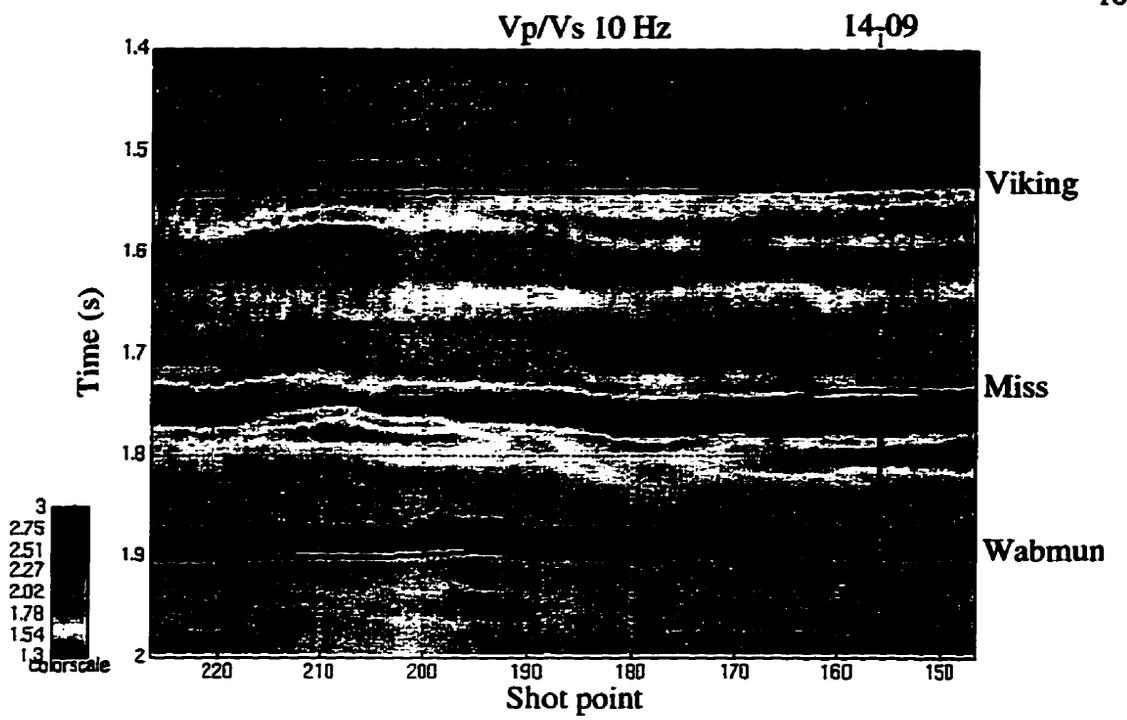

Figure 4.29. Vp/Vs section for the 10 Hz data. A Vp/Vs decrease is weakly coincident with the interpreted channel position between shotpoints 152 and 195.

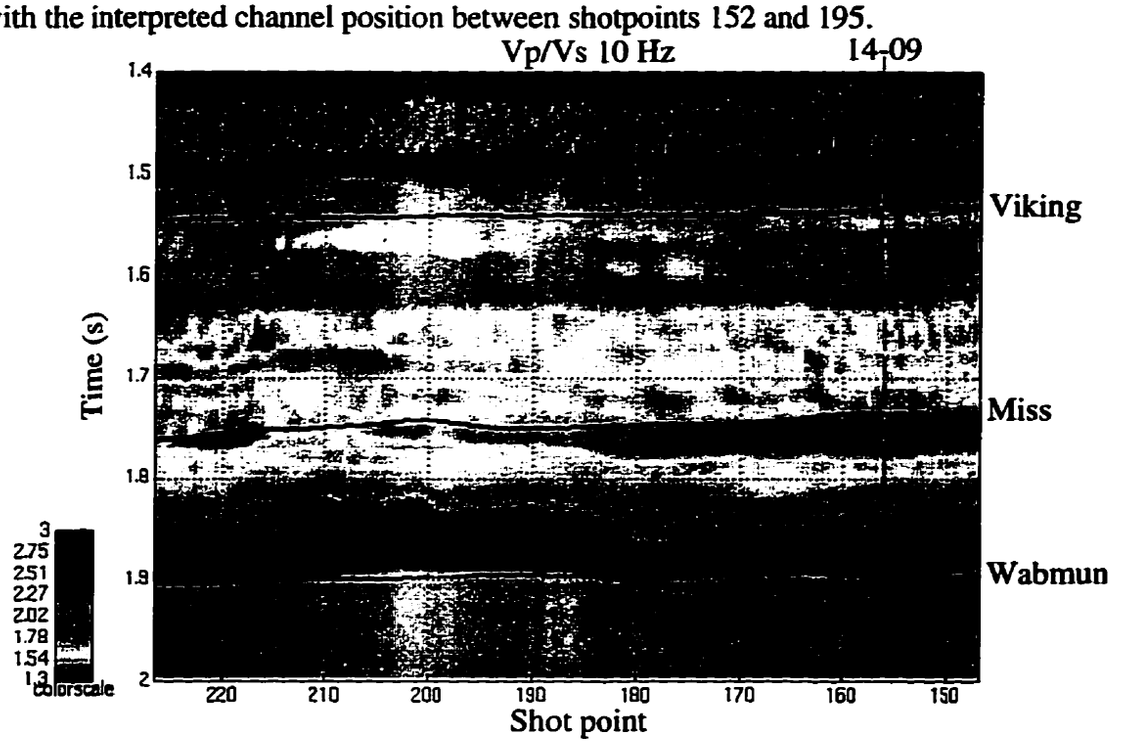

Figure 4.30. Vp/Vs section for the 10 Hz data. The BLIMP inversion was run with a 2 Hz frequency split. A Vp/Vs decrease is more strongly coincident with the interpreted channel position. The section is too noisy to provide an independent interpretation.

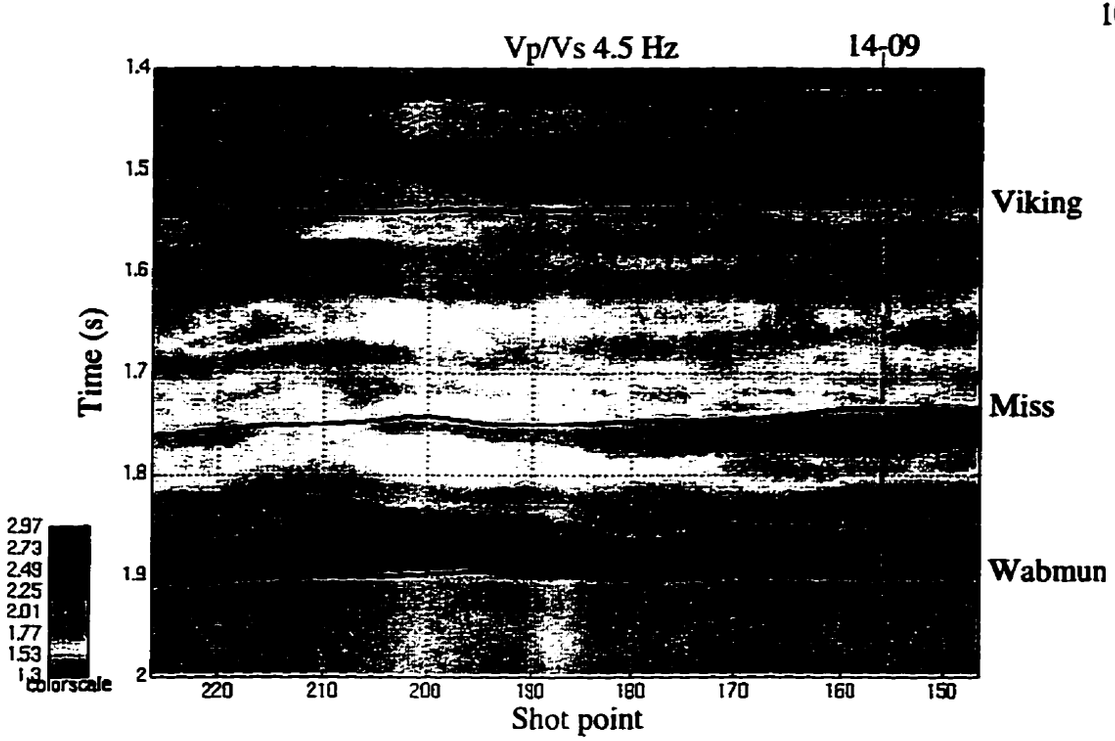

Figure 4.31. Vp/Vs section for the 4.5 Hz data. A Vp/Vs decrease is coincident with the interpreted channel position between shotpoints 170 and 187. The shape of the decrease is similar to that of the 2 Hz data.

4.6 Chapter summary

Inversion modeling of the Broad-band Blackfoot 3C-2D survey found that low-frequency filtering may be compromised by insufficient record length. The model inversion results showed that, when using a regional background model, inversion of the on-channel synthetic seismic data could not perfectly resolve the decreased Vp/Vs of the on-channel model. In future, models representing much longer reflection times, such as is the case with real seismic data, will be employed.

The processing of the Blackfoot field data showed that the P-P data had greater high-frequency content compared to the radial data (80 Hz vs. 60 Hz). The 2 Hz data were found to have more power in the low-frequency range (0 - 10 Hz) than the 10 Hz data. The 2 Hz vertical data were found to have an average of 3 dB more power in this range

than the 10 Hz data. The 2 Hz radial data were found to have an average of 2 dB more power than the 10 Hz data.

Processing flows were developed which allowed the P-S data to be processed pre-stack to facilitate P-S weighted stacking and inversion. Trace-to-trace equalization was found to eliminate coherent noise when applied pre-stack, but was not applied due to its deleterious effect on inversion results.

Comparisons of the final migrated sections showed the 2 Hz data were imaging additional events that the 10 Hz data could not. The 2 Hz P-P data were able to image an additional two events in an interpreted incised valley, the lower of the two was thought to be the top of the Mississippian. The 2 Hz P-S data were able to image an amplitude peak in the interpreted valley which had much greater amplitude than the corresponding peak on the 10 Hz data.

Inversions of the P-P data resulted in Vp sections which were quite similar in the velocity values resolved. A velocity decrease of 50 m/s was expected when encountering channel-sands but none was imaged by the 2 Hz, 4.5 Hz or 10 Hz data in the zone of interest. The 2 Hz and 10 Hz examples presented showed constant velocities of about 4000 m/s.

Inversions of the P-S resulted in sections which were quite different in the velocity values resolved. A velocity increase of 200 m/s was expected when encountering channel-sands. When using conventional frequency splits only the 2 Hz data were able to image a velocity increase consistent with the presence of a channel-sand.

The Vp and Vs sections were then used to generate Vp/Vs sections. A Vp/Vs decrease to 1.67 from 1.89 was expected when moving from regional shales to channel-sands. When using conventional frequency splits the 2 Hz data resolved the expected Vp/Vs decrease. The 4.5 Hz and 10 Hz inversions were run with a 2 Hz frequency split. Both data sets were able to resolve a Vp/Vs decrease with the 4.5 Hz data closely matching the 2 Hz data.

Chapter 5 CONCLUSIONS AND FUTURE WORK

5.1 Conclusions

P-S seismic data can be inverted to provide an estimate of the S-wave velocity (Vs) of the subsurface. By inverting the P-S stacking velocity, using an analogue of the Dix equation, a direct estimation of Vs is possible. The estimate is reliable only in a low-frequency sense if offset/depth ratios are kept below about 1.0.

P-S reflection amplitudes can be inverted using P-S weighted stacks and recursive inversion. The Vs estimates are, however, compromised by frequency-band limiting and phase distortion. Phase distortion is a problem that can be controlled in processing. Frequency-band limiting occurs at the acquisition stage, thus, careful processing and frequency-compensation must be applied to the data for reliable inversion results.

The BLIMP (Band Limited IMPedance) inversion, when modified for inverting P-S weighted stacks, provides very reliable Vs estimates. The frequency domain combination of the low-frequency trend of a log, with the Vs from a P-S weighted stack is a simple and efficient inversion method.

A constrained linear inversion can also be modified to invert P-S weighted stacks, but the algorithm developed to this point met with limited success. Moderately large numbers of trace samples were found to prevent convergence of the program to reasonable Vs values. The largest number of synthetic samples allowable were about 51 samples, and real data examples were limited to less than 20 samples.

Stack sections of the P-P data from the Blackfoot field have more high-frequency compared to the P-S data (80 Hz vs. 60 Hz). However, these values were measured after the processing contractors had applied a hyperbolic moveout. More high-frequency may be available in P-S stacks if shifted-hyperbolic moveout is used.

The 2 Hz data have more power in the low-frequency range (0 - 10 Hz) than the 10 Hz data. The 2 Hz vertical data have an average of 3 dB more power in this range than the 10 Hz data. The 2 Hz radial data have an average of 2 dB more power than the 10 Hz data.

The 2 Hz vertical data image two additional events in the zone of interest that the 10 Hz data miss, the lower of the two being the Mississippian marker. The 2 Hz P-S data image an amplitude peak in the zone of interest which is much less distinct on the 10 Hz data.

P-P inversion does not resolve the very small P-wave velocity change associated with the target channel sands, this holds for the 2 Hz, 4.5 Hz and 10 Hz data. In contrast, P-S inversion of the 2 Hz data yields a large S-wave velocity increase consistent with the presence of the channel sands. The 4.5 Hz also provides this result when it is inverted as though it is 2 Hz data. The resulting Vp/Vs for the zone of interest is also consistent with the presence of channel-sands.

5.2 Future work

Inversion of P-S stacking functions should be examined using shifted hyperbolic functions, which would result in greater picking accuracy during semblance analysis. This increase in accuracy would yield greater confidence in the resulting S-wave velocity estimates.

Other P-S inversion methods should be attempted, for example sparse-spike inversion. It could be re-cast to invert P-S weighted and may provide improved S-wave velocity estimates.

The P-S weighted stack algorithm should be expanded to accept P-S data which is binned as depth-variant CCPs as well as asymptotically-approximated CCPs. Both binning methods require assumptions about the Vp/Vs of the subsurface, but the depth-variant method would provide better inversion results in the shallow section.

More work is required to improve the performance of the constrained linear inversion developed in chapter 3. The problem of non-convergence might be solved by selecting a better set of convergence criteria, or by breaking the seismic trace into smaller, overlapping ranges.

Inversion modelling of the Broad-band Blackfoot 3C-2D data should be reexamined. The record lengths of the synthetic data were probably not long enough for reliable low-frequency filter performance. Extended models could be used to better predict inversion performance at the various low-frequency ranges.

The P-S data from the Broad-band Blackfoot 3C-2D should be reprocessed using stacking velocities based on shifted hyperbolic velocities. This should result in greater high-frequency detail in both the stacked sections and in the inversion results. True pre-stack migration should be applied to the P-S data prior to the P-S weighted stack. This would give greater confidence in the positioning and amplitude of the reflection data, and should provide more accurate S-wave velocity estimates.

REFERENCES

Aki, K., and Richards, P. G., 1980, Quantitative seismology: Theory and methods, v.1: W. H. Freeman and Co.

Anderson, D. L., and Leiberman, R. C., 1966, Sound velocities in rocks and minerals: VESIAC state -of-the-art report: 885-4-X, Univ. of Michigan, Ann Arbor.

Castanga, J P., Batzle, M. L., and Eastwood, R. L., 1985, Relationships between compressional-wave and shear-wave velocities in clastic silicate rocks: Geophysics, 50, 571-581.

Cooke, D. A., and Schneider, W. A., 1983, Generalized linear inversion of reflection seismic data: Geophysics, 48, 665-676.

Dix, H. C., 1955, Seismic velocities from surface measurements: Geophysics, 20, 68-86.

Domenico, S., N., 1977, Elastic properties of unconsolidated sand reservoirs: Geophysics 42, 1339-1368.

Domenico, S., N., 1984, Rock lithology and porosity determination from shear and compressional wave velocity: Geophysics, 49, 1188-1195.

Ferguson, R. J., and Margrave, G. F., 1996, A simple algorithm for band-limited impedance inversion: CREWES Project Research Report, 8, 21-1 - 21-10.

Gardner, G. H. F., Gardener, L. W., and Gregory, A. R., 1974, Formation velocity and density - the diagnostic basics of stratigraphic traps: Geophysics, 39, 770-780.

Gardner, G. H. F., and Harris, M. H., 1968, Velocity and attenuation of elastic waves in sands: 9th Ann. Log. Sympos., Soc. Prof. Well Log Analysts, Paper M.

Gregory, A. R., 1976, Dynamic elastic rock properties: key to pore fluid identity: Oil and Gas J., 74, 130-138.

Gulunay, N., 1986, F-X prediction and the complex weiner prediction filter for random noise reduction on stacked data: 56th Ann. Internat. Mtg., Soc. Expl. Geophys., Expanded Abstracts.

Han, D., Nur, A., and Morgan, D., 1986, Effect of porosity and clay content on wave velocities in sandstones: Geophysics, 51, 2093-2107.

Harrison, M. P., Processing of P-SV surface-seismic data; Anisotropy analysis, dip moveout, and migration: Ph.D. thesis, The University of Calgary.

Hendrick, N., and Hearn, S., 1993, Evaluation of seismic trace inversion techniques: Exploration Geophysics, 24, 549-560.

Ito, H., DeVilbiss, J., and Nur, A., 1979, Compressional and shear waves in saturated rock during water-steam transition: J. Geophys. Res., 84, 4731-4735.

Jeffrey, A., 1995, Handbook of mathematical formulas and integrals: Academic Press.

Lawton, D.C. and Howell, T.C., 1992, P-P and P-SV synthetic stacks: 62nd Ann. Intl. Mtg. Soc. Expl. Geophys., Expanded Abstracts, 1344-1347.

Lines, L. R., 1988, Inversion of Geophysical Data: Society of Exploration Geophysicists.

Lines, L. R., and Treitel, S., 1984, A review of least-squares inversion and its application to geophysical problems: Geoph. Prosp., 32, 159-186.

Menke, W., 1984, Geophysical data analysis: discrete inverse theory: International geophysics series, 45, Academic press.

Miller, S. L. M., Harrison, M. P., Lawton, D. C., Stewart, R. R., and Szata, K. J., 1995, Analysis of P-P and P-SV seismic data from Lousana Alberta: CREWES Project Research Report, 7, 7-1 - 7-24.

Murphy W. F. III, 1084, Seismic to ultrasonic velocity drift: intrinsic absorption and dispersion in crystalline rock: Geophys. Res. Let., 11, 1239-1242.

Nur, A., and Simmons, G, 1969a, Stress-induced velocity anisotropy in rock: an experimental study: J. Geophys. Res., 74, 6667-6674.

Nur, A., and Simmons, G, 1969b, The effect of saturation on velocity in low porosity rocks: Earth Planet Sci. Let., 7, 183-193.

Nur, A., 1971, Effect of stress on velocity anisotropy in rocks with cracks: J. Geophys. Res. 76, 2022-2034.

Oldenburg, D. W., Scheuer, T., and Levy, S., 1983, Recovery of the acoustic impedance from reflection seismograms: Geophysics, 48, 1318 - 1332.

Pickett, G. R., 1963, Acoustic character logs and their application in formation evaluation: J. Petr. Tech., 15, 659-667.

Russell, B., and Hampson, D., 1991, Comparison of post-stack seismic inversion methods: 61st Ann. Internat. Mtg., Soc. Expl. Geophys., Expanded Abstracts, 876 - 878.

Sheriff, R. E. and Geldart, L. P., 1983, Exploration seismology: Data-processing and interpretation: Cambridge University Press, v.2.

Slawinski, M. A., Slawinski, R. A., and Brown, R. J., 1995, Energy partition at the boundary between anisotropic media; part two: raytracing in layered, anisotropic media - comparison of synthetic and experimental results., CREWES Research Report, 7, 9-1 - 9-13.

Slotboom, R. T., Eaton, D. W., and Lawton, D. C., 1990, Improving converted-wave (P-S) moveout estimation: CREWES Research Report, 3, 80-88.

Smith, G. C., and Gidlow, P. M., 1987, Weighted stacking for rock property estimation and detection of gas: Geophysical Prospecting, 35, 993-1014.

Stewart, R. R., 1990, Joint P and P-SV inversion: CREWES Research Report, 2, 112-115.

Stewart, R. R., 1994, The present and promise of P-S seismic exploration: CREWES Research Report, 6, 1-1 - 1-31.

Stewart, R. R., 1995, The Blackfoot broad-band 3-C seismic survey: Introduction: CREWES Research Report, 7, 15-1 - 15-6.

Stewart, R. R., Ferguson, R. J., 1995, Dix interval velocity for shear-waves: CREWES Research Report, 7, 15-1 - 15-6.

Stewart, R. R., Ferguson, R. J., Miller, S., Gallant, E., and Margrave, G., 1996, The Blackfoot seismic experiments: Broad-band, 3C - 3D, and 3-D VSP surveys: CSEG Recorder, 6, 7 - 10.

Tatham, R. H., and McCormick, M. D, 1991, Multicomponent seismology in petroleum exploration: Society of Exploration Geophysicists.

Tessmer, G. and Behle, A., 1988, Common reflection point data-stacking technique for converted waves: Geophys. Prosp., 36, 661-688.

Tosaya, C., Nur, A., Vo-Thanh, D., and Da Prat, G., 1987, Laboratory seismic methods for remote monitoring of thermal EOR: Soc. Petr. Eng. Res. Eng., 2, 235-242.

Vestrum, R. W., and Stewart, R. R., 1993, Joint P and P-SV inversion: application and testing: CREWES Research Report, 5, 13-1 - 13-7.

Wang, Z., 1988, Wave velocities in hydrocarbons and hydrocarbon saturated rocks - with applications to EOR monitoring: Ph.D. thesis, Stanford University.

Wang, Z., and Nur, A., 1987, Wave velocities in hydrocarbon saturated rocks: 57th Ann. Internat. Mtg., Soc. Explor. Geophys., Expanded Abstracts, 1-5.

Waters, K. H., 1978, Reflection seismology: John Wiley and Sons.

Yilmaz, O., 1987, Seismic data processing: Soc. Expl. Geophys.

Zheng, C., and Stewart, R. R., 1991, Using P-SV waves to improve conventional AVO estimates: A synthetic study: CREWES Research Report, 3, 361-389